Raman and SERS studies of filamentous fungi

By
Fatemeh Farazkhorasani

A Thesis Submitted to the Faculty of Graduate Studies of

The University of Manitoba

in partial fulfillment of the requirement of the degree of

Master of Science

Department of Chemistry

University of Manitoba

Winnipeg, Canada

ABSTRACT

Fungal species perform many important roles in biotechnology and recycling and act as agents of disease and decay. The fungal wall preserves the cell against adverse environmental stress and plays a significant role in fungal physiology. The fungal cell wall has been studied as a great object for anti-fungal agents and a good model to address questions related to the cell wall. A better understanding of fungal growth, cell composition and interactions with their environment is important for the development of anti-fungal drugs.

Surface-enhanced Raman scattering (SERS) has attracted significant attention as an analytical method for chemical and biological identification. SERS enhancement is based on the intense electromagnetic fields in the close proximity of metallic surfaces. Noble metal nanoparticles (NPs) are favourable as SERS-active substrates due to their tunable optical properties and particularly surface plasmon resonance (SPR). SERS microscopy enables the detection of cellular components and NPs interaction with biological cells.

For SERS experiments, it is essential to generate gold nanoparticles (AuNPs) with proper sizes and shapes. Raman and SERS imaging of fungi via *in vivo* synthesis of AuNPs were used to explore cellular components of *Aspergillus nidulans* (*A. nidulans*) cell. Critical parameters including pH, temperature and metal concentration affect the sizes and shapes of the NPs. For better control of NP formation (size, shape and location), pre-formed NP were incubated with *A. nidulans* colonies. *Aspergillus nidulans* outer hyphal walls were coated with NPs. Raman and SERS imaging of fungal walls revealed that proteins, carbohydrates and lipids are the main constituents of fungal cell wall. Most

of the SERS responses were obtained from the outer surface proteins (mannoproteins). Similar SERS responses were achieved from AAE1 and AAE2 strains.

Additionally, Fourier transform infrared (FTIR) attenuated total reflectance (ATR), Raman, and SERS spectroscopy techniques were applied to characterize the composition of *Aspergillus nidulans* spores. FTIR-ATR and Raman spectra of five strains of *A. nidulans* engineered to have differing wall α-glucan content and these experiments revealed chemical composition variation. Analysis of FTIR-ATR and Raman spectra of these strains showed they had similar spectral features with a few differences mainly in the carbohydrate regions. The spectral resemblances are most likely due to their similar chemical composition as a result of their close relatedness. Raman spectra of germinated spore compared with the germ tube and different changes in spectral features were detected.

ACKNOWLEDGMENTS

I would like to express my deepest appreciation to my advisor, Dr. Douglas Goltz, for his guidance, support, and motivation. Without his supervision and constant help this dissertation would not have been possible.

I would like to thank my committee members, Prof. Michele Piercey-Normore, Dr. John Sorensen, and Dr. Jennifer van Wijngaarden.

I wish to thank my colleagues and friends at the Department of Chemistry.

Last but not the least, I would like to thank my family and friends. The most special thanks goes to my lovely husband, Hamed Aghakhani, who gave me his unconditional support and love through all this long process.

DEDICATION

To the four pillars of my life: God, my husband (Hamed), and my parents (Hassan and Ehteram). Without you, my life would fall apart.

I might not know where the life's road will take me, but walking with You, God, through this journey has given me strength.

Hamed, you are everything for me, without your love and understanding I would not be able to make it. I am truly thankful for having you in my life.

Hassan, whose good examples have taught me to work hard for the things that I aspire to achieve.

Ehteram, who has been a source of encouragement and inspiration during the challenges of graduate school and life.

We made it...

Table of Contents

List of Figures

List of Tables

Chapter 1: Introduction

1.1 Background

Fungi play several important roles in the environment, varying from helpful to extremely detrimental. Fungi affect humans in multiple ways from their roles in biotechnology and decomposing of nutrients to being harmful agents of disease and decay. Fungi can be used as experimental model organisms for eukaryotes due to shared origins of the genes responsible for essential biological functions.[1] The cell wall is one of the most striking differences between fungi and other eukaryotes.[2] The fungal cell wall performs an important function in fungal life.[3] The fungal wall has a dynamic and heterogeneous structure that maintains the cellular shape and integrity. In addition, the fungal cell interacts with the environment in reaction to environmental stresses through its wall.[4] The fungal cell wall composition varies along the length of the hypha as it becomes mature.[5] Due to the biological importance and structural specificity, the fungal cell wall has been examined as a good target for developing of anti-fungal drugs.[4]

Some fungi are considered to be a serious cause of infectious diseases. Fungal plants pathogens have a significant impact on most of crop plants and contaminate food by production of mycotoxins.[1] In the United States, the annual estimated damage of crop plants caused by fungi is ~33 billion dollars.[6] Similarly, the fungal infectious diseases are a growing threat to human and ecosystem health.[7] *Candida* and *Aspergillus* species are the most common fungal pathogens in HIV-related fungal infection and hospitalizations respectively.[8,9] Owing to all of the vital roles of fungi, it is necessary to have a better understanding of fungal cell, especially cell wall components, in order to control fungal activities.

1.2 Fungi

Fungi are important group of eukaryotic organisms that affect humans in multiple ways from their roles in biotechnology to being harmful agents of disease and decay. There are approximately 1.5 million fungal species; however, only 70,000 species have been identified already.[10,11] More than 200 fungal species impact humans either as pathogens or as organisms with no harm.[12] Humans use fungi in a variety of ways such as: a direct source of food or in the production and fermentation of foods and drinks,[13] manufacture of industrial chemicals like citric and lactic acids,[14] industrial production of drugs such as antibiotics,[15] and bioremediation for environmental detoxifying.[16] In addition, fungal species such as *Aspergillus nidulans,* are used as model organisms due to their short life cycle and easy reproduction in the laboratory. Therefore, they could provide information about more complex organisms, including humans. Due to lack of known sexual cycles, the study of *A. oryzae* (employed in the production of some beverages) and *A. fumigatus* (life-threatening human pathogen) depends on *A. nidulans* as a good genetic model.[17]

Fungi were initially considered to be part of the plant kingdom due to similar properties with plants such as immobility and presence of cell walls.[18] Unlike plants, fungi are unable to produce their food via photosynthesis and they obtain their nutrition from living or dead organisms. Such organisms are named heterotrophs and can be divided into several groups. Fungi that use dead organic matter as their food are called saprotrophs and they are known as nature's decomposers. Those fungi that derive their food from a living host may harm the host and are called parasites, while those that kill the host are named pathogens. Moreover, some fungi make a symbiotic relationship with

another living organism (e.g. the roots of trees or algae) and this association is mutually beneficial to both the plant or algae and the fungus.[19] Some fungi are harmful and cause human, crop, and animal diseases or stored food spoilage that have a negative effect on the human food supplies.[20] Since fungi play a critical role in ecosystem, it is important to get a better consideration of fungi and their interaction with environment in order to control their activities.

1.2.1 Fungal Structure

The vegetative forms of fungi include organisms such as simple, single-celled yeasts and complex, muticellular filaments. The life cycle of a fungus usually starts by germination from the spore in appropriate conditions (e.g., suitable substrate, nutrient). The germ tube is the first emergence of a germinating spore and is called a slender hypha (1-15 μm wide). The limited stored nutrients in a spore force the germ tube to extend into the nutrient- and water-rich environments for growth.[21] The vegetative body of filamentous fungi consist of hyphae, a system of branched, cytoplasm-filled, rigid tubular cells that grow at one end (tip) in order to take up nutrients (Figure 1.1). Hyphae usually grow by apical branching from the hyphal tip, or by lateral branching by emergence of new branches from sites below the hyphal tip.[22] During hyphal extension, cytoplasm, new wall material, and several organelles which are synthesized in regions distant from the tip, flow to the extreme apex to make the new wall at the tip.[21,23] A network of branched hyphae forms an individual fungus known as the mycelium.

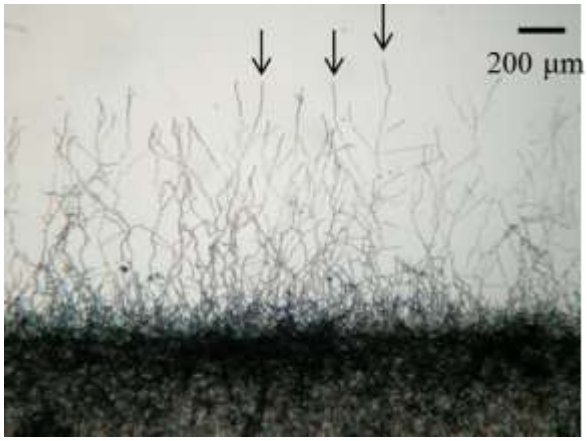

Figure 1.1: *Aspergillus nidulans* grown on glass microscope slide. Arrow show hyphal tips.

Hyphae are divided into compartments or cells by cross walls, called septa, displayed in Figure 1.2. Most septa are incomplete and they have pores which allow the passage of cytoplasm and organelles including mitochondria, vacuoles, and nuclei.[20] If the hyphae are aged or lysed, pores will be plugged by small, round, and electron rich materials called woronin bodies to avoid excessive cytoplasm leakage.[24] In most filamentous fungi, woronin bodies are located adjacent to the septal pores and when hyphae are injured, woronin bodies are released by a signal and then pores get blocked. In this case, transport of material to the apical region of the hyphae is prevented.[25] Blocking of septal pores has major roles in differentiation of hypha and protecting the mycelium when the hypha is damaged.[26, 27]

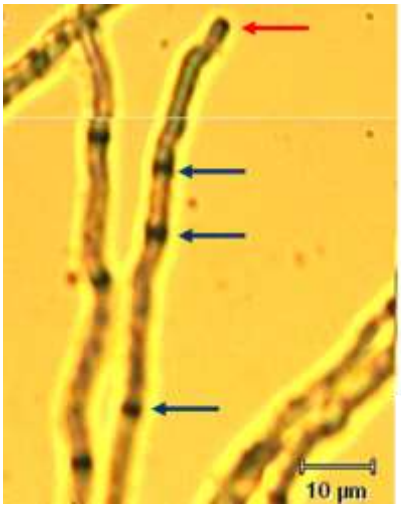

Figure 1.2: *Aspergillus nidulans* grown on a gold-coated silicon wafer substrate. Red arrow shows hyphal tip. The blue arrows indicate septa.

1.2.2 Fungal Cell Structure

Fungi share typical characteristics of eukaryotes; however, they have some unique organelles that give specialized functions. All the major organelles except chloroplasts are present in filamentous fungi. In addition, Golgi apparatus are infrequent among filamentous fungi.[21] The protoplast in fungi is bounded by a plasma membrane. The plasma membrane may be tightly attached to the hyphal wall. The plasma membrane contains lipids, proteins, and small amounts of carbohydrates. Sterols, sphingolipids, and glycerophospholipids are the main components of the fungal plasma membrane.[28] Fungal cytoplasm contains organelles including nuclei, mitochondria, vesicles, and vacuoles.

Nuclei are the most noticeable and in some species are the largest organelles within the cytoplasm. Nuclei of most filamentous fungi are the site of the genome and are around 1-3 µm in diameter. The nucleus of filamentous fungi is spherical and is surrounded by a double layer bounding membrane. The nucleolus is inside the nucleus and is the site of ribosome synthesis.[21] Mitochondria are energy producing organelles within the cells and are the sites of oxidative respiration. They are enclosed by two

membranes. The number of nuclei inside a hyphal compartment is variable due to nuclei migration via septal pores between neighbor compartments.[21] Vesicles are one of the main organelles within the filamentous fungal cell. Aggregations of vesicles are often located at the hyphal apex, branch points, and sites where germ tubes emerge.[21, 27] Vesicles from sub-apical (older regions) compartments of hyphae migrate through the septal pores to support the apical growth.[21] Vesicles might originate from Golgi and endoplasmic reticulum (ER).[21] Different kinds of vesicles such as cytoplasmic vesicles, apical vesicles, and wall vesicles are classified based on their functions. Clusters of vesicles in the hyphal apex wall suggest that hyphal cell wall synthesis occurs by vesicles.[5] Vacuoles are mostly observed in sub-apical compartments of hyphae. They are located in the active biomass area, between the active hyphal tip and dead mycelial part.[21] The vacuole main function is: cellular metabolite storage (e.g. enzymes and nutrients) and recycling, cytosolic ion and pH homeostasis, adoption to nutrient level variation.[21,27] Vacuoles are the main storage site of nitrogen, inorganic phosphorus (polyphosphate molecules) and some key ions such as Ca^{+2} and Mg^{+2}.[18,21] Vacuoles also eliminate toxic ions like Co and Pb from the cytosol.[21] Vacuole enzymes are effective in peptide recycling and this helps the fungus adapt to various nutrient conditions.[27]

1.2.3 Fungal Cell Wall

The cell wall is the outermost structure of the fungal cell which acts as the interface between the fungi and its environment. The cell wall is one of the key organelles in fungi that has several major functions. The fungal wall is a complex and rigid structure that supports the underlying protoplast from a variety of environmental stresses including toxic chemicals and changes in osmotic pressure.[21,27] Fungal cell

extension happens at the apex where the cell wall is viscoelastic.[29] As growth continues, fungal cells change rigidity and develop wall structure.[27] The structure and composition of the wall depends on the different phases of a species life cycle.[27] As an example, spore walls are thicker than the growing hyphal walls.[27] During the process of conversion of the viscoelastic to a rigid and mature wall, cell components are added to the wall structure and covalent bonds created among these components by exploitation of the enzymes exist in the wall.[29] The cell wall makes a barrier for molecules moving into or out of the fungal cells. There are some secreted enzymes in the structure of the wall or in the periplasmic area that do not pass throughout the wall.[30] For instance, some lytic enzymes including invertases break the nutrients into small molecules,[21] while other lytic enzymes like cellulase pass throughout the wall into the medium, perhaps from the porous wall of the hyphal tip.[21] The cell wall connects the cells with their surroundings and facilitates the adhesion of cells to hosts, substrates or other cells. In addition, it acts as a signaling center by triggering intracellular signal transduction pathways.[2,4] Cell wall damage can have a great impact on the fungal cell growth and structure, resulting in cell lysis and death.[4] Due to critical functions of the cell wall in the processes of fungal cell growth and development, it is essential to have a better knowledge about the cell wall and the creation of its components.[31]

1.2.4 Fungal Cell Wall Composition

Electron microscopy has revealed that the fungal plasma membrane is enclosed by electron-dense materials in layers of different thicknesses.[27] In some cases (e.g. spore walls), it is easy to correlate specific components to distinct layers, but, in hyphal cells, the layers are combined to make one structure.[21] The wall is thinner and more flexible at

the tip (primary wall) compared to the rigid wall in distal regions (secondary wall).[27] Chemical examination of the fungal cell wall showed that polysaccharides, proteins, and lipids are the main components while pigments are minor wall components.[29] Figure 1.3. shows a schematic of a fungal cell wall.

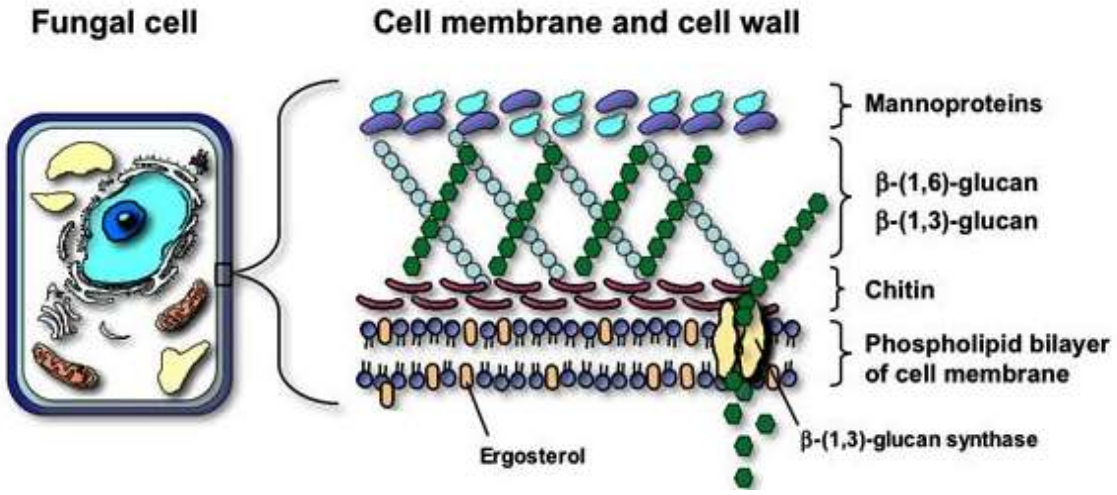

Figure 1.3. Schematic of fungal cell wall. Reprint and permission.[32]

Polysaccharides including chitin, chitosan, and glucans form the inner layer of the fungal wall. Chitin is a linear polymer of β (1,4)-linked of *N*-acetyl glucosamine. Chains of polysaccharide are linked by hydrogen bonds to make microfibrils. Chitin's unique molecular conformation provides strong rigid structure and mechanical strength.[21] Chitin microfibrils are the most internal segment of the wall and located near the plasma membrane.[2,21] Chitin synthesis occurs by chitin synthases which is a basic plasma membrane enzyme. This enzyme catalyzes glycosidic bond creation from uridine diphosphate (UDP)-*N*-acetyl glucosamine to produce a chain of chitin.[4] Chitosan is a polymer of β (1,4)-linked of glucosamine. Glucans are polymers of glucose units that are connected through a variety of bond linking. They could be classified as α-glucans

(glucose units are connected via an α-1,3-bond) and β-glucans (glucose units are linked by two different linkages, β-1,3-glucans or β-1,6-glucans).[29] Although β-1,3-glucans are the main components of the cell wall,[4] but they may exist intracellular or be exuded to the growth medium.[29] β-1,3-glucans are attached covalently with chitin and other cell wall structures.[4] It has been reported that β-1,6-glucans are not present in the cell walls of filamentous fungi such as *A. fumigatus.*[33] Like chitin, glucans are created on the plasma membrane.[4]

Mannoproteins, galactomannoproteins and xylomannoproteins are the main glycoproteins present in fungal walls.[21] Carbohydrate (mannan) binds to proteins in two forms; short chains of mannose O-linked to serine or threonine residues and long chains of mannose N-linked to asparagines.[29] Some cell wall proteins break down large molecules into small molecules providing cell nutrients,[34] while others are responsible for synthesis of wall components, interaction between the cell with its surroundings and facilitating absorption of molecules.[4,29] Most glycoproteins are created in the cytoplasmic secretory pathway. Primary synthesis occurs in the ER and the final glycosation process takes place through the Golgi vesicles.[29]

Lipids such as triglycerides, sterol and phospholipids are present in the cell walls of fungi.[29] Most of the lipids are covalently bonded to other cell wall components. Lipids give the cell wall a hydrophobic character and preserve it from drying out.[29] For some fungal species, cell wall lipids also participate in adhesion, protection, and signaling.[35]

Melanins and carotenoids are the two main pigments present in the fungal cell wall.[29] Melanins are dark pigments that originate from phenolic metabolites such as tyrosine.[21] They are located in the wall of spores and vegetative hyphae.[36] Sporopollenin

is a class of aromatic polymer that is present in the wall of many fungal spores.[36] Cell wall pigments give mechanical strength to the cell wall and protect the cells from environmental pressures including ultraviolet light, extreme dryness, and enzymatic lysis.[37]

1.2.5 Techniques Used to Study Fungi

There is an increasing demand to explore rapid and reliable detection and identification techniques of fungi particularly in the presence of mycotoxins. Several phenotypic and genotypic methods have been used for identification of fungi. Phenotypic methods are dependent on nutritional and physiological characteristics of fungi and morphology of the fruit body.[38] The drawbacks of these methods comprise low sensitivity and lengthy data process.[39] Genotypic techniques are based on molecular biological techniques such as amplified fragment length polymorphism (AFLP)[40] and polymerase chain reaction (PCR) of DNA.[41,42] Although, genetic analyses are fast and reproducible, they are high-priced and require skilled personnel.[43] Thus, there is a crucial need to introduce alternative new techniques for examination of fungi. Chromatographic approaches such as gas chromatography (GC) and gas chromatography-mass spectrometry (GC-MS) provide separation and identities of many of fungal components.[44] These techniques are destructive and not useful for analyzing the spatial distribution of the cellular components in regard to their location within the cell. The distribution of one or a few components may be examined with fluorescence labelling techniques.[45] High spatial resolution examination including scanning electron microscopy and atomic force microscopy are used to probe the fungal cell surface, without chemical component information.[46]

Vibrational spectroscopic methods, such as Fourier transform infrared (FTIR) and Raman spectroscopy as well as Surface Enhanced Raman Scattering (SERS) have been known as sensitive, accurate and rapid methods for recognition of fungi. These non-invasive techniques require minimum sample preparation with no chemical pretreatment and provide a highly specific spectroscopic fingerprint of biochemical composition of each fungus.[47-49] In addition, they allow the determination of spatial differentiation of cellular composition on a length scale of a few microns.[49,50-52]

The use of FTIR for fungal analyses has been explored since Michell & Scurfield published their work in 1967. In recent years, several studies have applied FTIR spectroscopy for rapid differentiation, classification and detection of fungi.[47, 53-55] FTIR microscopy provides sample molecular structure analysis with a high spatial resolution (≤ 10 μm).

Raman spectroscopy is a suitable technique to examine biological samples or to monitor living organisms because in contrast to IR absorption spectroscopy, it has narrow spectral bandwidths and low water background.[56] Raman measurements can be used for the analysis of aqueous samples. In combination with a microscope, Raman microscopy offers spatial resolution in the range of 1-2 μm that allows the possibility to identification of cellular and subcellular structures inside fungal cells with a size of 1-15 μm in diameter.[57] During recent years, Raman spectroscopy has been used ever more for detection of fungi and fungal spores.[47,48,58-60]

Surface enhanced Raman spectroscopy (SERS) is a sensitive, selective and high spatial resolution method that offers a considerable enhancement of Raman signal intensity of a molecule that is in close vicinity to a suitable metal substrate. SERS

substrates could be either noble metal colloids or metallic nanopatterned surfaces.[61] SERS is an excellent spectroscopic technique for the study of microbial cells. SERS has been extensively used for the study of bacterial cells.[62-64] To date few manuscripts have been published using the SERS for analysis of yeast and fungal cells.[52,56, 65]

1.3 Principles of Vibrational Spectroscopy

Vibrational spectroscopy is used to study molecular vibrations. It involves several different techniques mainly infrared (IR) and Raman spectroscopy. Both IR and Raman spectroscopy offer complete chemical information for classification and detection of molecular structure of systems.

1.3.1 Electromagnetic Radiation

Electromagnetic radiation is defined by its wavelength, λ, frequency, ν, and wavenumber $\bar{\nu}$. These parameters are related by the following relationship:

$$\bar{\nu} = \frac{1}{\lambda} = \frac{\nu}{c} \tag{1.1}$$

where c is the speed of light. In quantum theory, radiation is produced by a source in discrete units termed photons. Photon energy is given by:

$$E = h\nu \tag{1.2}$$

where h is the Planck's constant ($h = 6.626 \times 10^{-34}$ J s).

1.3.2 Molecular Vibration

Every molecule has 3N degrees of freedom (N is the number of atoms in the molecule). Three of these degrees are translation and three denote rotations. The remaining degrees of freedom offer a non-linear molecule 3N-6 vibrational motions.

1.3.3 Classical Harmonic Oscillator

A vibrating molecule describes with a diatomic molecule with two masses m_A and m_B that are coupled by a spring. The restoring force *F* describes by Hook's law:

$$F = -\frac{dV(x)}{x} = -kx \tag{1.3}$$

Where V is the potential energy, *k* is the force constant of the spring, and *x* is the displacement of each mass from equilibrium. Integration results

$$V(x) = \frac{1}{2}kx^2 \tag{1.4}$$

A plot of the change in potential energy of a harmonic oscillator as a function of X (interatomic distance) is symmetric about the equilibrium interatomic distance (X_e) and shown in Figure 1.4.

The classical vibrational frequency (ν) for a diatomic molecule is determined by the reduced mass and the force constant of the bond and described as:

$$\nu = \frac{1}{2\pi}\sqrt{\frac{k}{\mu}} \tag{1.5}$$

In this expression, μ is the reduced mass and is based on the individual atoms in the bond. The reduced mass (μ) is defined as:

$$\frac{1}{\mu} = \frac{1}{m_A} + \frac{1}{m_B} \tag{1.6}$$

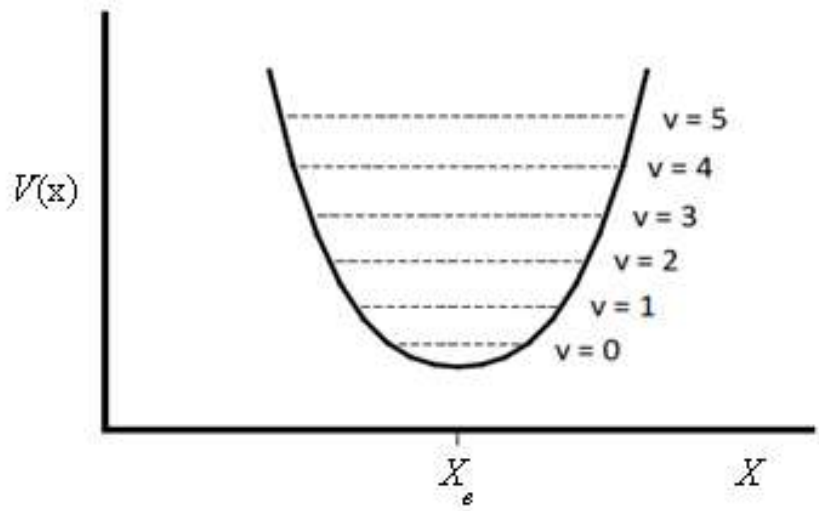

Figure 1.4: Potential energy, *V(x)*, versus interatomic distance *(X)* for a diatomic harmonic oscillator. *Xe* is the equilibrium bond length and dotted lines show vibrational energy levels of quantum number v.

1.3.4 Quantum Mechanical Harmonic Oscillator

Based on quantum mechanics, molecules are in definite quantized energy levels. In harmonic potentials, energy level given by

$$E_i = \left(V_i + \frac{1}{2}\right) h\nu \tag{1.7}$$

where h is Planck's constant, ν is the vibrational frequency of the oscillator and V_i is the vibrational quantum number. In the harmonic oscillator model, only transitions to adjacent levels, $\Delta V = \pm 1$, are allowed. Therefore, the harmonic oscillator is only accurate for low vibrational quantum numbers. A more realistic approach for higher vibrational quantum numbers is anharmonic oscillator approximation which predicts the dissociation energy and shown in Figure 1.5. In anharmonic oscillator, increase in the vibrational quantum number results greater deviation from harmonic oscillation. At higher vibrational levels, adjacent levels separation becomes smaller until the dissociation limit is reached and the bond breaks.

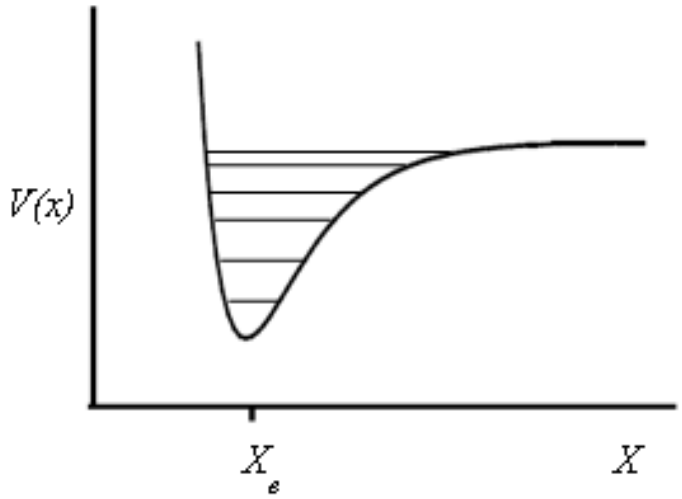

Figure 1.5: Potential energy, *V(x)*, versus interatomic distance *(X)* for a diatomic anharmonic oscillator. The equilibrium bond length is marked by *Xe*.

1.4 Raman Spectroscopy

Raman spectroscopy is an effective spectroscopic method for recognition of molecules which depends on the inelastic scattering of light through the interaction of molecules with an incident laser light. It was first predicted by Smekal in 1923 and then demonstrated in 1928 by Raman and Krishnan. The weak Raman effect has experienced growth and widening of interest due to use of the laser as a monochromatic light source as well as advances in detector (CCD) and filter. These technical advances make Raman as an appropriate method to a variety of research fields including geology, chemistry, biology, pharmaceutics and forensics. Raman spectroscopy is among the best choices for on-site and *in-vivo* examination, due to its non-destructive character and great potential to provide molecular composition at a micrometer scale, and high tolerance for aqueous samples.

1.4.1 Theory of Raman Spectroscopy

When a monochromatic light interact with a molecule, a portion is elastically scattered with similar frequency as the incident photons known as Rayleigh scattering. Smaller portion (1 photon in 10^7) of light will be scattered inelastically known as Raman scattering resulting in either frequencies or higher frequencies than the incident light.[66]

1.4.2 Quantum Description of Raman Spectroscopy

Quantum theory explains the relationship between molecular properties and Raman scattering. The simplest way of describing the scattering phenomenon is an energy exchange between the scattering molecule and the incident light. Rayleigh and Raman are processes and their energy diagram is shown in Figure 1.6.

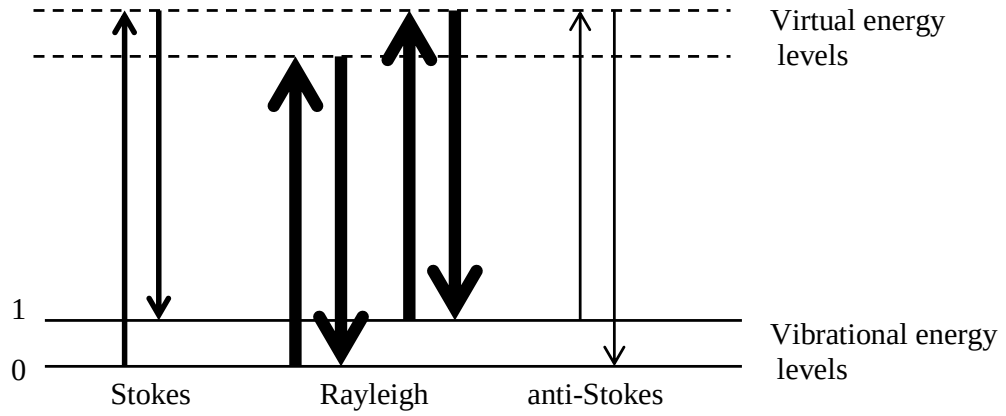

Figure 1.6: Energy diagram of Rayleigh and Raman scattering process.

In Rayleigh scattering, the incident photon absorbed by a transition from a ground vibrational energy level to a virtual state (a non- stable, short-lived energy level lower in energy than the first electronic excited state) and a new photon is generated and scattered when a photon goes back to the ground vibrational energy level resulting in no energy exchange. In Stokes Raman scattering, the incident photon absorbed by a transition from

a ground vibrational energy level (v=0) to a virtual state and a new photon is scattered when a photon returns back to the excited vibrational energy level. In this process, energy is transferred from the photon to the molecule, so it causes a shift of the scattered photon to lower energy and frequency. In anti-Stokes Raman scattering, the incident photon absorbed by a transition from an excited vibrational energy level (v=1) to a virtual state and a scattered photon generates from a transition from the virtual state back to the ground vibrational energy level. In this case, energy is shifted from the molecule to the photon, causing a shift of the scattered photon to higher energy and frequency. The inelastic scattering are described by Eqs. (1.8) and (1.9):

$$hc\bar{\nu} = hc(\bar{\nu} - \bar{\nu}_m) = hc\bar{\nu}_m, \text{ Stokes scattering} \quad (1.8)$$

$$hc\bar{\nu} + hc\bar{\nu}_m = hc(\bar{\nu} + \bar{\nu}_m), \text{ anti-Stokes scattering} \quad (1.9)$$

In these equations, h is Planck's constant, c the velocity of light, $\bar{\nu}$ and $\bar{\nu}_m$ is as the wavenumber (cm^{-1}) of the incident radiation and the Raman shift (energy difference between the lowest and first excited vibrational levels) respectively. Raman shift in wavenumber (cm^{-1}) is determined as,

$$\bar{\nu}_m = \frac{1}{\lambda_{inc}} - \frac{1}{\lambda_{sc}} \quad (1.10)$$

Where λ_{inc} and λ_{sc} are incident and Raman scattered photon wavelengths (in cm) respectively. At ambient temperature, the majority of the molecules are in the ground vibrational state. Therefore Stokes scattering is more severe than anti-Stokes.[66-68]

1.4.3 Classical Description of Raman Spectroscopy

The classical theory is the most basic explanation of Raman spectroscopy and is dependent on the wave nature of light and the interaction between a molecule's electron

cloud and the electromagnetic radiation. The oscillating electric field strength (E) of incident light (laser beam) changes with time is given by

$$E = E_0 \cos 2\pi\nu_0 t \quad (1.11)$$

Where E_0 is the maximum amplitude and ν_0 is the frequency of the incident laser light. The electromagnetic field slightly alters the distribution of electrons and an electric dipole moment P is induced:

$$P = \alpha E = \alpha\, E_0 \cos 2\pi\nu_0 t \quad (1.12)$$

Here α is the polarizability of the molecule. The induced dipole moment happens due to molecular polarizability. The nuclear displacement (q) for a vibrating molecule with a given frequency is:

$$q = q_0 \cos 2\pi\nu_m t \quad (1.13)$$

Where q_0 is the vibrational amplitude. When q is small, α varies linearly with vibration of the molecule. Hence:

$$\alpha = \alpha_0 + \left(\frac{\partial\alpha}{\partial q}\right)_0 q_0 + \cdots \quad (1.14)$$

Where α_0 is the polarisability at an equilibrium position and creates elastic scattering, and $\left(\frac{\partial\alpha}{\partial q}\right)_0$ is change of α regarding to the change in q at this point that produces inelastic scattering. Combining the previous three equations, dipole moment P can be written as:

$$P = \alpha\, E_0 \cos 2\pi\nu_0 t + \frac{1}{2}\left(\frac{\partial\alpha}{\partial q}\right)_0 q_0 E_0[\cos\{2\pi(\nu_0 + \nu_m)t\} + \cos\{2\pi(\nu_0 - \nu_m)t\}] \quad (1.15)$$

The first expression is Rayleigh scattering that occurs with a frequency similar to the incident light ν_0 . The second term represents the Raman scattering, Stokes and anti-Stokes, with frequencies $\nu_0 - \nu_m$ and $\nu_0 + \nu_m$ respectively. The vibration is not Raman-

active when $\left(\frac{\partial \alpha}{\partial q}\right)_0$ is zero. Thus, in Raman scattering, the molecular selection defines the polarizability must change during the molecular vibration.

Figure 1.7 displays the reaction of a non-polar diatomic molecule when an electric field exist. When the oscillating electric field of the incident radiation interacts with a molecule, it will force the charged particles of the molecule to move. Thus, the outer electrons are attracted to the positively charged plate, whereas the negatively charged plate attracts the nuclei. This charge separation results in an induced dipole moment.[68]

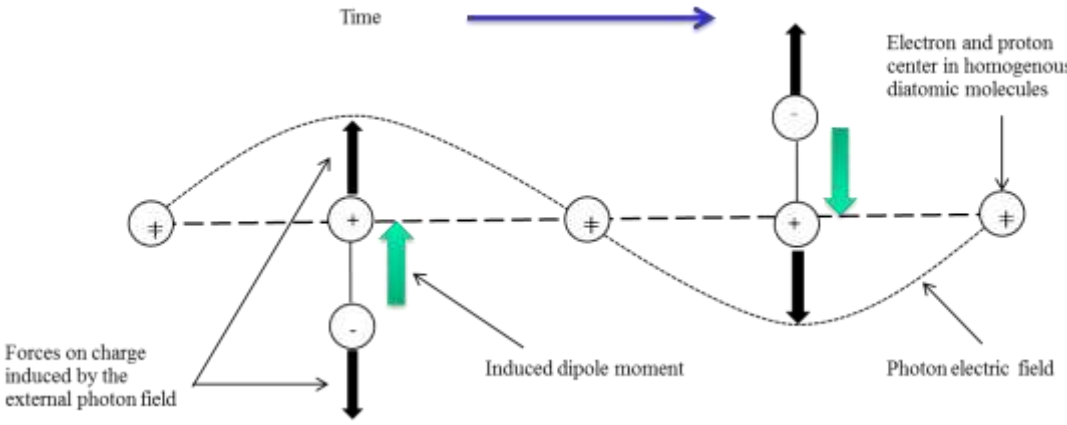

Figure 1.7: Induced dipole moment of a non-polar diatomic molecule results from the oscillating electric field of the incident light.

The intensity of Raman scattered light I_{NRS} observed at $\nu_0 \mp \nu_m$ is given by:

$$I_{NRS} = N(\nu_0 \mp \nu_m)^4 I_0 \left(\frac{\partial \alpha}{\partial q}\right)^2 \quad (1.16)$$

Where N is the number of molecules, I_0 is the intensity of incident light of frequency ν_0, and ν_m expresses the Raman shift. The $\left(\frac{\partial \alpha}{\partial q}\right)^2$ is the change in polarisability of the molecule during vibration. This formula denotes that the intensity of Raman scattering is

proportional to the fourth power of the frequency of ν_0 of the scattered light $\mp \nu_m$ (expresses the ν^4 rule), intensity of the incident light I_0 and the square of the change in molecule polarizability.[67,69]

Raman productivity of a scatterer is indicated by its cross section, σ, which is based on $\left(\frac{\partial \alpha}{\partial q}\right)$. The cross section can be defined as "the probability of an incident photon being scattered as a Raman shifted photon".[69,70] The sample cross section is one of the major factors that influences the intensity of Raman scattering.

1.4.4 Instrumentation of Raman Spectroscopy

A Raman instrument consists of an excitation source, spectrometer, detector, and collection optics.

1.4.5 Excitation Source

Since Raman spectroscopy measures a shift in wavelength, it is important to use a monochromatic excitation source such as a laser. The best lasers for using in Raman spectroscopy are the ones with clean, narrow bandwidth, stable frequency and no mode hop. The quality of the Raman peaks is directly altered by stability and sharpness and of the excitation source.

The question in deciding the proper laser wavelength for particular experiments is whether or not the sample fluoresces. The NIR lasers emit at high wavenumbers which are utilized to diminish the fluorescence effect for samples with high fluorescence probability. The two most common NIR lasers are diode laser with line in the region of 780 nm and Nd:YAG laser that provides 1064 nm line. For weakly fluoresce samples,

high power lasers, such as Ar^+, He-Ne or Kr^+ lasers that provide the lines in the range of 470-650 nm are preferred.[69]

1.4.6 Spectrometer

A spectrometer measures the scattered signal intensity versus the Raman shift. Dispersive and non-dispersive are the two main types of spectrometers. In dispersive spectrometers, a grating diffracts the scattered light on a multichannel detector. The dispersive spectrometers may employ a 420 to 785 nm laser excitation. Sensitivity (high S/N ratio) is the main advantage of these spectrometers which offers to use lower laser power. Non dispersive Raman spectrometers employs an interferometer and uses a Fourier Transform program to generate the spectrum.[69,71] Since dispersive instrument was used in this work, discussion is only limited to this approach.

The dispersive spectrometer is supplied with entrance and exit slits, collecting mirror, exit focusing mirror, and three different diffraction gratings of 1200, 1800, and 2400 grooves/mm. The scattered light is diffracted into its different wavelengths at different angles by diffraction grating. A single monochromator requires the use of a holographic notch filter for selective rejection of the photons before they moved into the spectrometer. The notch filter blocks the signals below 200 cm^{-1} and Raman signal cannot be measured in this range.[69,70,72]

1.4.7 Raman Microscopy

Raman microscopy offers coupling a microscope to a Raman spectrometer with 180º orientation of the laser beam along the microscope optical axis. Raman microscopy is well suited for microanalysis and enables the user to examine extremely small samples and therefore, to distinguish small amounts of material. The technique provides the

capability to obtain Raman spectra with 1μm spatial resolution. Raman mapping and imaging of the sample can be facilitated by the use of automated stages.

Raman microscope contains an optical microscope with excitation and collection optical paths. The excitation optical path contains optics to sharpen the line shape of the laser beam and direct it into the microscope. The laser spot is focused on the specimen with one of the 4 different microscope objectives (5, 20, 50, 100x). Then, the scattered light is collected at 180º from the specimen. A notch filter is utilized to filter out the Rayleigh scattered light before the light enters the spectrometer. A diffraction grating disperses the Raman scattered light and sends it to a CCD detector to be read out by a computer. To collect the spectrum in an extended scan, the diffraction grating position is automatically changed to get each portion of the spectrum.

Point-by-point mapping and line scanning are the two most common methods used for collecting a Raman map. In the first method, the laser is point focused, and the position of the sample under test is moved using an *x-y* automated stage regarding to the laser focus to examine various regions of the sample. It involves collecting a Raman spectrum for each pixel of the image therefore, this method requires a long time to obtain a Raman map. In line scanning, the laser is stationary and is focused on a line, and the sample is moved beneath it. Multiple spectra are collected along the line simultaneously. Then, the measurement time to obtain these spectra is significantly shorter than the first method.[72,73]

1.4.8 Raman Scattering vs. Fluorescence

One problem in utilizing Raman-based technologies is the interference of strong background, mostly fluorescence background. Fluorescence is usually ~ 10^3 and ~ 10^{11} -

times stronger than resonant and non-resonant Raman scattering respectively. The fluorescence background originates from samples with fluorophores such as fluorescent molecules.[74]

One way to decrease fluorescence background is to use NIR laser excitation. As stated earlier, the intensity of Raman scattering is proportional to the fourth power of incident light frequency. Then, by using a short wavelength laser (UV laser), the intensity of Raman signal is improved and better signal-to-noise ratio (SNR) provided, while UV laser due to its high energy could damage the sample.

The NIR lasers are usually utilized for examination of biological systems (e.g., microorganisms, cells, tissues, animal and human bodies). In this case, fluorescence is decreased and there is smaller risk of sample damage. However, such lasers use lower energy photons compared to visible excitation and provide poorer Raman signal. Near IR lasers have the advantage of providing low energy photons that cause minimal damage to the sample (fluorescence). Furthermore, NIR lasers are capable of providing sub-surface spectra as these wavelengths can penetrate living tissues to depths of > 1cm.

1.5 Surfaced Enhanced Raman Scattering

In spite of its many advantages, Raman scattering is a weak and inefficient technique with small scattering cross sections, since, a small fraction (only 1 in every 10^6-10^8) of photons are inelastically scattered. Therefore, elevated laser power and lengthy signal collection are required. Impurities and weakly fluorescent molecules can also dominate the spectrum and affect sensitivity of the Raman signal detection. These limitations can be overcome by a more sensitive technique called Surface Enhanced Raman scattering (SERS). SERS phenomenon enhances the Raman cross section of the

molecules by a factor of 10^6-10^8 or higher when the analyte is in close vicinity to an appropriate roughened surface of a suitable metal.[61]

Surface enhanced Raman scattering was first discovered in 1974 by Fleischman and his coworkers,[75] who observed enhanced Raman scattering from pyridine placed on an electrochemically roughened silver electrode. They ascribed this discovery to an increase in the electrode surface area. In 1977, two groups independently noted that the huge intensity (10^6) from the roughening of the surface was not a result of increase in surface area (less than a factor of 10) and each group suggested a mechanism. Jeanmarie and Van Duyne confirmed the Raman scattering enhancement and attributed it to an electromagnetic (EM) enhancement effect.[76] Later, Albrecht and Creighton suggested a chemical or charge-transfer (CT) effect for the enhancement.[77] This huge signal enhancement makes SERS a sensitive and selective technique that provides information in areas such as bioanalysis and nanotechnology.

Silver and gold are the most effective metals have SERS effect. Other metals including copper, palladium, platinum, sodium, and lithium have also been shown to be good SERS substrates.[78,79]

1.5.1 Theory

Metal surfaces are covered with electrons. Electron density of metals expands with a significant distance from the surface and electrons freely move along the surface. When incident light interacts with surface electrons, they start to oscillate across the surface and oscillations are called surface plasmons. Surface plasmons could be either from the thin metal films with propagating plasmons, known as surface plasmon polaritons or from metallic nanostructures with the localized surface plasmon resonance

(LSPR). In localized surface plasmon, incident radiation interacts with small particles (particle diameters are less than the incident wavelength) and it generates an oscillating plasmon all around the surface of the particle (Figure 1.8).[80]

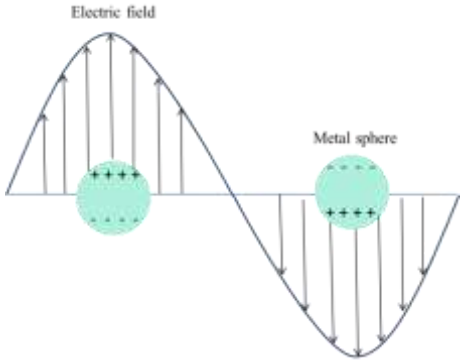

Figure 1.8: Schematic diagram displaying a localized surface Plasmon.

The resonance frequency is varied with the metal type and the nature of the surface. The reasons that gold and silver used as SERS-active substrates are due to their relative stability and resonance plasmon frequencies in the visible region. Metals can both absorb and scatter the light and the ratio depends on the metal type. Silver known to have the greatest enhancement at mid-visible wavelengths where its localized surface plasmon exists. Gold has the advantages of greater stability and bio compatibility with many molecules and provides enhancement at near-IR wavelengths that is suitable for biological applications. The dielectric constant of the metal can be described as real and imaginary parts which are linked to the absorption and scattering respectively. Metals with a negative real and small positive imaginary dielectric constant can yield a surface plasmon resonance (SPR). On a smooth surface, oscillation is along the plane of the surface because electrons are bound to the surface. Therefore, absorption of light occurs but light will not be scattered. For scattering, it is necessary to have an oscillation perpendicular to the surface plane which occurs by roughening the surface. Also, the

nature of the surface roughness is crucial. When there is a range of surface roughness with various dimensions, the plasmon of the surface shows a broad range of wavelengths. While for mono-dispersed colloids, the range of the absorption frequencies is much narrower expressing a better surface roughness.[69,71] The enhancement achieved by SERS is not dispersed evenly over the metallic surface generating some spatially localized parts with enhancement up to $\sim 10^{14}$ called 'hot-spots'.[81,82]

The surface enhanced Stokes Raman signal in SERS (I_{SERS}) is proportional to the number of involved molecules in SERS (N_{SERS}), the intensity of incident light (I_0) of frequency ν_0, the Raman cross section of adsorbed molecules ($\sigma \frac{R}{ads}$) and the electromagnetic enhancement of the electric fields for both the incident A_{ν_0} and scattered A_{ν_s} frequency.[83]

$$I_{SERS} = N_{SERS} I_0 \left|A_{\nu_0}\right|^2 \left|A_{\nu_s}\right|^2 \sigma \frac{R}{ads} \tag{1.17}$$

1.5.2 Electromagnetic Enhancement (EM)

In EM enhancement, the analyte is in close vicinity to the metal surface or is adsorbed onto the metal and an interaction take place between the molecules adsorbed on the roughened surface and the plasmons. When incident light illuminates a roughened surface, an energy shift from the plasmon to the molecule occurs followed by production of an electric field enhancement and finally a Raman process.[69]

The simplest illustration model of electromagnetic SERS is dependent on a small metallic sphere at a distance d from a molecule that is subjected to an incident electromagnetic field (E_0) from the laser (Figure 1.9).

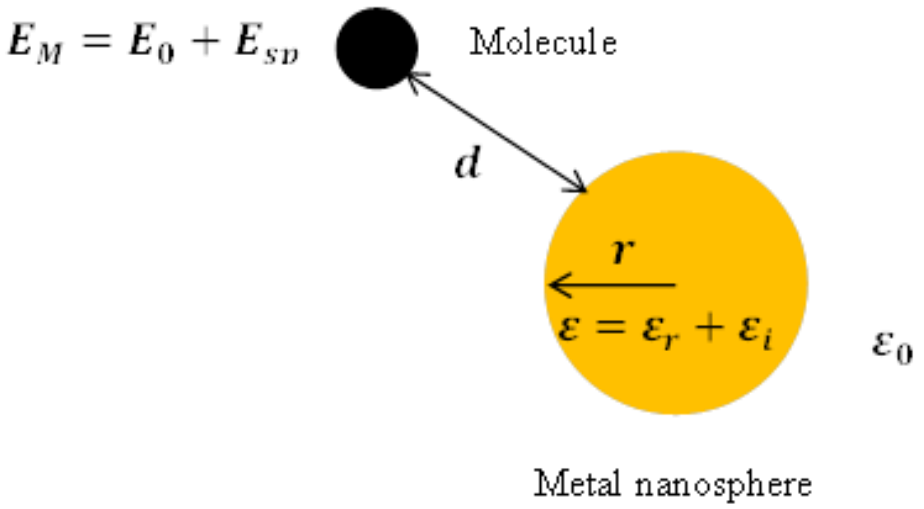

Figure 1.9: Schematic diagram of electromagnetic SERS effect.

The incident field induces a dipole moment in the metal nanosphere with E_{sp} electric field. The experienced field by the molecule E_M is:

$$E_M = E_0 + E_{sp} \tag{1.18}$$

The induced dipole moment in the metal nanosphere is:

$$E_{sp} = r^3 \frac{\varepsilon - \varepsilon_0}{\varepsilon + 2\varepsilon_0} E_0 \frac{1}{(r+d)^3} \tag{1.19}$$

ε_0 and ε are the dielectric constants of the medium surrounding the metal nanosphere and of the metal nanosphere respectively. The diameter of the sphere 2r is estimated to be much smaller than the wavelength of light λ ($2r \ll \lambda$). ε_0 is usually close to 1 and large enhancements are obtained when the real part of the dielectric constant (ε_r) is equal to -2ε_0, and the imaginary part of the dielectric constant (ε_i) is small. At this point, a maximum local field is experienced by the molecule adsorbed on the metal nanosphere surface.[71]

This experienced enhancement field is expressed as the field enhancement factor $A(\nu)$ and is described as the ratio of the field when the molecule is in the proximity of a metal nanosphere and the incident electric field.

$$A(\nu) = \frac{E_M(\nu)}{E_0(\nu)} \sim \frac{\varepsilon - \varepsilon_0}{\varepsilon + 2\varepsilon_0} \frac{r^3}{(r+d)^3} \tag{1.20}$$

The scattered field also will be improved when it is in resonance with the metal nanosphere surface plasmons.[84] The total electromagnetic enhancement factor $G_{em}(\nu_s)$ which is the combination of enhancement factors of both the incident $|A(\nu_0)|^2$and the Raman scattered $|A(\nu_s)|^2$ fields is given by:

$$G_{em}(\nu_s) = |A(\nu_0)|^2 |A(\nu_s)|^2 \sim \left|\frac{\varepsilon(\nu_0) - \varepsilon_0}{\varepsilon(\nu_0) + 2\varepsilon_0}\right|^2 \left|\frac{\varepsilon(\nu_s) - \varepsilon_0}{\varepsilon(\nu_s) + 2\varepsilon_0}\right|^2 \left(\frac{r}{(r+d)}\right)^{12} \tag{1.21}$$

Therefore, when the excitation and scattered fields are in resonance with the surface plasmons, the Raman signal is strong and rises to the fourth power of the local field of the metal nanosphere.[84,85] For the electromagnetic enhancement, it is not essential to have a direct contact between molecule and metal. Based on the Eq. 1.21, the enhancement field is inversely proportional to $\left(1/d\right)^{12}$ and for $d > r$, the magnitude of the SERS enhancement decreases when molecule is distanced from the metal surface.[86]

1.5.3 Chemical Enhancement

The chemical effect is based on the charge transfer mechanisms due to the electron pairing between the molecule and the metal and can be described by two observations. The first observation requires direct contact between the molecule and metal surface known as first layer effect. The interaction between metal electrons and adsorbate molecules involves in the creation of a bond between the analyte and the metal surface. The electron wave functions of the metal and adsorbate molecule overlap

resulting in the charge transfer from the metal to the molecule and back to the metal again.[71] There is a significant increase in the polarizability of the molecule upon interaction with electrons of the metal. Based on the first observation, chemical enhancement occurs via presence of new electronic states due to chemisorption (formation of bond between the metal and molecule).[71] It is believed that these new states serve as resonant intermediates in Raman scattering.[71] The second observation is explained the electronic levels in the absorbed molecule being shifted and broadened compared with free molecule due to its interaction with the metal surface.[87]

1.5.4 SERS Active Substrates

Successful fabrication of the SERS substrates is essential due to the fact that SERS applications depend on the activity and reproducibility of the substrate. SERS substrates can be classified as: 1) Metallic nanoparticles in solution, such as metal colloidal solutions, 2) planar metallic structures, like arrays of metallic nanoparticles maintained on a planar substrate (glass, silicon, metals) and 3) metal electrodes.[88] Among SERS substrates, metallic nanoparticles different shapes and sizes fabricated by wet chemical methods are the most used SERS substrates. These classes of SERS substrates are very useful due to their low cost and easy preparation compared to the other two classes. The most common types of metallic colloids are silver and gold colloids, and are mainly made by reduction of salts with organic agents or by laser ablation. Reduction of salts usually occurs when a stabilizing agent is present which coats the colloids surface and prevents them to form aggregation.[88] Therefore, these colloids are stable for longer time compared to non-coated colloids.[88,89] Planar metallic structures can be created simply by drying colloidal solutions on underlying substrates such as silicon or glass, or

by roughening metallic surfaces. A novel method to produce highly ordered planar SERS substrates is self-organization like patterning through nano-lithography and island lithography techniques. These techniques provide good control over the homogeneity and geometry of the patterned elements and therefore, better control of their plasmon resonances.[88,89]

1.6 Introduction to Nanomaterials

Metallic nanoparticles were first studied by Michael Faraday in 1857. He was the first synthesized colloidal gold solutions and discovered the red color in stained glass was as a result of small size of gold particles. These solutions are still on display in the British Museum in London. [90] Nanotechnology is the engineering of matter on an atomic and molecular scale. Nanoparticles are defined as particles with size ranging from 1-100 nm (Figure 1.10).

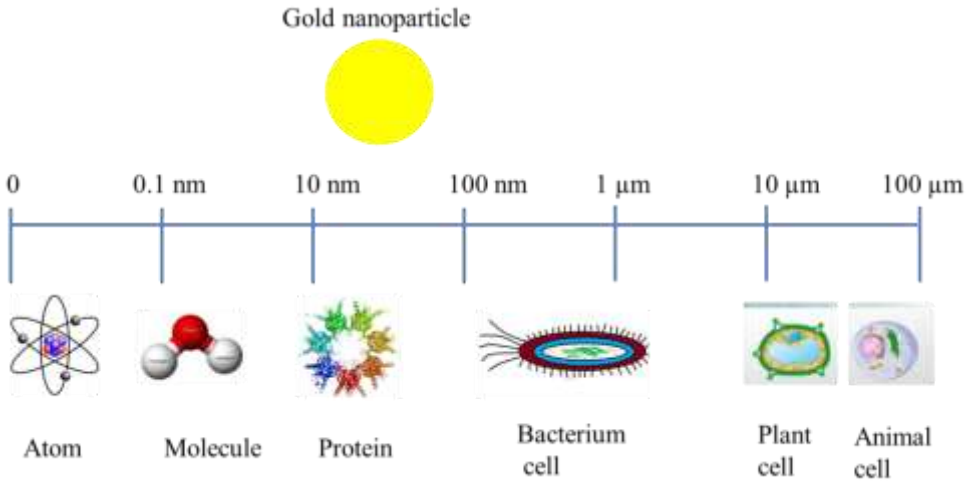

Figure 1.10: The comparison of the size of metal nanoparticle with other biological objects.

Nanoparticles exhibit size-related properties (electronic, optical, magnetic and catalytic) which are different from those observed in both the constituent atoms or molecules and the bulk counterparts. The unique properties of nanoparticles are due to

their large surface to volume properties as well as their (excitation) wavelength to particle radius. Optical properties of metal nanoparticles are due to their unique interaction with light and depend on the shape, size, and the dielectric constant of the surrounding medium.[91] Localized surface plasmon resonance generate optical properties of metal nanoparticles. In general, when the incident electromagnetic radiation interacts with particles much larger than the incident wavelength, the plasmon oscillates around the metal nanoparticle known as localized surface plasmon resonance (LSPR).[80] For noble metals, such as Au, Ag, and Cu nanoparticles, the surface plasmon resonance occurs in the visible frequency region. Surface plasmon absorption band for gold and silver nanoparticle with the diameter between 50-100 nm is around 520 and 390 nm respectively. As the nanoparticle size increases (the number of electrons increases) and reaches the wavelength of light, the plasmon band is broadened and red-shifted due to the size dispersion of the colloidal nanoparticles.[92]

There are two approaches to the synthesis of nanomaterials: top-down and bottom-up. The top-down method requires breaking down bulk material into nanosized particles; for example, by film deposition and growth, lithographic techniques, laser-beam processing and mechanical techniques. In the bottom-up method, small building blocks are brought together to make larger assemblies. Chemical synthesis for the synthesis of nanoparticles is a good example of a bottom-up approach. Very fine features and state-of-the-art structures are provided by the bottom-up approach.[93,94] Recently biogenic synthesis of nanoparticles by using biological cells such as bacteria, fungi, and lichens attracts more attention. This technique provides an eco-friendly approach, as no toxic chemical and elevated temperature is involved.[95]

1.7 Infrared Spectroscopy

Infrared (IR) spectroscopy is the study of the interaction of infrared light with matter. Infrared spectroscopy may be used to determine the functional groups in a molecule.

1.7.1 Attenuated Total Reflectance (ATR)

Attenuated total reflectance (ATR) is a widely used FTIR sampling technique utilizing an internal reflection element (ATR crystal of a high refractive index) that is in direct contact with the sample (Figure 1.11). Total internal reflectance occurs when an incident beam penetrating the ATR crystal which has greater angle of incidence compared to the critical angle. The incident radiation field penetrates further than the surface of the ATR crystal into the sample where it loses some of its energy due to sample adsorption.[68]

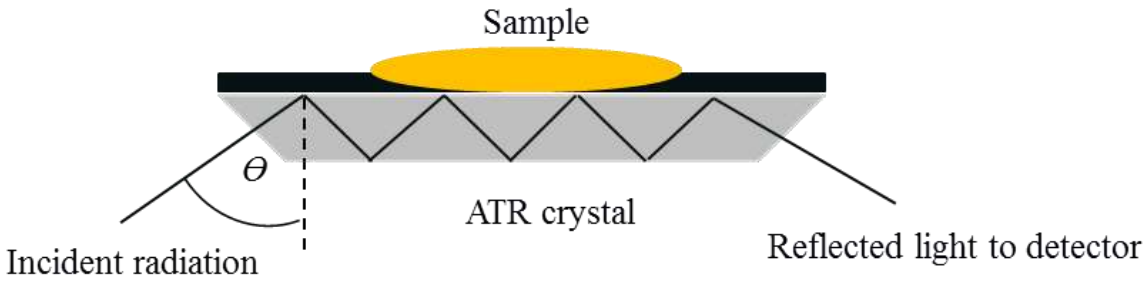

Figure 1.11: Schematic of attenuated total reflectance.

In ATR, the depth of penetration, d_p, depends on the wavelength, λ, the refractive indices of the sample and the crystal, n_1 and n_2, and the incident angle of radiation, θ (Eq. 1.28).

$$d_p = (\lambda/n_1)\,/\{2\pi[\sin\theta - (n_1/n_2)^2]^{1/2}\} \qquad (1.28)$$

Zinc Selenide (ZnSe) and Germanium are the most commonly used materials used in ATR cells.[96]

1.7.2 Infrared Analysis of Biological Samples

Infrared spectroscopy is an efficient molecular structure method for the study of biological systems, including animal and plant tissues, microorganisms, clinical samples, and food. Water, lipids, proteins, carbohydrates and nucleic acids are present in all of the biological systems.[97] Vibrational spectra provide specific molecular information about the biochemical structure. Infrared bands can be narrow (1-2 cm^{-1}) when they are due to vibration of a specific chemical bond in the molecule.[98] Broad band absorption occurs when there are many functional groups with overlapping peaks. An IR spectrum of a fungal spore is shown in Figure 1.12.

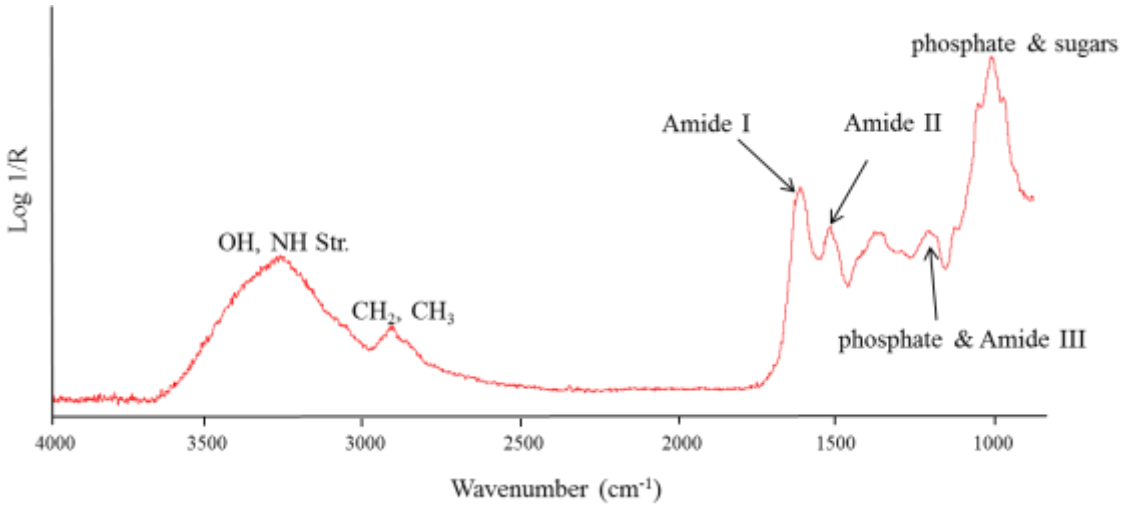

Figure 1.12: FTIR-ATR spectrum of *A. nidulan*s fungal spore. The spectrum shows absorption bands for the functional groups found in biological samples.

In FTIR spectra, lipids mainly contribute to C-H stretching vibrations. The lipid contents can be found at 2956 cm^{-1} (asymmetric stretching vibration of CH_3 of acyl chains), 2922 cm^{-1} (asymmetric stretching vibration of CH_2 of acyl chains), 2874 cm^{-1}

(symmetric stretching vibration of CH_3 of acyl chains), 2852 cm^{-1} (symmetric stretching vibration of CH_2 of acyl chains), and 1600–1800 cm^{-1} (C=O stretching vibrations of the ester functional groups in phospholipids). Biological samples display three absorbance bands which attributed to the amide bonds of protein as: the amide I, resulting from C=O stretching vibration at 1650 cm^{-1}, the amide II arising N-H bending vibration coupled to C-N stretching at 1500-1600 cm^{-1}, and the amide III from C-N stretching and N-H in plane bending at 1220-1350 cm^{-1}. Bands at 1220–1240 cm^{-1} and 1040–1100 cm^{-1} have been assigned to asymmetric and symmetric stretching vibrations of P=O in nucleic acids (DNA, RNA) and phosphodiesters. Carbohydrates and other phosphates can be found around 1117 cm^{-1} (C-O stretching vibration of C-OH group of ribose) and 1050–70 cm^{-1} (C-O-C ring vibrations). Table 1.1 shows a complete assignment of the IR bands of biological systems.[48,98-100]

Table1.1: Assignment of IR bands of biological systems.

Wavenumber (cm^{-1})	Assignment
3200-3100	υ OH, NH
2958-2954	υ_{asym} CH_3
2930-2918	υ_{asym} CH_2
2876-2870	υ_{sym} CH_3
2854-2850	υ_{sym} CH_2
1750-1735	υ C=O fatty acid ester
1690-1610	υ C=O (amide I)
1600-1500	υ CN; δ NH (amide II)
1350-1220	υ CN; δ NH (amide III)
1240-1220	υ_{asym} P=O
1100-1075	υ_{sym} P=O
1200-900	υ CO
1070-1050	δ COC

υ= stretching, δ= deformation

1.8 Goals of the Thesis

In this thesis, *Aspergillus nidulans* are investigated at the molecular level using FTIR, Raman, and SERS microscopy. These techniques have the advantage of preserving sample integrity while providing detailed chemical information at the micrometer scale which is not easy to obtain by other approaches.[60]

The overall objective of this research is to study fungal cell and cell wall components by utilization of synthesized gold nanoparticle (AuNP) as SERS substrates. The specific goals of this project are:

Goal 1: Synthesize stable AuNP with appropriate size and shape to employ as SERS substrates to study the cellular composition of *A. nidulans* hyphal cell.

Goal 2: Develop methodology for reproducible SERS spectra of cell wall components from synthesized AuNP.

Goal 3: Apply the use of AuNP and SERS to investigate chemical composition of other strains of *A. nidulans*.

In order to achieve the goals described above, two methods for synthesis of AuNP were used. In one method, the capability of fungal cells to create NPs and the use of these particles as SERS substrates was examined to study fungal cell and cell wall components. Details of this method are provided in chapter 2. In the second method, AuNPs were synthesized separately by addition of monosodium glutamate (MSG) to $HAuCl_4$ solution. These NPs showed a good stability over time, through the presence of a persistent Surface Plasmon Resonance (SPR) band. The NP-containing solution was then added to the fungal colonies and fungal cell components were investigated by SERS microscopy. A summary of the *A. nidulans* (AAE1 and ugmA) SERS results from these

preparations are discussed in chapter 3. Although the work described in this thesis mainly focuses on SERS studies of *A. nidulans* hyphae, several Raman, SERS and FTIR-ATR spectra of *A. nidulans* conidia were also acquired and presented in chapter 4.

1.9 References

1. J. E. Galagan, M. R. Henn, L. Ma, C.A. Cuomo, B. Birren, *Genom Res*, 2005, 15, 1620-1631.

2. S. M, Levitz, *PLoS Pathog*, 2010, 6, e1000758.

3. R. Tada, J. P. Latge, V. Aimanianda, *Curr Pharm Des*, 2013, 19, 3738-3747.

4. S. M. Bowman, S. J. Free, *BioEssays*, 2006, 28, 799–808.

5. S. Bartnicki-Garcia, *Annu Rev Microbiol*, 1968, 22, 87-108.

6. L. V. Madden, M. Wheelis, *Annu Rev Phytopathol*, 2003, 41, 155-176.

7. M. N. Swartz, *Proc Natl Acad Sci*,1994, 91, 2420-2427.

8. E. J. Dasbach, G. M, Davies, S. M. Teutsch, *Clin Infect Dis*, 2000, 31, 1524-1528.

9. O. Gudlaugsson, S. Gillespie, K. Lee, J. Vande Berg, J. Hu, S. Messer, L. Herwaldt, M. Pfaller, D. Diekema, *Clin Infect Dis*, 2003, 37, 1172-1177.

10. D. L. Hawksworth, *Mycol Res*,1991, 95, 641-655.

11. D. L. Hawksworth, P. M. Kirk, B. C. Sutton, D. N. Pegler. Ainsworth and Bisby's Dictionary of the Fungi. Wallingford : CAB International, 1995.

12. M. Buckley. The fungal kingdom:diverse and essential roles in earth's ecosystem. Washington : American Academy of Microbiology, 2008.

13. J. Piskur, E. Rozpedowska, S. Polakova, A. Merico, C. Compagno, *Trends Genet*, 2006, 22, 183-186.

14. H. G. Schlegel. General Microbiology. Cambridge : Cambridge University Press, 1993.

15. A. A. Brakhage, P. Sprote, Q. Al-Abdallah, A. Gehrke, H. Plattner, A. Tuncher, *Advances Biochem Eng Biotechnol*, 2004, 88, 45–90.

16. G. M. Gadd. Fungi in Bioremediation. Cambridge : Cambridge University Press, 2001.

17. J. E. Galagan et al. *Nature*, 2005, 438, 1105-1115.

18. J. W. Deacon. Modern Mycology. Oxford : Blackwell Science, 1997.

19. S. L. Stephenson. The Kingdom Fungi: The Biology of Mushrooms, Molds, and Lichens. Cambridge : Timber Press, 2010.

20. D. H. Griffin. Fungal Physiology. New York : Wiley-Liss, 1994.

21. N. A. R. Gow, G. M. Gadd. The growing fungus. Oxford : Chapman & Hall, 1995.

22. S. D. Harris, *Mycologia*, 2008, 100, 823-832.

23. L. J. McKerracher, I. B. Health, *Exp Mycol*,1987, 11, 79-100.

24. P. G. Markham, *Mycol Res*, 1994, 98, 1089–1106.

25. S. Bloemendal, U. Kuck, *Naturwissenschaften*, 2013, 100, 3–19.

26. D. H. Jennings, G. Lysek. Fungal Biology: Understanding the Fungal Lifestyle. New York : Springer, 1999.

27. S. Isaac. Fungal-plant interactions. Cambridge : Chapman & Hall, 1992.

28. F. J. Alvarez, L. M. Douglas, J. B. Konopka, *Eukaryot Cell*, 2007, 6, 755-763.

29. J. Ruiz-Herrera. Fungal cell wall: Structure, synthesis, and assembly. New York : Taylor & Francis group, 2012.

30. P. J. Kuhn, A. P. J. Trinci, M. J. Jung, J. W. Gooday, L.C. Copping. Biochemistry of cell walls and membranes of fungi. Berlin : Springer-Verlag, 1989, 5-30.

31. D. K. Arora, P. D. Bridge, D. Bhatnagar. Handbook of fungal biotechnology. New York : Marcel Dekker Inc., 2004, 1-8.

32. M. H. Kirsch**,** doctor fungus, http://www.doctorfungus.org/thedrugs/antif_pharm.php.

33. T. Fontaine, C. Simenel, G. Dubreucq, O. Adam, M. Delepierre, J. Lemoine, C. E. Vorgias, M. Diaquin, J. Latge, *J Biol Chem*, 2000, 275, 27594–27607.

34. D. Adams, *Microbiology*, 2004, 150, 2029-2035.

35. C. Mille, J. Janbon, F. Delplace, S. Ibata-Ombetta, C. Gaillardin, G. Strecker, T. Jouault, P. A. Trinel, D. Poulain, *J Biol Chem*, 2004, 279, 47952-47960.

36. G. Turian, H. R. Hohl. The Fungal Spore: Morphogenetic Controls. New York : Academic Press, 1981.

37. H. M. Wheeler, A. A. Bell, *Curr Top Med Mycol*, 1988, 2, 338-387.

38. P. R. Murray, E. J. Baron, M. A. Pfaller, F. C. Tenover, R. H. Yolken. Manual of clinical microbiology. Washington : ASM Press, 1999, 193-201.

39. V. Shapaval, J. Schmitt, T. Moretro, H.P. Suso, I. Skaar, A.W. Asli, D. Lillehaug, A. Kohler, *J Appl Microbiol*, 2012, 114, 788-796.

40. S. Rosendahl, J. W. Taylor, *Mol Ecol*, 1997, 9, 821–829.

41. M. A. Pfaller, *Emerg Infect Dis*, 2001, 7, 312-318.

42. K. A. Haynes, T. J. Westerneng, J. W. Fell, W. Moens, *J Med Vet Mycol*, 1996, 33, 319-325.

43. S. R. Jordan, R. Limburn, C. Baylis. Fungal forensics: an evaluation of three commercial identification and characterisation systems. UK: Campden : BRI, 2010.
44. I. Brondz, K. Hoiland, D. Ekeberg, *J Chromatogr B*, 2004, 800, 303-307.
45. S. G. W. Kaminskyj, *Fungal Genet Biol*, 2000, 31, 105-113.
46. S. G. W. Kaminskyj, T. E. S. Dahs, *Micron*, 2008, 39, 349-361.
47. K. Maquelin, C. Kirschner, L. P. Choo-Smith, N. A. Ngo-Thi, T. van Vreeswijk, M. Stammler, H. P. Endtz, H. A. Bruining, D. Naumann, G. J. Puppels, *J Clin Microbiol*, 2003, 1, 324-329.
48. M. Harz, P. Rosch, J. Popp, *Cytome Part A*, 2009, 75A, 104-113.
49. K. Maquelin, L. P. Choo-Smith, C. Kirschner, N. Ngo-Thi, D. Naumann, G. J. Pupples. Handbook of Vibrational Spectroscopy. Chichester : John Wiley, 2002, 3308-3334.
50. K. Jilkine, K. M. Gough, R. Julian, S. G. W. Kaminskyj, *J Inorg Biochem*, 2008, 102, 540-546.
51. S. G. W. Kaminskyj , K. Jilkine, A. Szeghalmi, K. M. Gough, *FEMS Microbiol Lett*, 2008, 284, 1-8.
52. A. Szeghalmi, S. G. W. Kaminskyj, P. Rosch, J. Popp, K. M. Gough, *J Phys Chem B*, 2007, 111, 12916-12924.
53. D. Naumann, D. Helm, H. Labischinski, *Nature*, 1991, 351, 81-82.
54. G. Fischer, S. Braun, R. Thissen, W. Dott, *J Microbiol Methods*, 2006, 64, 63-77.
55. A. Naumann, *Analyst*, 2009, 6, 1215-1223.
56. R. Petry, M. Schmitt , J. Popp, *ChemPhysChem*, 2003, 4, 14-30.
57. L. Baia, K. Gigant, U. Posset, G. Schottner, W. Kiefer, J. Popp, *Appl Spectrosc*, 2002, 56, 536-540.
58. K. De Gussem, P. Vandenabeele, A. Verbeken, L. Moens, *Spectrochim Acta A*, 2005, 61, 2896-2908.
59. K. De Gussem, P.Vandenabeele, A.Verbeken, L. Moens, *Anal Bioanal Chem*, 2007, 387, 2823-2832.
60. S. Ghosal, J. M. Macher, K. Ahmed, *Environ Sci Technol*, 2012, 46, 6088-6095.
61. C. L. Haynes, R. P. Van Duyne, *J Phys Chem B*, 2003, 107, 7426-7433.

62. Z. Xiaoyu, M. A. Young, O. Lyandres, R. P. Van Duyne, *J Am Chem Soc*, 2005, 12, 4484-4489.

63. S. Efrima, L. Zeiri, *J Raman Spectrosc*, 2009, 40, 277-288.

64. R. M. Jarvis, R. Goodacre, *Chem Soc Rev*, 2008, 37, 931-936.

65. M. A. Prusinkiewicz, F. Farazkhorasani, J. J Dynes, J. Wang, K. M. Gough, S. G. W. Kaminskyj, *Analyst*, 2012, 137, 4934-4942.

66. W. R. Browne, J. J. McGarvey, *Coord Chem Rev*, 2007, 251, 454-473.

67. J. R. Ferraro, K. Nakamoto, C. W. Brown. Introductory Raman Spectroscopy. San Diego: Elsevier, 2003.

68. P. J. Larkin. Infrared and Raman spectroscopy: principles and spectral interpretation. s.l. : Elsevier, 2011.

69. S. Sasic. Pharmaceutical applications of Raman spectroscopy. New Jersey : Wiley-interscience, 2008.

70. R. L. McCreery. Raman Spectroscopy for chemical analysis. s.l. : Wiley-interscience, 2000.

71. E. Smith, G. Dent. Modern Raman spectroscopy-A practical approach. Chichester : Wiley-interscience, 2005.

72. P. Matousek, M. Morris. Emerging Raman Applications and Techniques in Biomedical and Pharmaceutical Fields. Berlin : Springer, 2010, 1-24.

73. J. Chan, S. Fore, S. Wachsmann-Hogiu, T. Huser, *Laser & Photon Rev*, 2008, 2, 325-349.

74. H. Kim, K. M. Kosuda, R. P. Van Duyne, P. C. Stair, *Chem Soc Rev*, 2010, 39, 4820-4844.

75. M. Fleischman, P. J. Hendra, A. J. McQuillan, *Chem Phys Lett*, 1974, 26, 163-166.

76. D. L. Jeanmaire, R. P. Van Duyne, *J Electroanal Chem*, 1977, 84, 1-20.

77. M. G. Abrecht, J. A. Creighton, *J Am Chem Soc*, 1977, 99, 5215-5217.

78. J. M. Sanz, D. Ortiz, R. Alcaraz de la Osa, J. M. Saiz, F. González, A. S. Brown, M. Losurdo, H. O. Everitt, F. Moreno, *J Phys Chem C*, 2013, 117, 19606-19615.

79. Z. Q. Tian, B. Ren, D.Y. Wu, *J Phys Chem B*, 2002, 106, 9463-9483.

80. K. Willets, R. P. Van Duyne, *Annu Rev Phys Chem*, 2007, 58, 267-297.

81. C. Farcau, S. Astilean, *J Phys Chem C*, 2010, 114, 11717-11722.

82. K. Kneipp, Y. Wang, H. Kneipp, I. Itzkan, R.R. Dasari, M. S. Feld, *Phys Rev Lett,*1996, 76, 2444-2447.

83. K. Kneipp, I. Kneipp, I. Itzkan, R.R. Dasari , M. S. Feld, *Chem Rev,* 1999, 99, 2957-2976.

84. K. Kneipp, H. Kneipp, I. Itzkan, R. R. Dasari, M. S. Feld, *J Phys Condens Matter,* 2002, 14, R597-R624.

85. C. L. Haynes, A. D. McFarland, R. P. VanDuyne, *Anal Chem,* 2005, 77, 338-346.

86. R. Aroca. Surface-enhanced vibrational spectroscopy. West Sussex : Wiley interscience, 2006.

87. A. Campion, P. Kambhampati, *Chem Soc Rev,* 1998, 27 241-250.

88. E. C. Le Ru, P. G. Etchegion. Principles of Surface-Enhanced Raman Spectroscopy and related plasmonic effects. Oxford : Elsevier, 2009.

89. S. Schlucker. Surface Enhanced Raman spectroscopy: Analytical, biophysical and life science applications. Weinheim : Wiley-vch, 2011, 39-70.

90. P. P. Edwards, J. Meurig Thomas, *Angew Chem Int Ed,* 2007, 46, 5480–5486.

91. M. R. Ivanov, H. R. Bednar, A. J. Haes, *ACS Nano,* 2009, 3, 386–394.

92. M. El-Sayed, S. Link, *Int Rev Phys Chem,* 2000, 19, 409-453.

93. V. Rotello. Nanoparticles: Building Blocks for Nanotechnology. New York : Springer, 2004, 29-85.

94. F. Sanchez, K. Sobolev, *Constr Build Mater,* 2010, 24, 2060-2071.

95. M. Rai, N. Duran. Metal Nanoparticles in Microbiology. New York : Springer, 2011, 1-16.

96. B. Stuart, Infrared Spectroscopy: Fundamentals and Applications. New York : John Wiley & Sons, Ltd, 2004, 16-44.

97. D. Naumann, *Appl Spectrosc Rev,* 2001, 36, 239-298.

98. Z. Movasaghi, S. Rehman, I. U. Rehman, *Appl Spectrosc Rev,* 2008, 43, 134-179.

99. W. Petrich, *Appl Spectrosc Rev,* 2001, 36, 181-237.

100. R. A. Meyers. Encyclopedia of Analytical Chemistry. Chichester : Wiley-interscience, 2000, 102-131.

Chapter 2: SERS Imaging of *Aspergillus nidulans* Hyphae via *In vivo* Synthesis of Gold Nanoparticles

First published in Analyst, 2012, 137, Martin A. Prusinkiewicz*, Fatemeh Farazkhorasani* James J. Dynes, Jian Wang, Kathleen M. Gough, and Susan G. W. Kaminskyj

Author contributions: M. A. P and F. F contributed equally to this work. F. F. prepared samples for white light microscopy, UV-Vis spectroscopy and Raman and SERS measurements. F. F. designed, performed and analyzed the white light microscope images, UV-Vis adsorption, Raman and SERS imaging. F. F. wrote the materials and methods part for UV-Vis spectroscopy, Raman measurement and table contents. F. F. made final changes of all the figures and texts and submitted the manuscript to the Analyst journal. K. M. G and S. G. W. wrote the main manuscript. J. J. D. and J. W. designed, performed, analyzed and wrote the STXM section.

2.1 Introduction

Filamentous fungi including *Aspergillus nidulans* affect humans through their roles in biotechnology and recycling, as well as being agents of disease and decay. The similarities and differences between these metabolic activities will be the key to better exploitation and/or control strategies. High spatial resolution, high sensitivity spectrochemical analysis of hyphal composition[1, 2] was coupled with molecular genetics and microscopy.[3-6] The hypotheses that relate fungal cell structure and function to colony

growth and development, and to fungal interactions with their environment are tested. Together, these methods will enable to assess factors expected to be critical for fungal growth and reproduction. Importantly, they will allow researchers to have a better understanding of fungal responses to stressful environments, such as those created by anti-fungal drugs.

Over the last century, the average human life span in the developed world has increased from 50 to 80 years, mostly due to better public health measures, vaccinations, and antibacterial drugs. Still, millions of people die every year from infections, with systemic fungal infections emerging as being amongst the most dangerous.[7] In the USA in 2008, the cost of treating human fungal diseases was ~ $33 billion.[8] Once a fungal infection has invaded an organ or the bloodstream, a cure means being symptom-free for six months. The risk of infection is unavoidable since there are potentially dangerous airborne spores in every breath we take. Our major defense is our immune system, which is weaker in the young, the old, and the sick. Physiologically, fungi respond to stressful environments by reallocating their internal resources[9,10] and by up regulating their cell wall integrity pathways.[11,12] Fungi can also adapt through mutation.[13]

The use of high spatial resolution spectrochemical methods to study cytoplasm has considerable promise as part of a suite of correlated approaches to elucidate structure and function in hyphal growth processes. For example, infrared spectroscopy, Raman spectroscopy, and Surface Enhanced Raman Scattering (SERS) were used to obtain spatially resolved biochemical information about *Aspergillus nidulans*[9] and *Curvularia protuberata*.[14] SERS, which can be several to many orders of magnitude more sensitive

than Raman spectroscopy,[15-17] has been achieved from hyphae grown across a nanopatterned gold substrate.[18]

Gold nanoparticles (AuNPs) created through the addition of gold chloride ($HAuCl_4$) to liquid growth medium that contained live *A. nidulans* fungal colonies from overnight growth. The shape, size and distribution of AuNPs were characterized using scanning transmission X-ray microscopy (STXM), UV-Vis absorption, fluorescence light microscopy and transmission electron microscopy (TEM). SERS spectra obtained from these samples provide proof-of-principle that these AuNPs are SERS active. Analysis of the results demonstrates the potential for greater control over location and activity.

2.2 Materials and Methods

2.2.1 Gold Nanoparticle (AuNP) Generation in Fungal Cells

The wild type morphology of *A. nidulans* strain AAE1 was maintained as described.[3] For AuNP production spores were germinated in potato dextrose broth (PDB, Difco) adjusted to pH 6.5 with 1 M NaOH. Previously, an initial pH of 6.5 was determined to be optimal for *A. nidulans* culture.[9]

To prepare colonies for fluorescence microscopy, TEM and STXM, ~500 *A. nidulans* spores (10 μL of a 50,000 spore/mL stock, stored in sterilized distilled water for up to 7 d at 4 °C) were added to 0.5 mL PDB in 1.5 mL microfuge tubes. These were sealed with Parafilm®, placed in a 125 mL Erlenmeyer flask, and germinated overnight at 37 °C, with shaking at 270 rpm. The resulting colonies were white, globose, and 1- 2 mm diameter. The precise number of spores was not crucial: due to space constraints, this method produced ~ 10 colonies. Colonies were treated with 0.5 - 5 mM $HAuCl_4$, diluted from a 100 mM aqueous stock solution. PDB does not have substantial buffering

capacity: following germination at pH 6.5, overnight growth of *A. nidulans* acidified PDB to pH 5.5. Addition of 5 mM $HAuCl_4$ further acidified it by up to 2 pH units. To compensate, the initial pH of the PDB was adjusted to 7.5 in subsequent preparations, so that following overnight growth and $HAuCl_4$ addition solution pH was ~ 6. Colonies were treated with $HAuCl_4$ for 150 minutes before harvest and preparation for microscopy, described below.

Colonies for UV-Vis and SERS spectroscopic analysis were grown in a similar manner. Twenty microlitre aliquots of spores, freshly harvested or stored up to 7 days in ultrapure water at 4 °C, were added to 1.5 mL microfuge tubes containing 1.0 mL PDB pH 6.5, and shaken overnight at 37 °C. For 1 mM $HAuCl_4$, 46 μL of 0.5 % $HAuCl_4$ was added; pH was adjusted by addition of 1-2 drops of 0.1 M NaOH, to achieve a pH of ~6. The microfuge tubes were shaken at 37 °C as described above, then removed and stored at 4 °C. To assess hyphal viability, colonies treated with 1 mM or 5 mM $HAuCl_4$ for up to 150 minutes were transferred to potato dextrose agar plates and incubated at 37 °C.

2.2.2 Methods for Characterization of AuNP

Colonies that had been treated with 1 mM and with 5 mM $HAuCl_4$ for 150 minutes were prepared for TEM and STXM as described.[19] Hyphae were fixed in 1 % glutaraldehyde, rinsed 3× in buffer, post-fixed in 1 % osmium tetroxide, dehydrated, and embedded in Epon 812, which was polymerized at 60 °C. Following mounting and trimming, TEM silver sections (~75 nm thick) and STXM gold sections (~100 nm thick) were collected on Formvar-coated single slot copper grids. The pale grey interference colour of these Formvar films indicated a thickness of 60-75 nm.

STXM imaging and spectromicroscopy were carried out at the Canadian Light Source (CLS) SM beamline, 10ID-1. Whole AuNP containing colonies were transferred to Formvar coated Cu EM slot grids. The excess PDB medium was wicked away using a filter paper triangle and the colony was air-dried at room temperature. The Cu grids were attached to an aluminum STXM sample holder, and examined at the C K-edge and Au $M_{4,5}$-edges. For the Au reference, a 5 μL drop of 100 mM $HAuCl_4$ was dried onto part of a 500 nm thick silicon nitride window. Thin sections of hyphae were prepared as for TEM, above. All image and spectral processing was performed with aXis2000 software.[20]

Absorption at the C K-edge was used as a proxy for biological materials. Qualitative carbon maps were obtained from the difference of optical density (OD) images recorded at 288.2 eV (absorption maximum for the C 1s π*C=O protein peak) and 280 eV (baseline before peak onset).[21] The energy scale at the C K-edge was calibrated using the Rydberg peaks of CO_2.

Qualitative Au maps were obtained from the difference of OD images recorded at 2150 eV (below the Au M-edge) and 2370 eV (centre of the $M_{4,5}$-edge peak). Quantitative mapping of Au in whole fungal cells was achieved by spectral fitting of the Au image sequence using a singular value decomposition linear regression procedure.[22] These maps were based on the $HAuCl_4$ reference spectrum, placed on a linear absorbance scale by matching it to the predicted response for the compound based on its elemental composition and density (3.9 g cm^{-3}),[23] and using tabulated continuum absorption coefficients.[24] Transmitted signals (I) were converted to optical densities (OD) [absorbance, OD = -ln (I/I_0)] using the incident flux (I_0) measured through sections

devoid of fungal cells, to correct for absorbance by Formvar and Epon. The absolute energy scale of the Au $M_{4,5}$ edge was set by assigning the onset of the Au M5-edge of $AuCl_3$ to 2206 ± 5 eV.[25]

UV-Vis absorption spectra of liquid from each microfuge tube were acquired with a UV-2101 spectrometer (Shimadzu), from 190 to 900 nm, at 1 nm spectral resolution, against a water blank (Milli Q) in matching 1 cm path-length, 1 mL quartz cuvettes.

Some colonies that had been treated with $HAuCl_4$ were stained with Calcofluor in order to visualize hyphal walls and septa[26] and assess AuNP spatial distribution. Fluorescence images were acquired with a Zeiss AxioImager Z1 equipped with a 63×, N.A. 1.4, Plan Apochromat objective, a light emitting diode at 365 ± 10 nm, and filters for Calcofluor excitation, captured with a Zeiss Axiocam.

For TEM, sections were post-stained with uranyl acetate and lead citrate. In addition, 5 µL samples of the growth medium from AuNP-producing colonies were applied to Formvar coated single-slot Cu grids, air-dried, negative stained with phosphotungstate, and examined. Images were obtained with a Philips CM10 transmission electron microscope operating at 60 kV and captured on X-ray sheet film. Films were digitized at 1200 dpi following development.

2.2.3 SERS Analysis

For SERS, $HAuCl_4$-treated colonies were transferred whole to clean glass microscope slides, then PDB was wicked away with a filter paper triangle. Samples were immediately frozen on a metal shelf at -80 °C for 5 minutes, then air dried at room temperature. A reference Raman spectrum was obtained from a clean glass microscope

slide. For Raman spectroscopy of the growth medium, a drop of PDB was dried onto a gold-coated substrate.

SERS spectra were acquired using a Renishaw inVia Raman microscope, equipped with a high sensitivity, ultra-low noise CCD, and a motorized x-y sample stage for automated mapping. Samples were illuminated with a 785 nm diode laser with a 1200 grooves/mm holographic grating. The Raman spectrometer wavelength was automatically calibrated using the center frequency of the silicon band (520 cm^{-1}) from a silicon reference wafer.

The CCD detector in this instrument can accommodate a spectral width of ~400 cm^{-1} for a given grating position. Extended scan maps were created by collecting data at sequential grating settings to yield a spectrum from 200-1800 cm^{-1} for each pixel, and raster scanning across a predetermined area; exposure times were 1 to 10 s per pixel, with 50× objective and a 785 nm diode laser. The inVia Streamline option, which utilizes a multiplexed line focus illumination method and fast CCD readout, was used to create SERS maps with < 1 s laser exposure per pixel and a single grating setting, providing a 400 cm^{-1} segment of the entire spectrum. Multiple images were acquired sequentially, from overlapping spectral windows, in order to build up the entire spectrum for each map.

2.3 Results

Aspergillus nidulans colonies grown in PDB changed from white to coloured during incubation with $HAuCl_4$ (Figure 2.1). The rate of change as well as the final colour achieved varied with the $HAuCl_4$ concentration and duration of exposure. After 150 minutes at 37 °C, colonies exposed to 1 mM $HAuCl_4$ were pink-purple (Figure

2.1A), whereas those exposed for the same time to 5 mM $HAuCl_4$ were golden (Figure 2.1B). Individual hyphae from the 1 mM $HAuCl_4$ treatment also had a purple hue (Figure 2.1C), but distinct particles were not seen. Large (> 1μm) golden shapes (presumably AuNPs) were detected in the dried medium surrounding the golden colonies from the 5 mM treatment (Figure 2.1D). Identification of these NP as gold and the range of AuNP sizes and shapes were documented with STXM, UV-Vis absorption spectroscopy, fluorescence microscopy and TEM.

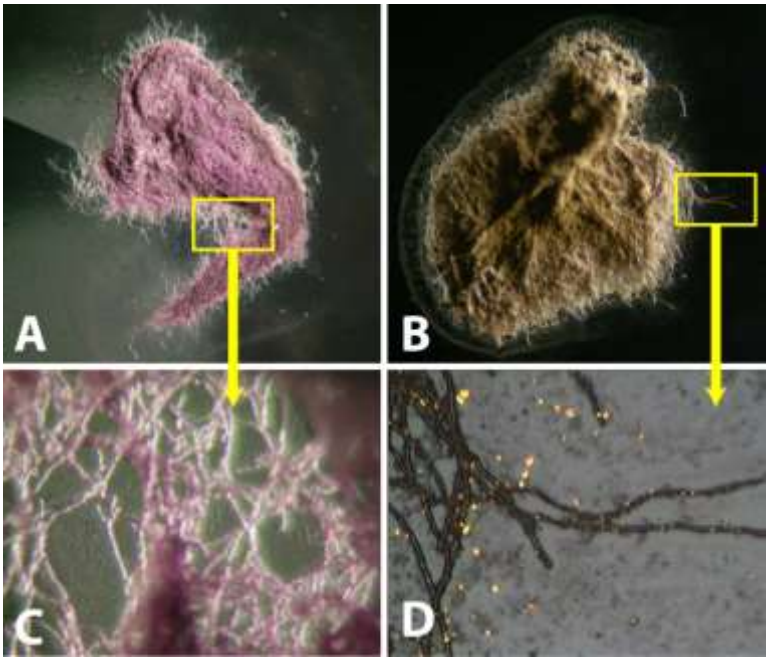

Figure 2.1: *Aspergillus nidulans* colonies incubated for 150 minutes at 37 °C in PDB (A, 4x;C,40x) 1 mM $HAuCl_4$ and (B, 4x;D,40x) 5 mM $HAuCl_4$; colonies were illuminated from above. Pink-purple color in (A, C) is characteristic of 50–70 nm gold nanoparticles (AuNP). Metallic golden color in (B) is characteristic of larger particles, some of which are visible at 40x (D).

Viability studies following AuNP induction showed that peripheral hyphae from *A. nidulans* colonies grown for up to 150 minutes in 1 mM $HAuCl_4$ were able to grow

vigorously and sporulate on PDB solidified with agar. Cultures treated with 5 mM $HAuCl_4$ had reduced viability after 30 minutes.

2.3.1 Characterization of Gold Nanoparticles in *Aspergillus nidulans* Cultures

2.3.1.1 Scanning Transmission X-ray Microscopy

Whole colonies and 100 nm thick TEM sections of *A. nidulans* were examined with STXM (Figure 2.2). The Au $M_{4,5}$-edge spectrum from the reference gold is an excellent match to the spectrum from putative AuNPs in whole hyphae (Figure 2.2A). The latter spectrum was obtained by masking pixels from obvious electron dense NP in the whole *A. nidulans* colonies, and processing as described.[27] Hyphae were visualized from the qualitative image of the C distribution (Figure 2.2B) based on the differences in on- and off-resonance OD maps for the intensity at the $C_{C=O}$ K-edge, a protein-associated signal. A smaller area from this map (red box in Figure 2.2B, magnified in 2.2C) was imaged for C (red) and randomly distributed AuNPs (green). The quantitative spectral fitting procedure for Au was applied to a small region (yellow box in Figure 2.2C). Based on the quantitative fit, the brightest green corresponds to particles that are ~2 μm thick.

STXM maps of 100 nm thick sections of *A. nidulans* hyphae treated with 5 mM $HAuCl_4$ are shown in Figure 2.2D-F. It was not possible to detect a signal at the Au $M_{4,5}$-edge for the STXM sections due to thinness of the material. However, the 280 eV image is below the onset of the C 1s absorption, thus compounds lacking carbon would be structureless at this energy.[21] Because the cross-section for heavy, electron rich elements (i.e., Au) is very high, the Au is expected to be the dominant non-biological heavy

element component of these systems and thus the 280 eV image is ascribed to the spatial distribution of Au. This was confirmed for clusters imaged at the Au $M_{4,5}$-edge spectrum, above (Figure 2.2 C).

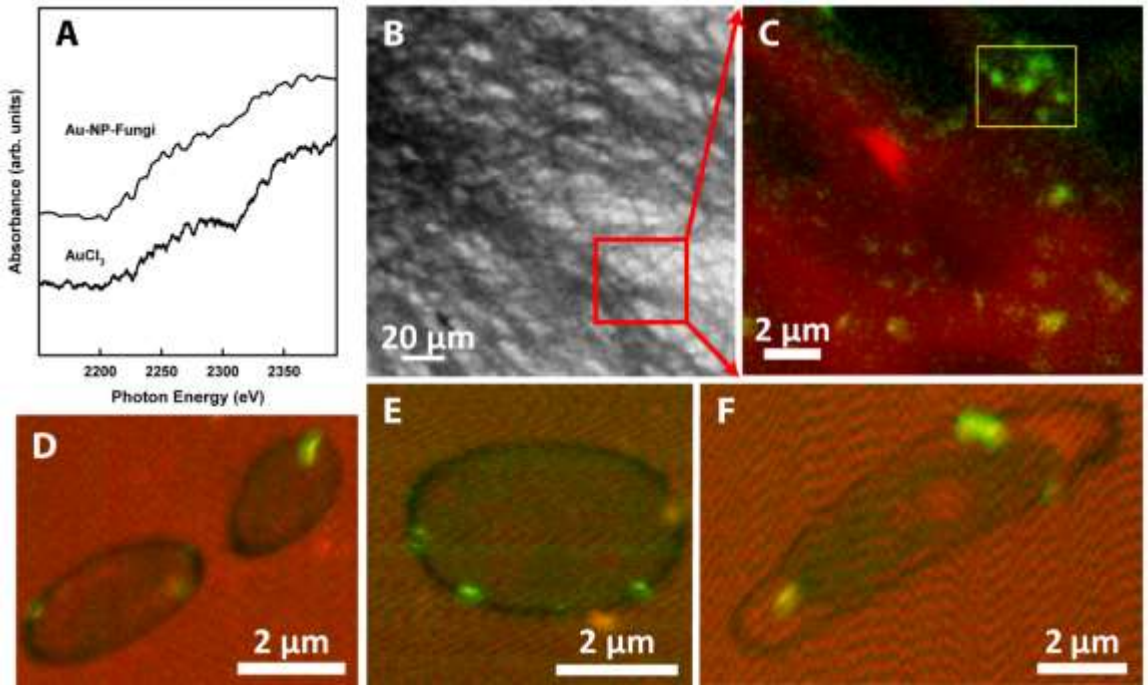

Figure 2.2: STXM analysis of NP produced in *Aspergillus nidulans* following incubation with 5 mM $HAuCl_4$. (A) STXM spectra of NP in whole hyphae and of Au reference in Au $M_{4,5}$ edge region. (B) Intensity at 2150 eV qualitative carbon image, hyphae are grey to black. (C) Expanded from red box in (B), showing carbon (red) and Au (green) in whole hyphae. Yellow box shows where quantitative stack data were acquired. (D–F) Qualitative images from thin sections of hyphae showing carbon (red) and Au (green).

2.3.1.2 UV-Vis Spectroscopy-Absorption and Fluorescence

UV-Vis absorption spectra of growth medium withdrawn from typical overnight colonies, and again following 20 to 200 minutes incubation in 1 mM $HAuCl_4$, are shown in Figure 2.3. The spectra display a strong surface plasmon resonance (SPR) band with a maximum at ~543 nm, attributed to AuNP on the order of 50 -70 nm.[28] Incubation of pure PDB with $HAuCl_4$ showed that the growth medium is also capable of chemical

reduction leading to formation of large AuNP, as evidenced by a broad, low SPR band (maximum at 570 nm, FWHM from 525 to 750 nm) measured after 2 hours incubation. Further experiments using minimal medium for growth are underway, in an effort to limit medium-driven reduction of gold.

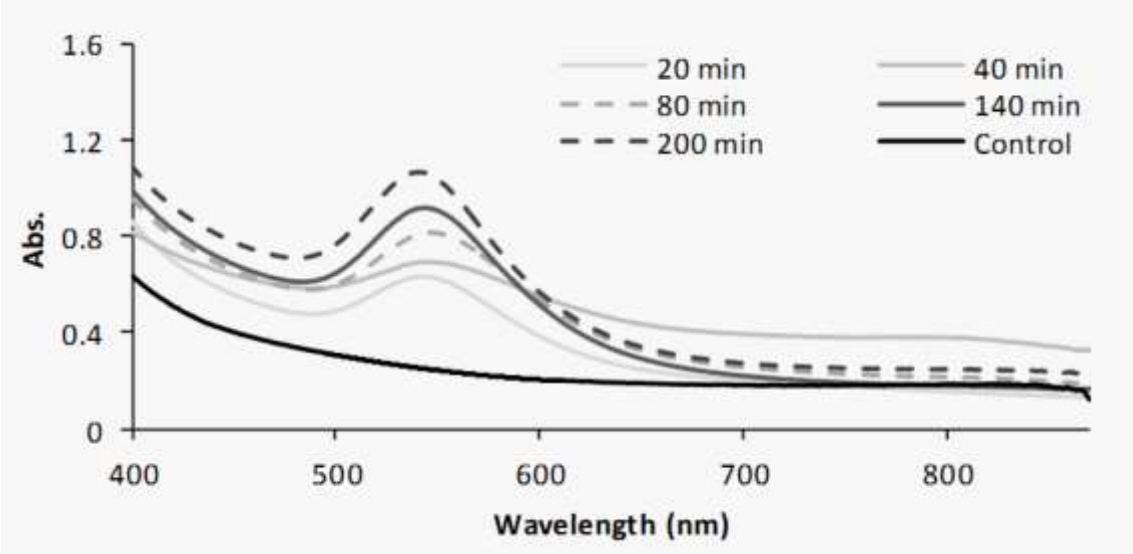

Figure 2.3: UV-Vis absorption spectra of supernatant PDB, extracted from microfuge tubes in which *Aspergillus nidulans* colonies were germinated and incubated with 1 mM $HAuCl_4$; initial pH adjusted to 6.5. Spectra are on a common scale, and are compared to spectrum of broth prior to addition of Au solution (control).

Some *A. nidulans* colonies were stained with Calcofluor for fluorescence imaging of their cell walls and septa, following 150 minutes growth in 1 mM $HAuCl_4$ (Figure 2.4). Dark triangular and irregular hexagonal objects are consistent with the presence of micron-size AuNPs (Figure 2.4).

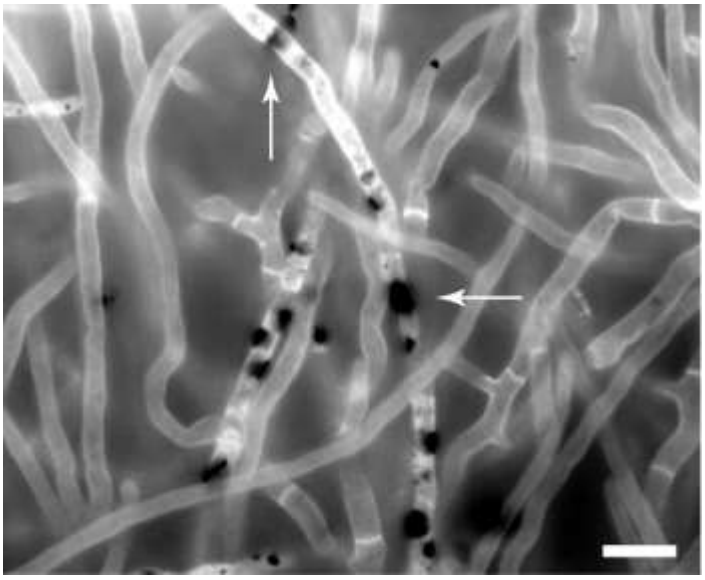

Figure 2.4: *Aspergillus nidulans* hyphae treated with 5 mM $HAuCl_4$ to induce AuNP formation for 150 minutes at 37 C, and stained with Calcofluor to visualize cell walls. Bar = 10 mm. AuNPs appear as black spots, some of which have triangular (vertical arrow) or hexagonal (horizontal arrow) profiles.

2.3.1.3 Transmission Electron Microscopy

Transmission electron micrographs of *A. nidulans* hyphae incubated in $HAuCl_4$ are shown in Figure 2.5. A near-median section of an *A. nidulans* hypha from a colony incubated with 5 mM $HAuCl_4$ (Figure 2.5A-C) shows profiles of large flat AuNPs associated with the cell membrane and with the outer surface of the cell wall (black arrows in Figure 2.5A). Electron-dense objects, tentatively identified as polyhedral AuNPs, were associated with the near-apical Spitzenkörper region (large arrowhead in Figure 5A; higher magnification in Figure 2.5B). Globose AuNPs (small arrowheads in Figure 2.5A) were associated with the peripheral cytoplasm. Tiny (~ 10 nm) electron-dense particles assumed to be AuNPs (white arrows in Figure 2.5B; and in Figure 2.5C) were found throughout the cytoplasm. A TEM cross-section of a hypha from a colony incubated in 1 mM $HAuCl_4$ (Figure 2.5E) contains many tiny ~10 nm particles dispersed

throughout the cytoplasm; however, most of the particles were found as clumps associated with the outer cell wall surface.

2.3.2 Surface Enhanced Raman Scattering Activity

AuNPs associated with *A. nidulans* colonies treated with 0.5 to 5.0 mM $HAuCl_4$ showed SERS activity. Many images were recorded, under different collection parameter settings, with different laser powers and exposure times. Images obtained with the extended scan option permitted collection of the entire spectrum at each pixel in a map. Some spectra from extended scan maps showed intense SERS activity (Figure 2.6); other spectra showed strong graphite peaks that indicated some carbonization due to the longer exposure to the laser, despite the low power.

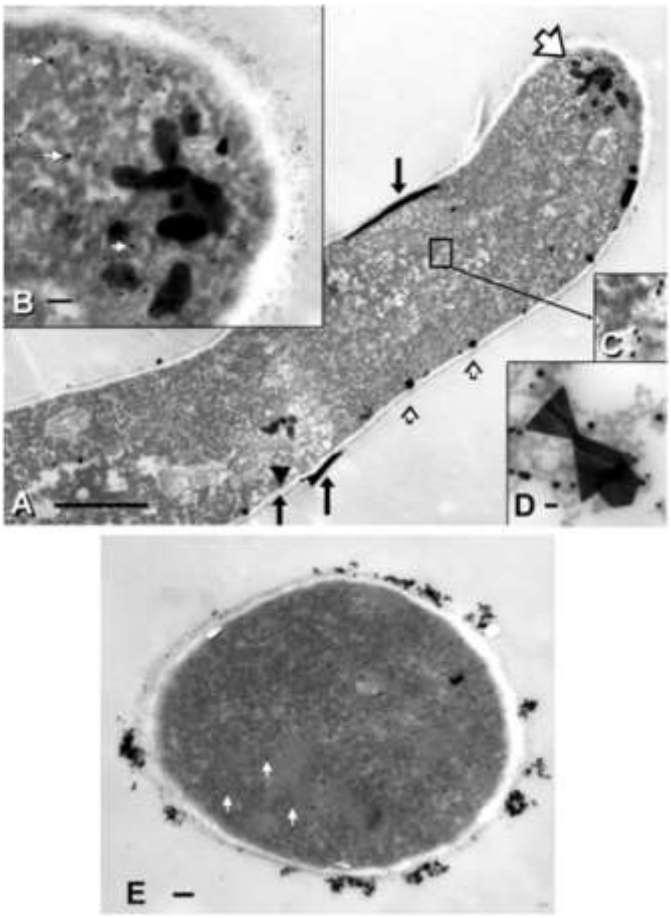

Figure 2.5: Transmission electron micrographs of an *Aspergillus nidulans* hypha (A–C) induced to form AuNP by incubation in 5 mM $HAuCl_4$ for 150 minutes. (D) AuNP formed in conditioned medium containing 5 mM $HAuCl_4$. (E) Cross-section of an *A. nidulans* hypha incubated in 1 mM $HAuCl_4$. Bar in A =1mm; bar in B, D, E= 100 nm, C is same scale. (A–C) Near-median, longitudinal section of an *A. nidulans* hyphal tip with small globose (small arrowheads) and large flat (black arrows) AuNP in the cytoplasm and adjacent to the wall surface. A cluster of polyhedral AuNP (large arrowhead in A; detail in B) formed associated with the Spitzenkörper region at the hyphal tip. Flat AuNP associated with the peripheral cytoplasm and outer wall surface are seen in cross-section. Tiny globose AuNP (white arrows in B, detail in C) are abundant throughout the cytoplasm. (D) AuNP formed in conditioned growth medium containing 5 mM $HAuCl_4$ has characteristic shapes from minute dots to large triangular plates. (E) TEM of an *A. nidulans* hypha induced to form AuNP by incubation in 1 mM $HAuCl_4$ for 150 minutes. The cytoplasm contains tiny 8 to 10 nm AuNPs (white arrows) but most AuNP form clumps on the external surface of the cell wall.

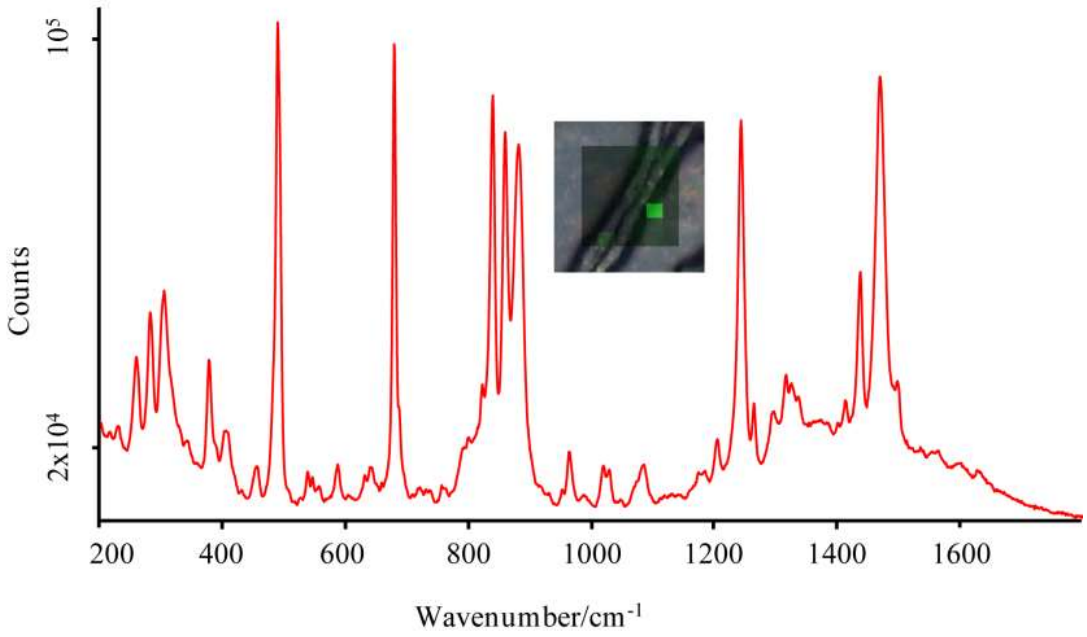

Figure 2.6: Spectrum from extended scan SERS map (green pixel), demonstrating the existence of SERS-active AuNP, generated in a fungal colony incubated for 2 h in PDB with 0.5 mM $HAuCl_4$, pH 4.5. SERS was excited at 785 nm with laser power of 1% (6–10 mW) and exposure time 10 s.

Rapid scan images (80 to 300 ms per pixel) were acquired with the Streamline option, which limited the spectral range to a single segment of ~400 cm^{-1}. In these cases, a complete spectrum was constructed by mapping the same sample area multiple times at different grating positions, with overlapping segments for each spectral range. Images showing *A. nidulans* hyphae and locations with SERS activity are shown in Figure 2.7. The reconstructed Streamline spectrum of a clean glass substrate is shown for comparison (Figure 2.7, spectrum 1). Several hyphae lie flat on the glass slide, at the periphery of the dried colony (Figure 2.7A). Weak fluorescence from these hyphae elevates the baseline relative to surrounding glass substrate, revealing their outline (Figure 2.7B, spectra 2 and 3). Several SERS active spots were found in this small area; at least one was possibly associated with a hypha. Reconstructed complete spectra are

taken from points that illustrate both reproducibility and variability in such images (Figure 2.7C, spectra 4 and 5). The extended scan Raman spectrum of PDB on gold-coated substrate is shown below (Figure 2.7, spectrum 6).

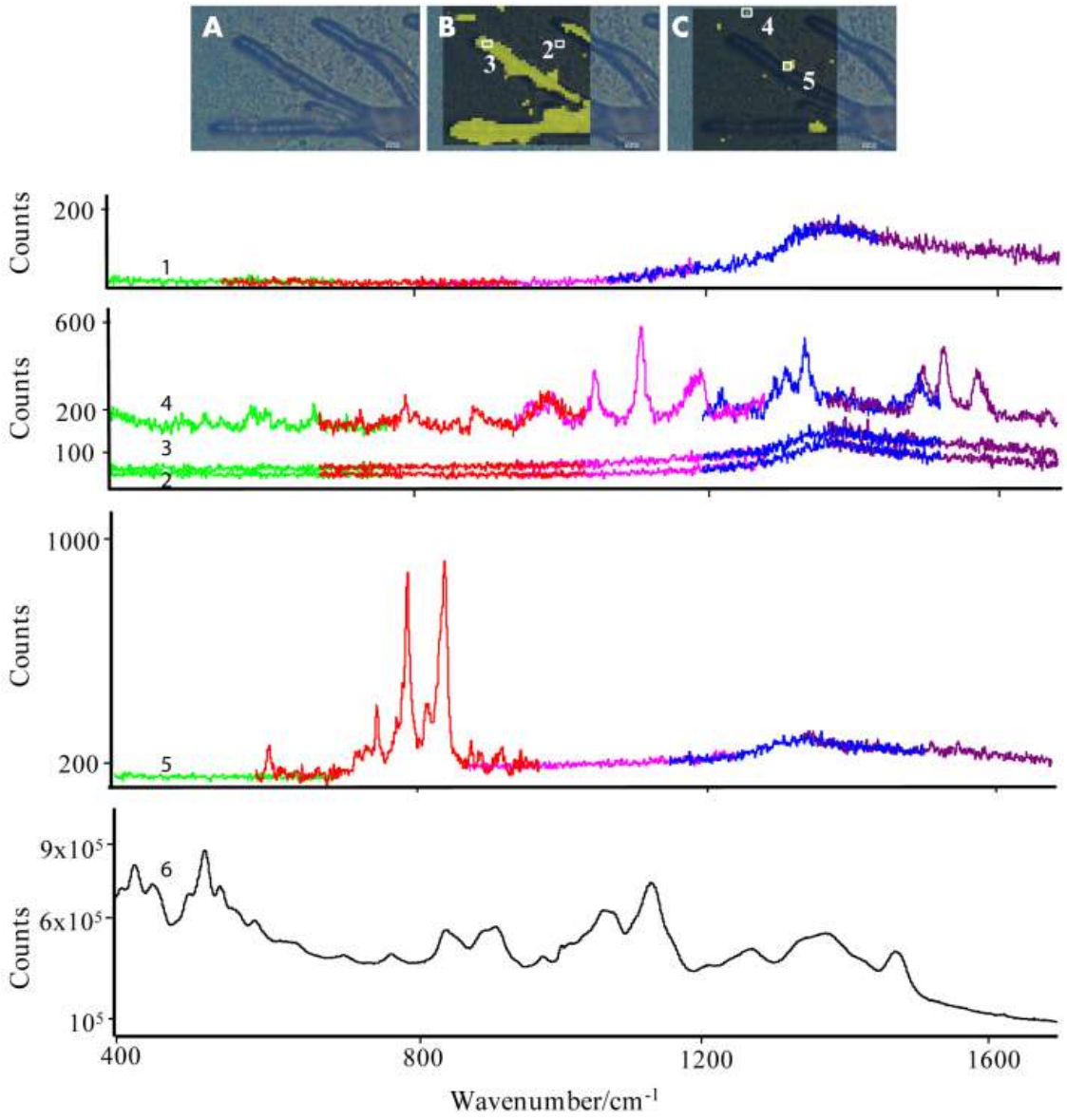

Figure 2.7: SERS imaging from colony incubated with 5 mM $HAuCl_4$ for 70 minutes, shaking at 270 rpm, 37°C. All spectra were recorded with 785 nm laser, 6–10 mW. Exposure times: 1 s (Streamline); 10 s (extended scan). (A) Photoimage of colony on microscope slide, under white light, 50x objective. Scale bar = 10 mm. (B) Same area overlaid with Streamline map from 1400–1750 cm^{-1} segment, processed to show intensity at 1550 cm^{-1}. (C) Same area, overlaid with Streamline map from 900–1300 cm^{-1} segment, processed on peak height at 1344 cm^{-1}. Streamline spectrum 1 is from a clean glass slide. Streamline spectra 2–5 are from the same series of maps and are displayed on a common scale; spectra 2–4 are shown as recorded, without offset. In each Streamline spectrum, green represents data from first map, then red, light purple, blue and dark purple from subsequent maps; wavelength ranges overlap. Raman spectrum 6: PDB.

2.4 Discussion

The goal of this study was to demonstrate that in vivo synthesis of SERS active AuNPs can be achieved. Microorganisms are thought to have major roles in biomineralization.[29] Furthermore, bacteria and fungi,[30-38] as well as plant extracts,[39] are being proposed as alternative, green technology vehicles for nanoparticle synthesis. AuNP generation is clearly not difficult. The next focus was on the creation of synthesis conditions that permit SERS activity, preferably from AuNP generated in specific locations, while preserving cell viability. Nanoparticle sizes and shapes are critical to their function,[40] so in addition to AuNP synthesis *per se*, I was interested in factors that control location, size and shape.

The fungal wall is the interface between the cytoplasm and the cell's environment and mediates interactions, such as symbiosis and pathogenesis, with organisms. It is likely that metallic NP generation is part of an adaptive (defense) mechanism.[33,41] *A. nidulans* is able to generate metallic NPs when challenged with solutions of group VIII and IB transition metal salts including $AgNO_3$, $CuSO_4$, $PdCl_2$, K_2PdCl_4 and K_2PtCl_4 (data not shown), consistent with results from Neurospora crassa.[36]

2.4.1 $HAuCl_4$-treated *Aspergillus nidulans* Hyphae Form AuNPs

Aspergillus nidulans colonies grown in PDB rapidly changed colour following addition of $HAuCl_4$ solution, consistent with the formation of AuNPs (Figure 2.1). This provided an immediate preliminary indication of AuNP presence, albeit without nm-scale spatial resolution. The 1 mM treatment produced a colour change from white to pink-purple, but no particles were detectable with light microscopy. Incubation in 5 mM $HAuCl_4$ resulted in the production of golden particles (triangles, irregular hexagons)

greater than 1 μm in size, readily observable under white light. Such microparticle shapes and sizes have been reported elsewhere.[40, 42, 43] This variation also demonstrated that $HAuCl_4$ starting concentration and duration of incubation can be useful variables for control of NP formation.

Near-edge X-ray absorption fine structure (NEXAFS) is used in scanning transmission X-ray microscopy (STXM) to qualitatively and quantitatively map chemical species with a spatial resolution of better than 40 nm. Components in a natural river microbial biofilm including metals and biopolymers have been quantitatively mapped using STXM.[44] Here, STXM data was used to confirm the identity of the AuNPs, and to provide qualitative images and calibrated quantitative images from sequences at specific energies.[22]

The $M_{4,5}$-edge absorption profiles from the NPs in whole hyphae and from the $AuCl_3$ standard were found to be similar, and matched that of Au metal,[25] confirming their identity as AuNPs (Figure 2.2 A). Qualitative images, overlaid to compare C and Au at higher spatial resolution, showed that the AuNPs were scattered throughout the mycelium (Figure 2.2 B, C) in a sample exposed to 5 mM $HAuCl_4$. Quantitative spectral fitting of an AuNP cluster gave a maximum effective thickness of ~2 μm, with the effective thickness of obvious individual AuNPs being 1.0 ± 0.6 μm. Other shapes, including cubes >1 μm, were observed in the extracellular medium. These dimensions were consistent with the visible images and the later results.

Qualitative carbon images from 100 nm thick sections showed hyphal outlines, but the background from the embedding material and Formvar support film obscured many details, since the 228.2 eV carbon peak can contain smaller contributions from

lipid and polysaccharide-like components (Figure 2.2 D-F). The cytoplasm was a brighter red, suggesting higher relative protein content, whereas the cell wall was dark. Although proteins are found in cytoplasm and walls, *Aspergillus* cell walls are ~ 80 % carbohydrate. This presumably reduced the 288.2 eV signal, facilitating contrast with the cytoplasm.

Qualitative mapping of Au in thin TEM sections confirmed that AuNPs were located beside, as well as within, hyphae (Figure 2.2 D-F). Large AuNPs were associated with hyphal walls, and were similar in size and distribution to those from our TEM results. Au was not detected in fungi exposed to 1 mM $HAuCl_4$, likely because it was below the sensitivity limit of our STXM instrumentation.

The UV-Vis spectra of conditioned medium following incubation of *A. nidulans* with 1 mM $HAuCl_4$ (Figure 2.3) showed an SPR band that was consistent with the visible purple-pink colour that developed in these colonies. By 20 minutes incubation, the UV Vis spectrum of the growth medium showed a strong SPR peak at ~540 nm, typical of AuNP in the 50-70 nm size range;[28] peak height increased with length of incubation. At times (e.g.: at 40 minutes, in this particular experiment), a new minor band appeared at longer wavelengths, here ~820 nm. Such bands are attributed to changes in particle size, shape, state of aggregation and local environment.

Fluorescence microscopy and TEM also showed abundant NP formation, including NPs associated with walls and cytoplasm of fungal cells, or distributed freely in the growth medium. Calcofluor stained the lateral walls and septa (Figure 2.4) in 5 mM $HAuCl_4$-treated hyphae; as expected, these hyphae had wild type morphology. Non-fluorescent (dark) objects, some of which appeared to be triangular or hexagonal, were

associated with some hyphae. Since AuNPs were expected to be dark, i.e.: no stain or fluorescence under these conditions, these shapes were interpreted to be large AuNPs. No unattached extracellular NPs were observed; most likely such NPs were washed away during the staining procedure.

TEM images of hyphae following exposure to 1 mM or 5 mM $HAuCl_4$ showed electron dense structures presumed to be AuNPs. These were located within and adjacent to fungal cells, as well as in the growth medium (Figure 2.5). Both 1 mM and 5 mM $HAuCl_4$-treated hyphae had many 8-10 nm AuNPs in their cytoplasm. These were about twice the size of ribosomes, similar in size and with equivalent electron density to chemically synthesized AuNPs used for immunogold electron microscopy. Following 1 mM (but not 5 mM) $HAuCl_4$ treatment, *A. nidulans* hyphae also had clusters of ~20-30 nm globose AuNPs that remained associated with the outer cell wall surface after preparation for TEM.

The Spitzenkörper region of a hypha treated with 5 mM $HAuCl_4$ contained polyhedral AuNPs suggesting that the cell was actively growing when those AuNPs were formed. Similarly, a small cluster of polyhedral AuNPs about 8 μm behind the tip might be associated with a future branching event. Compared to TEM results for control and 1 mM $HAuCl_4$ treated hyphae fixed at the same time, the cytoplasm in the 5 mM $HAuCl_4$ treatment was less dense. In 5 mM (but not 1 mM) $HAuCl_4$-treated cells, AuNPs included flat plates that could be up to a micrometer in length. It is possible that these NP damaged the cell membrane as they grew, perturbing ion gradient homeostasis.

The AuNP shapes in the growth medium (Figure 2.5D) are consistent with AuNPs found within cells and on their surfaces in the fluorescence images (Figure 2.4).

Given the dimensions of cytoplasmic AuNPs compared to the expected pore size of Aspergillus cell walls (~ 2 kDa), it is most likely that the cytoplasmic AuNPs formed in situ. This is consistent with our earlier suggestion that AuNP formation is a defense or detoxification mechanism.[33,41]

The cytoplasm and exterior of living cells experience very different chemical conditions. Ion concentration in the cytoplasm of a living cell is highly regulated, [47, 48] whereas the outside surface of the cell wall is strongly influenced by its environment. Consistent with this, colonies treated with 1 mM $HAuCl_4$ for 150 minutes were still able to grow vigorously, whereas colonies treated with 5 mM $HAuCl_4$ displayed reduced growth after 30 minutes treatment. It is possible that the polyhedral AuNPs associated with the Spitzenkörper region, which were not seen in extracellular AuNPs, reflect a particular cytoplasmic chemistry. Taken together, there are multiple lines of consistent evidence of AuNP synthesis in *A. nidulans* hyphae, most likely while they were alive, regardless of concentration or length of exposure.

2.4.2 AuNPs -associated with *Aspergillus nidulans* Hyphae are SERS-active

Colonies of *A. nidulans* that contained AuNPs, mounted and dried onto glass, showed a range of SERS activity when examined with Raman microscopy. Often, spectra from an extended scan map showed significant SERS activity, for example, in Figure 2.6, where signal intensities are on the order of 10^5 counts. However, spectra from other pixels in this map showed two strong graphite bands between 1300-1550 cm^{-1}, indicating that the sample had overheated and burned. Assignment of the observed bands in SERS spectra is challenging. The spectrum in Figure 6 came from within a mass of hyphae,

making it impossible to assign location; given the possibility of partial oxidation, spectral assignment was not pursued in this case.

While the SERS intensity was several orders of magnitude greater than normal Raman, the extended scan recording conditions were not optimal. Ideally, scans should be rapid, with low laser power, to reduce the possibility of carbonization as well as to increase the efficiency of data collection for large scale studies. A good signal to noise ratio should be obtainable in less than 1 s from SERS-active AuNPs. The Streamline mode in the Renishaw inVia enables a very rapid scan, as fast as ~30 ms laser exposure per pixel, for a single grating setting. Such maps must be taken at several grating settings (about 400 cm^{-1} each), in order to build up the entire spectrum.

Typically, Streamline images were recorded over several intact hyphae located at the periphery of the colony, such as those shown in Figure 2.7. Since this colony was withdrawn from the growth chamber, the region around the hyphae contains dried exudate, PDB and cellular debris, as well as free AuNPs, based on other observations and characterization. Most, but not all, SERS hot-spots remained active throughout acquisition of the required series of grating settings. The spectrum of the clean glass displays a broad weak band with maximum ~1400 cm^{-1}. With the exception of a few extra-cellular SERS hot spots, spectra from the extra-cellular region exhibit this same profile, while those coming from hyphae are similar but uniformly elevated across the entire spectral range (Figure 2.7, spectra 2 and 3, respectively). The spectra are shown as recorded, without offset, on a common scale. The elevation in spectrum 3 was attributed to the broad background fluorescence from hyphae; hence, by processing only for the

relative background intensity, I was able to delineate the location of the hyphae in the yellow false-colour image; the individual spectra carry no spectrochemical information.

Spectrum 4 from this series is a genuine SERS spectrum and typifies an ideal situation. The point remained SERS-active throughout the experiment. Bands did not change from image to image at the different grating settings: peaks in the 400-800 cm^{-1} scan were also present in the 700-1100 cm^{-1} scan. Absence of peaks was also consistent: there were no bands where the segments overlapped, e.g.: ~1300-1400 cm^{-1}. This result is particularly promising, since the sample was not heat damaged (no graphite bands).

The spectrum from point 5 illustrates one of the as-yet uncontrolled aspects of SERS imaging. In the first map, the pixel was silent, and continued to be so in segments 3, 4 and 5. However, while segment 2 was recorded, some NP(s) in this region suddenly responded actively, before falling silent again. Notably, this point was also graphite-free, thus carbonization was not an issue. One possible explanation for this event is that the laser beam position shifted slightly during that pass, and the NP was suitably excited on that occasion only. A solution to this problem is to record a much broader segment of the spectrum at one time, but this would require a different detector arrangement. Nevertheless, it was concluded that a SERS signal only appears when AuNPs are present, whether in the PDB or the hyphae.

Table 2.1: Tentative band assignments from SERS spectra of *A. nidulans*, Figure 7, Spectra 4 and 5.

Raman shift (cm^{-1})		Tentative assignment
#4	#5	
548		COC deformation (glycosidic ring)
646		C-C deformation
	750	OPO symmetric stretching (phosphodiester)
	810	OPO antisymmetric stretching (phosphodiester)
836		CC stretching
951		Ring vibrations
1082		CC & CO stretching
1162		CC & CN stretching
1282		Amide III
1297		CH_2 deformation (lipid)
1325		Amide III, CH deformation
1500		Amide II, C=C stretching
1530		N-H bending, C=C stretching (protein)
1582		C=C stretching (protein)

SERS spectra from the hyphae or surroundings do not match the PDB spectrum and must derive from the hyphal components. Assignment of bands from these spectra was attempted, with reference to literature values for common biochemical cell components (Table 2.1).[49-51] In this, it was assumed that the SERS signal was arising from a general enhancement in the vicinity of AuNP; the degree of signal enhancement did not suggest single molecule detection, nor could identify a likely single source. There are numerous candidates, including bands common to proteins, carbohydrates and lipids. Currently it is impossible to arrive at a unique solution, since the signals must arise from highly localized components, but the number and type could vary, especially for large biomolecules such as proteins.

It was shown that AuNPs produced by incubation of *A. nidulans* in $HAuCl_4$ were SERS active. Rapid scanning rates of less than 1 s/pixel were required to eliminate carbonization. Peak assignment represents a considerable challenge, in part because it is as yet difficult to unambiguously correlate AuNP location and SERS signal generation. Having shown that incubation in 1 mM $HAuCl_4$ does not impair hyphal vigor and results in AuNPs on the wall outer surface, our next goal is to achieve better control over the size and sites of AuNP formation. AuNPs thus created could serve as SERS probes for wall biochemistry. The use of such AuNPs with *A. nidulans* strains that have been deleted for one or more genes in the Galf biosynthesis pathway, which affects cell wall structure and composition.[3-6] Site-specific generation of AuNPs could permit directed high spatial resolution analyses with biochemical specificity.

2.5 Conclusions

Aspergillus nidulans colonies can generate AuNPs within and adjacent to hyphae. Examination of *A. nidulans* colonies incubated in $HAuCl_4$, using light microscopy, UV-Vis spectroscopy, fluorescence microscopy, TEM and STXM, provided complementary identification and characterization. AuNP synthesis is straightforward; NPs have characteristic shapes comparable to those generated by other microorganisms or by chemical reduction. These AuNPs exhibit surface plasmon resonance and can be used as substrates for SERS spectra, enhancing the scattering intensity by several orders of magnitude. Both 1 mM and 5 mM $HAuCl_4$ treatments produced SERS-active particles. Methods for better control of NP formation and for assignment of bands, as well as protocols for SERS imaging from AuNPs in living *A. nidulans* hyphae were developed.

These experiments also demonstrated that PBD is capable of causing NP formation. AuNP formed in PDB would interfere with the SERS studies of fungal cell components. In addition, parameters such as temperature, pH, exposure time to metal, biomass and metal concentration affect the growth conditions (size and shape), cellular activities, and enzymatic processes. Nanoparticle sizes and shapes are critical to their function for SERS experiments. Since NPs were synthesized by live cells, it was very difficult to control their sizes, shapes, and locations. This lack of control limited their utilization for SERS investigation of fungal cell, particularly cell wall. Therefore this method was abandoned and a chemical method using monosodium glutamate for synthesis of NPs was developed; details of this method are provided in chapter 3.

2.6 References

1. S. G. W. Kaminskyj, A. Szeghalmi, K. Jilkine, K. M. Gough, *FEMS Microbiol Lett*, 2008, 284, 1-8.

2. G. Srinivasan. Vibrational Spectroscopic Imaging for Biomedical Applications. NewYork : McGraw-Hill Professional, 2010, 125-152.

3. A. M. El-Ganiny, D. A. R. Sanders, S. G. W. Kaminskyj. *Fungal Genet and Biol*, 2008, 45, 1533-1542.

4. A. M. El-Ganiny, I. Sheoran, D. A. R. Sanders, S. G. W. Kaminskyj, *Fungal Genet Biol*, 2010, 47, 629-635.

5. S. Afroz, A. M. El-Ganiny, D. A. R. Sanders, S. G. W. Kaminskyj, *Fungal Genet Biol*, 2011, 48, 896-903.

6. B. C. Paul, A. M. El-Ganiny, M. Abbas, S. G. W. Kaminskyj, T. E.S. Dahms, *Eukaryot Cell*, 2011, 10, 646-653.

7. M. C. Fisher, D. A. Henk, C. J. Briggs, J. S. Brownstein, L. C. Madoff, S. L. McCraw, S. J. Gurr, *Nature*, 2012, 484, 186-194.

8. L. Cowen, *Nat Rev Microbiol*, 2008, 6, 187-198.

9. A. Szeghalmi, S. G. W. Kaminskyj, K. M. Gough, *Anal Bioanal Chem*, 2007, 387, 1779-1789.

10. K. Jilkine, K. M. Gough, R. Julian, S. G. W. Kaminskyj, *J Inorg Biochem*, 2008, 102, 540-546.

11. B. B. Fuchs, E. Mylonakis, *Eukaryot Cell*, 2009, 8, 1616-1625.

12. F. Dirr, B. Echtenacher, J. Heesemann, P. Hoffmann, F. Ebel, J. Wagener, *Int J Med Micro*, 2010, 300, 496-502.

13. L. A. Walker, N. A. R. Gow, C. A. Munro, *Fungal Genet Biol*, 2010, 47, 117-126.

14. M. Isenor, S. G. W. Kaminskyj, R. J. Rodriguez, R. S. Redman, K. M. Gough, *Analyst*, 2010, 135, 3249-3254.

15. W. E. Smith, *Chem Soc Rev*, 2008, 37, 955-964.

16. P. L. Stiles, J. A. Dieringer, N. C. Shah, R. P. Van Duyne, *Ann Rev Anal Chem*, 2008, 1, 601-626.

17. J. A. Dieringer, K. L. Wustholz, D. J. Masiello, J. P. Camden, S. L. Kleinman, G. C. Schatz, R. P. Van Duyne, *J Am Chem Soc*, 2009, 131, 849-854.

18. A. Szeghalmi, S. G. W. Kaminskyj, P. Roesch, J. Popp, K. M. Gough, *J Phys Chem B*, 2007, 111, 12916-12924.
19. S. G.W. Kaminskyj, *Fungal Genet Biol*, 2000, 31, 105-113.
20. A. P. Hitchcock, http://unicorn.mcmaster.ca/aXis2000.html.
21. J. J. Dynes, J. J. Lawrence, D. R. Korber, G. D. W. Swerhone, G. G. Leppard, A. P. Hitchcock, *Sci Total Environ*, 2006, 369, 369-383.
22. J. J. Dynes, T. Tyliszczak, T. Araki, J. R. Lawrence, G. D. W. Swerhone, G. G. Leppard, A. P. Hitchcock, *Environ Sci Technol*, 2006, 40, 1556-1565.
23. R. C. Weast, M. J. Astle. CRC Handbook of Chemistry and Physics. Florida: CRC Press Inc.,1980.
24. B. L. Henke, E. M. Gullikson, J. C. Davis, *At Data Nucl Data Tables*, 1993, 54, 181-342.
25. A. Owens, S. C. Bayliss, P. J. Durham, S. J. Gurman, G. W. Fraser, *Astrophys J*, 1996, 468, 451-454.
26. S. G. W. Kaminskyj, *Fungal Genet Newsl*, 2001, 48, 25-31.
27. K. V. Kaznatcheev, C. Karunakaran, U. D. Lanke, S. G. Urquhart, M. Obst, A. P. Hitchcock, *Nucl Instrum Meth A*, 2007, 582, 96-99.
28. W. Haiss, N. T. K. Thanh, J. Aveyard, D. G. Fernig, *Anal Chem*, 2007, 79, 4215-4221.
29. S. K. Das, E. Marsili, *Rev Environ Sci Biotechnol*, 2010, 9, 199-204.
30. P. Mukherjee, A. Ahmad, D. Mandal, S. Senapati, S. R. Sainkar, M. I. Khan, R. Ramani, R. Parischa, P. V. Ajayakumar, M. Alam, M. Sastry, R. Kumar, *Angew Chem Int Ed Engl*, 2001, 40, 3585-3588.
31. N. Vigneshwaran, N. M. Ashtaputre, P. V. Varadarajan, R. P. Nachane, K. M. Paralikar, R. H. Balasubramanya, *Mater Lett*, 2007, 61, 1413-1418.
32. Z. Sadowski, I. H. Maliszewska, B. Grochowalska, I. Polowczyk, T. Koźlecki, Mater Sci-Poland, 2008, 26, 419-424.
33. F. Reith, B. Etschmann, C. Grosse, H. Moors, M. A. Benotmane, P. Monsiers, G. Grass, C. Doonan, S. Vogt, B. Lai, G. Martinez-Criado, G. N. George, D. H. Niles, M. Mergeay, A. Pring, G. Southam, J. Brugger, *Proc Natl Acad Sci USA.*, 2009, 106, 17757-17762.

34. R. Bhambure, M. Bule, N. Shaligram, M. Kamat, R. Singhal, *Chem Eng Technol*, 2009, 32, 1036-1041.
35. S. Karmakar, S. Kundu, K. Kundu, *Artif Cell Blood Sub*, 2010, 38, 259-266.
36. E. Castro-Longoria, A. R. Vilchis-Nestor, M. Avalos-Borgia, *Colloids Surf B*, 2011, 83, 42–48.
37. P. Singh, R. B. Raja, *Asian J Exp Biol Sci*, 2011, 2, 600-605.
38. N. Jain, A. Bhargava, S. Majumdar, J. C. Tarafdar, J. Panvar, *Nanoscale*, 2011, 3, 635-64.
39. S. S. Shankar, A. Rai, B. Ankamwar, A. Singh, A. Ahmad, M. Sastry, *Nature Mater*, 2004, 3, 482-488.
40. C. S. S. R. Kumar. Metallic Nanomaterials: Nanomaterials for the Life Sciences. Weinheim: Wiley-VCH, 2009.
41. J. F. Stolz, R. S. Oremland. Microbial Metal and Metalloid Metabolism: Advances and applications. Washington: ASM Press, 2011, 213-246.
42. N. C. Bigall, M. Reitzig, W. Naumann, P. Simon, K. V. Pee, A. Eychmuller, *Angew Chem Int Ed*, 2008, 47, 7876-7879.
43. S. K. Das, A. R. Das, A. K. Guha, *Small*, 2010, 6, 1012-1021.
44. A. P. Hitchcock, J. J. Dynes, J. R. Lawrence, M. Obst, G. D. W. Swerhone, D. R. Korber, G.G. Leppard, *Geobiology*, 2009, 7, 432- 453.
45. P. W. J. de Groot, B. W. Brandt, H. Horiuchi, A. F. J. Ram, C.G. de Koster, F. M. Klis, *Fungal Genet Biol*, 2009, 46, S72-S81.
46. A. Tripathy, A. M. Raichur, T. C. Prathna, N. Chandrasekaran, A. Mukherjee, *J Nanopart Res*, 2010, 12, 237-246.
47. H. D. Osiewacz. Molecular biology of fungal development. New York: Marcel Dekker Inc., 2002, 29-58.
48. R. R. Lew, *Nature Rev Microbiol*, 2011, 9, 509-518.
49. Z. Movasaghi, S. Rehman, I. U. Rehman, *Appl Spectrosc Rev*, 2007, 42, 493-541.
50. A. Sujith, T. Itoh, H. Abe, K. Yoshida, M. S. Kiran, V. Biju, M. Ishikawa, *Anal Bioanal Chem*, 2009, 394, 1803-1809.
51. K. A. Willets, *Anal Bioanal Chem*, 2009, 394, 85-94.

Chapter 3: Raman and SERS Imaging of *Aspergillus nidulans* Hyphae via Gold Nanoparticles Synthesized by Monosodium Glutamate

3.1 Introduction

There is a great need for rapid and precise methods for detection and classification of fungi particularly for the microbial diagnosis.[1] The conventional methods for fungal identification have several limitations including lack of specificity, extensive sample preparation and high cost. Therefore, alternative approaches for biochemical detection of fungi are required. Raman spectroscopy has demonstrated its high potential as a rapid and reliable technique for the analysis of biological samples.[2] Raman spectroscopy is a noninvasive and label-free technique that requires minimal sample preparation and provides comprehensive information about the chemical structure of the complex biological samples on a molecular level.[3,4] Raman microscopy, which couples Raman spectroscopy with an optical microscopy, is a suitable method to achieve spatial resolution of the samples in the range of ~1 μm.[1,5] It allows the examination of small sample volumes (< 1 μm^3) such as fungal hyphae with a size of about 10 μm in diameter.[2] The Raman effect is an inherently weak process (only 1 in 10^8 of the incident photons are inelastically scattered). Thus, Raman spectroscopy requires high laser powers and it takes long time to collect Raman spectra.

Surface enhanced Raman scattering (SERS) can improve the Raman cross section by 4-6 orders of magnitude. This is due to intense electromagnetic enhancement that results from surface plasmon oscillations of a metal colloids or roughened metal

surface.[6,7] SERS is a selective and sensitive spectroscopic technique that has shown profound potential for the analysis of microorganisms. SERS has been extensively used to examine the chemical composition of bacterial and yeast cells.[8-12] Some works have been published for the SERS analysis of fungal cells.[13,14] One of the challenges faced by scientists is acquiring reproducible SERS spectra from biological samples particularly microorganisms with complex biochemical structure. This problem may be due to several experimental factors, such as particle morphology, analyte-metal interface geometry and saturation of the particle surface.[2,15]

Fungi are a group of eukaryotic organisms that play important roles in the biosphere. Fungi can be used as experimental model organisms for other eukaryotes due to shared origins of the genes responsible for essential biological functions.[16] Fungal hyphae usually grow by apical branching from the hyphal tip.[17] The fungal cell wall is one of the unique structures that has specialized functions. The wall is thinner and more flexible at the tip compared to the rigid wall in basal regions.[18] Chemical analysis of the fungal cell wall has shown that polysaccharides, proteins, nucleic acids and lipids are the main components of the wall.[19] The cell wall connects the cells with their surroundings and facilitates the adhesion of cells to hosts, substrates or other cells. Cell wall damage can have a great impact on the fungal cell growth and structure, resulting in cell lysis and death.[20] Therefore, the fungal cell wall is often considered a great target for the development of anti-fungal agents.[20]

In this chapter, gold colloids were prepared from the reduction of chloroauric acid ($HAuCl_4$) by monosodium glutamate (MSG). These particles were characterized with UV-Vis spectroscopy and exhibit a surface plasmon resonance (SPR) peak. Incubation of

A. nidulans colonies with pre-formed AuNPs was also performed to investigate the feasibility of using SERS for the analysis of the fungal cell wall. As the overall objective of this work was to explore cell wall composition of *A. nidulans* hyphae, both Raman and SERS techniques were used.

3.2 Materials and Methods

3.2.1 Fungi

Two strains of *Aspergillus nidulans* used in this study were supplied by Prof. Susan Kaminskyj from the Biology Department, University of Saskatchewan. AAE1 is a wild type strain and AAE2 is a mutant which differs from AAE1 in one gene. Galactose is a common monosaccharide; in mammals, it is in the six-membered ring form named galactopyranose (Gal*p*), while in many microorganisms cell wall such as fungi, galactose is observed in the five-membered form, galactofuranose (Gal*f*).[21,22] UDP-galactopyranose mutase (UGM) is an enzyme capable of conversion of UDP-galactopyranose to UDP-galactofuranose.[23] Gal*f* is essential for wild type growth and is observed in most of the pathogenic species. Since Gal*f* is absent from mammals and higher plants, its biosynthetic pathways could be useful targets for anti-fungal drug development.[21] The UGM gene has been deleted in AAE2 and compared to wild type strain, it generates wide, highly branched hyphae with thicker cell walls (~204 nm compared to ~54 nm in wild type). As a consequence of UGM deletion, sporulation is delayed and reduced in AAE2 strain.[22]

All strains were grown on Potato Dextrose Agar (PDA) at 37 ºC for 3 days. The growth medium pH was adjusted to 6.5 with 1 M NaOH.

3.2.2 Gold Colloid Preparation

Gold nanoparticles were prepared according to the method of monosodium glutamate (MSG) reduction reported by Sugunan et al.[24,25] This method involved adding 0.84 mL of 0.5 % (21 mM) $HAuCl_4$ solution to 50 mL doubly distilled, deionized water. The mixture is brought to boiling. Then, 2.8 mL of 0.42 % (25mM) of MSG was added to the solution which was stirred and boiled until the color changed from light yellow to red. The reaction was removed from the heat and the solution was cooled in an ice bath. Gold colloidal solution was stored in the dark at 4 °C. A schematic of the NP synthesis with MSG is represented in Figure 3.1. The colloidal solution of AuNPs prepared by this method was characterized using UV-visible absorption spectroscopy and dynamic light scattering (DLS).

UV-Vis absorption spectra of Au colloidal solution and liquid from colonies exposed to colloidal solution of AuNPs were taken with a UV-2101 spectrometer (Shimadzu), from 190 to 900 nm, at 1 nm spectral resolution, against a water blank (Milli-Q) in matching 1 cm path-length, 1 mL glass cuvettes.

3.2.3 Raman and SERS Microscopy

Raman and SERS spectra were obtained with a Renishaw inVia Raman microscope in conjunction with a high sensitivity, ultra-low noise CCD, and a motorized x–y stage for map creation. Measurements were carried out using a 785 nm diode laser giving a power of ~0.1-30 mW at the sample, and a 50x objective. The Raman spectrometer wavelength calibrations were performed using the center frequency of the silicon band (520 cm^{-1}) from a silicon reference wafer. The CCD detector accommodates a spectral width of 400 cm^{-1} for a given grating position. Raman maps were generated by

collecting data either with an extended scan from 400-1800 cm^{-1} or by sequential static (400 cm^{-1} segment) scan to create a spectrum between 400 and 1800 cm^{-1}. For each pixel of extended scan, exposure time was 10 seconds with 1-10 scans. For instance, if we have two pixels, the exposure time will be 20 seconds and so on. In this experiment time is a very important parameter as the time required to acquire a full spectrum will be significantly longer than a typical SERS event. Furthermore, if longer exposure times are used, the spectra will contain a mixture of Raman and SERS signals.

For SERS analysis of hyphae, 1 mL freshly prepared spore suspension was transferred to a 15 mL conical tube containing 7 mL potato dextrose broth (PDB) adjusted to pH 6.5 with 1 M NaOH. Spores were germinated overnight at 30 ºC with shaking at 190 rpm. Then, PDB was removed and colonies were washed 3 times with 25 mM of freshly prepared MSG solution. Colonies were re-suspended in 2 mL MSG solution and 2 mL of Au colloidal solution was added and mixed. The conical tube was shaken at 25 ºC with 190 rpm. A brief description of SERS sample preparation procedure is given in Table 3.1.

Table 3.1: Sample preparation procedure for SERS measurement.

Colony growth AAE1or AAE2	Wash colonies with diluted MSG	Reaction of colonies and AuNP
Germination overnight in: 7 mL PDB Shake at 30°C, 190 rpm pH 6.5	Remove PDB (pipet) (Add diluted MSG, remove)x3 Add 2 mL MSG solution	Add 2mL AuNP+MSG solution to colonies: Shake at 25°C, 150 rpm Variable times: 0 – 24 hrs

Colonies exposed to Au colloidal were transferred whole to ZnSe window or commercially used aluminum foil slide and excess solution was wicked away with filter

paper. Samples were frozen at -80 ºC and then dried at room temperature. Spectra of hyphae exposed to Au colloidal were obtained with low laser power of ~ 0.3-3 mW to avoid laser-induced degradation of the samples. Control samples were prepared from the colonies that had not been exposed to Au colloidal solution. Control spectra of hyphae were acquired with laser power of ~ 3-30 mW. The number of AAE1 and AAE2 hyphae examined with Raman and SERS are shown in Table 3.2.

Table 3.2: Number of hyphae examined for each strain with Raman and SERS.

Technique	Substrate	# of hyphae (AAE1)	# of hyphae (AAE2)
Raman	ZnSe	5	4
	Aluminum foil	4	4
SERS	ZnSe	10	8
	Aluminum foil	16	13

A reference Raman spectrum of MSG was acquired from MSG powder placed on a commercially used aluminum foil slide. In addition, a Raman spectrum of Au colloid was obtained from a dried droplet of Au colloidal solution on a commercially used aluminum foil slide.

3.3 Results and Discussion

3.3.1 Characterization of Gold Nanoparticles

3.3.1.1 UV-Vis Spectroscopy

Colloidal AuNPs were synthesized by the reduction of chloroauric acid ($HAuCl_4$) with MSG, as shown in Figure 3.1.[24,25]

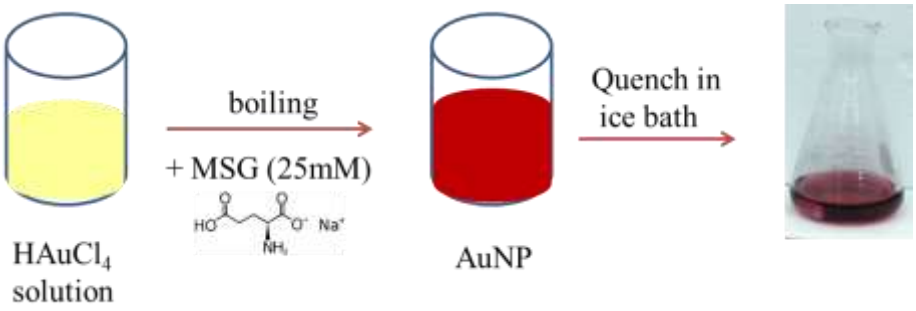

Figure 3.1: Schematic of AuNP synthesis by MSG.

UV-Vis absorption spectra of AuNP solution were monitored over time and depicted in Figure 3.2. The spectrum of Au colloidal solution right after preparation (fresh) shows a surface plasmon resonance (SPR) peak with a maximum at ~529 nm, ascribed to AuNP with the average size of ~ 50 nm.[26] As shown in Figure 3.2, there is no obvious difference in the position of the absorption peak over 21 days. These spectra demonstrated that AuNP colloidal solutions were stable for at least 3 weeks.

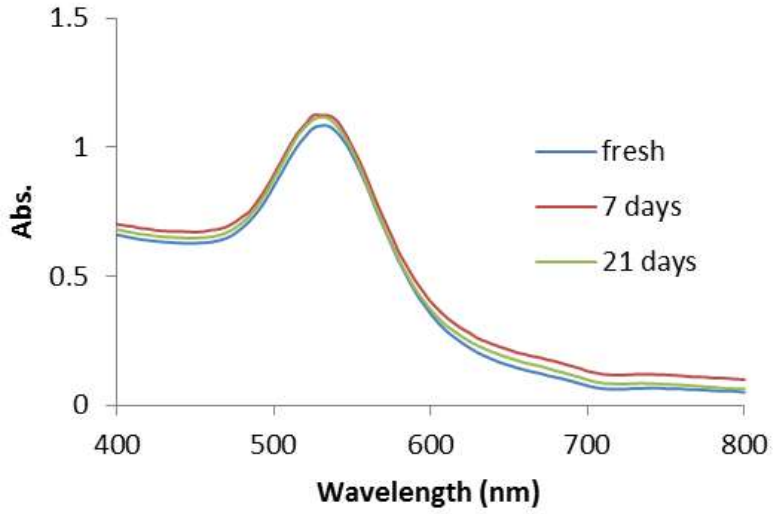

Figure 3.2: Absorption spectra of AuNP prepared by the reduction of MSG and stored at different times: fresh (blue line), 7 days (red line) and 21 days (green line).

3.3.1.2 Raman of MSG and AuNPs Stabilized by MSG

The negatively charged MSG was used as reducing and stabilizing agent which can modify the surface of AuNPs and preserve them from aggregation.[27] The Raman spectra of the MSG and the AuNPs capped by MSG were recorded in the range of 300-1800 cm^{-1} and are displayed in Figure 3.3. Large differences in band intensities were observed in this work as well as by others.[30] Raman spectrum of MSG exhibits bands in the regions of 1585-1665, 1555-1605, 1490-1540 and 1315-1340 cm^{-1} which can be assigned to NH_3^+ deformation, COO^- asymmetric stretching, NH_3^+ deformation and CH deformation respectively.[28,30] The bands at 1417 and 1440 cm^{-1} in the spectrum of MSG corresponds to symmetrical stretching mode of COO^- group and bending modes of CH_2 group respectively. The strong band at 1345 and the shoulder at 1317 cm^{-1} are assigned to the CH_2 deformation and twisting modes respectively. The NH_3 rocking mode is observed at 1081 cm^{-1}. The strong band at 936 cm^{-1} is assigned to C-C stretching mode and the bands at 883 and 860 cm^{-1} corresponds to the CH_2 rocking mode and to the deformation mode of COOH group respectively.[29] Adsorption of the MSG on the AuNPs surface can occur via the lone pair electrons of nitrogen atom of the NH_2 group and the oxygens of the carboxyl group.[30] Figure 3.3 shows the effect of the adsorption of MSG on the Au surface by the observed changes in the characteristic bands of the carboxylate (COO^- stretching mode) group and the C-C stretching bands. This effect was also observed by other researchers which they have attributed to indicate binding of the MSG molecule via chemisorbed species.[30]

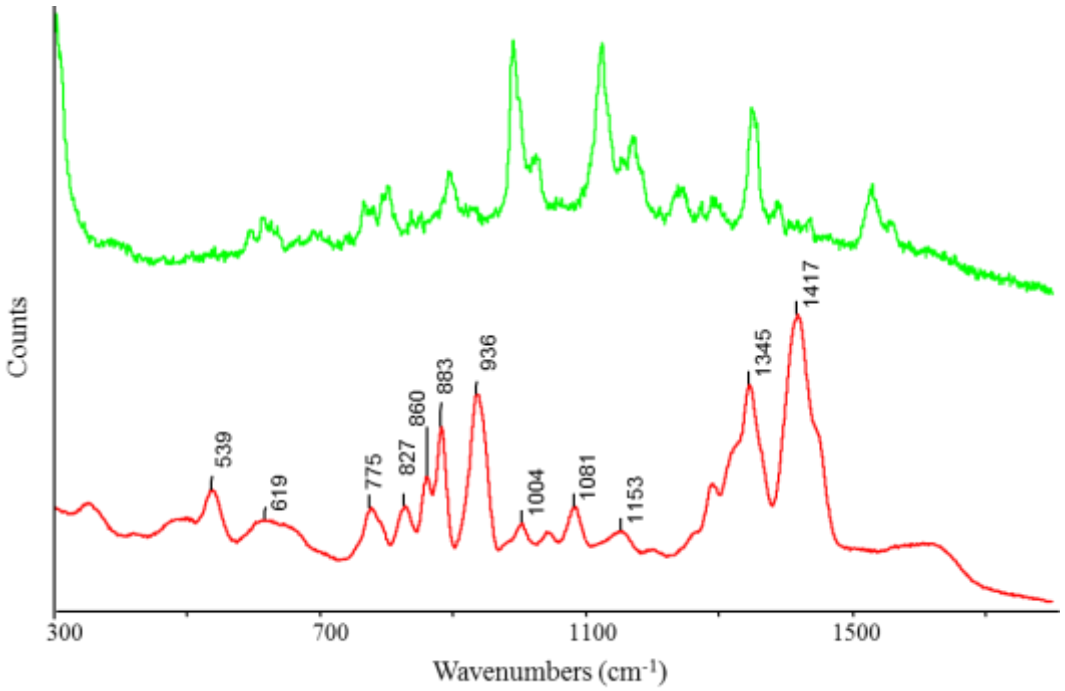

Figure 3.3: Comparison of Raman spectra of MSG (1M) (red) and AuNPs capped by MSG (green). A single droplet of each was dried on commercially used aluminum foil. Spectra were recorded with 785 nm laser, ~15 mW, 1 scan and 10 s exposure time. The spectra are presented on a common scale and offset for clarity.

It is difficult to see from Figure 3.3 if peaks have shifted because the peak intensities changed significantly. For example, the peak intensity at 860 cm^{-1} decreased considerably. A possible explanation for differences in the spectra is powder (MSG) vs solution (AuNPs capped by MSG). Previous workers have shown that the SERS spectra changes significantly but wavelengths for most of peaks were reasonably consistent (within ~2 cm^{-1}).[30]

3.3.1.3 UV-Visible Spectroscopy of Gold Colloids with Fungal Cells

UV-visible absorption spectra of Au colloidal solution incubated with fungal cells at 3 different incubation times are shown in Figure 3.4A. The spectrum of the colloidal

solution after incubation (t=0) shows an absorbance peak with a maximum at 529 nm. Significant reduction in absorbance peak at 529 nm and an additional absorbance peak at 650 nm were observed when the colloidal Au solution was exposed to the fungal cells for 18 and 24 hours (Figure 3.4A). The color of Au colloidal solution changes from red at time zero to dark purple after 18 hours (Figure 3.4B). This change in color and reduction in absorbance peak (at 529 nm) might be due to consumption of the glutamate ions by the fungi.[24] Furthermore, aggregation of AuNPs from the Au colloidal solution onto the fungal wall resulted in broadening and the red-shift of their plasmon resonance spectra. It is possible the glutamate ion removal from the Au colloidal solution de-stabilized the charged AuNPs and the particles accumulated on the hyphal wall. Since both the gold and hyphal surfaces are hydrophobic, accumulation of NPs on the fungal walls may be attributed to the interaction of two hydrophobic surfaces. As shown in Figure 3.4C, the fungal hyphae were coated by AuNPs during incubation. Coating likely occurs due to electrostatic or covalent interactions between the biological compounds of the hyphal walls and the NPs. Other workers have observed a similar change in the visible absorbance with MSG-AuNPs and fungi. In this study, [24] aggregations took significantly longer (2 weeks) however the same results (aggregation of AuNP) were observed.

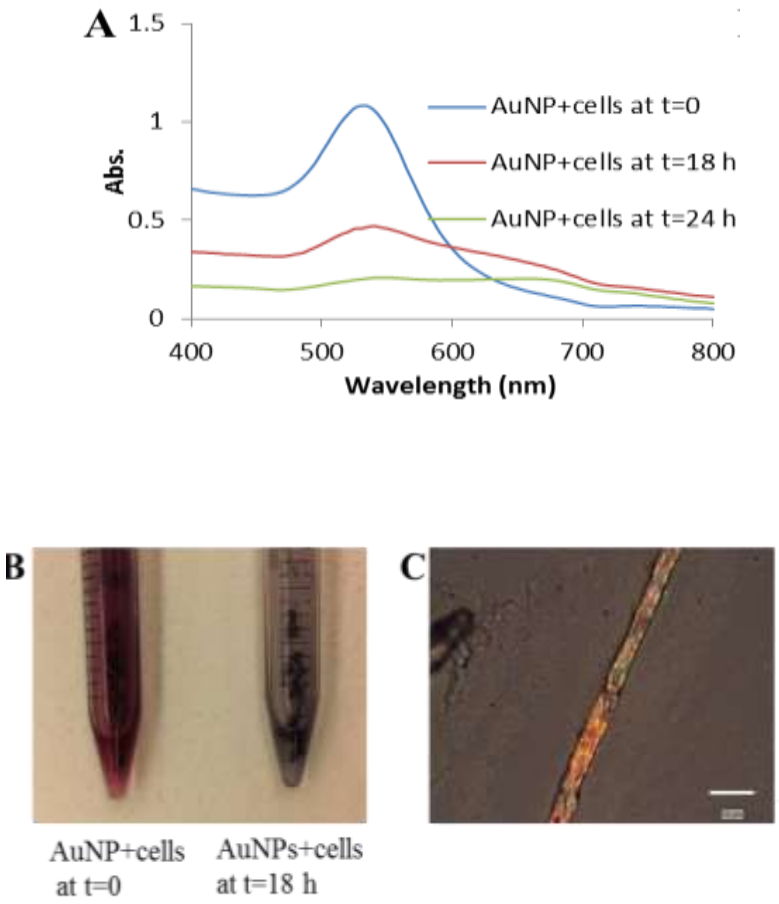

Figure 3.4: A) Absorption spectra of AuNP exposed to *A. nidulans* cells at different incubation times. B) Photo of the Au colloidal solution incubated with *A. nidulans* cells right after and 18 hours after exposure. C) *A. nidulans* hypha exposed to Au colloidal solution for one hour. AuNPs coated the hypha cell wall.

3.3.2 Substrate

To determine a good substrate for SERS study of fungi, the Raman spectra of several blank substrates in the region of 400-1800 cm^{-1} were recorded and shown in Figure 3.5. Minimal spectral interference with the sample spectrum, cost and availability were the main factors considered in substrate selection. As shown in Figure 3.5, the Raman spectra of the microscope glass slide showed a broad band at ~1390 cm^{-1}. The Raman spectra of the aluminum foil slide and ZnSe window display the minimal spectral

features compared to the Raman spectra of other substrates. Therefore, SERS measurements of fungi were obtained using ZnSe window or aluminum foil slide.

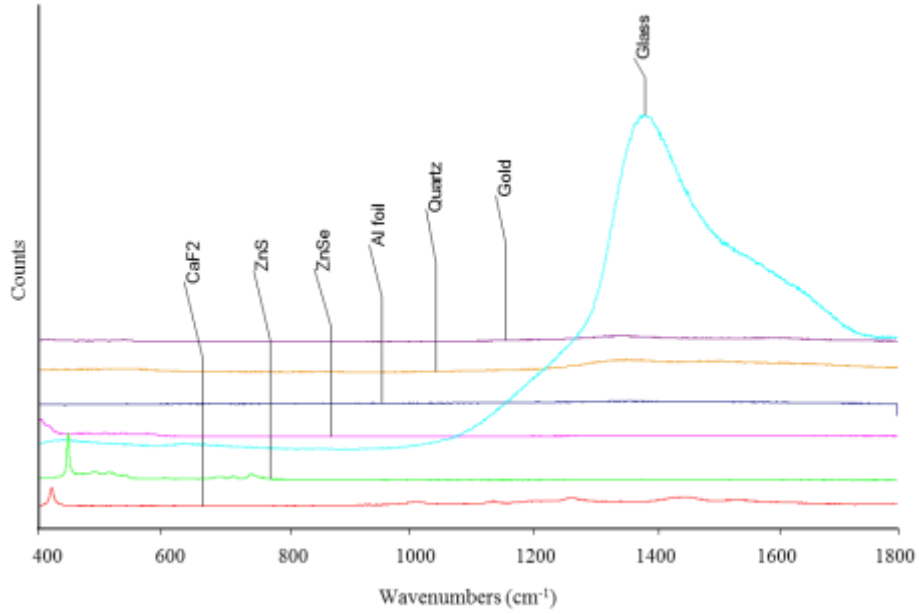

Figure 3.5: Comparison of Raman spectra of different substrates. Spectra are on a common scale and offset for clarity.

3.3.3 Surface Enhanced Raman Scattering Activity of *A. nidulans* Hyphae

Figure 3.6 shows Raman and SERS spectra of a selected AAE1 cell wall. Both spectra were recorded with 785 nm excitation wavelength with a 10 s exposure time and 3 scans in the 400-1800 cm^{-1} spectral region. For the Raman measurements, the sample was mounted and dried onto ZnSe window and examined using a ~30 mW laser. For SERS measurements, AAE1 colonies were incubated with gold colloidal solution for 30 minutes and the colonies were dried onto ZnSe window. SERS spectra were collected with ~0.1 mW laser. The Raman spectrum provides information about the AAE1 chemical composition of the whole cell of which the cell wall is a small percentage. However, it is limited to a few bands with poor signal definition. In addition, high laser

power (~30 mW) was required to collect the Raman spectra with sufficient signal-to-noise ratios.

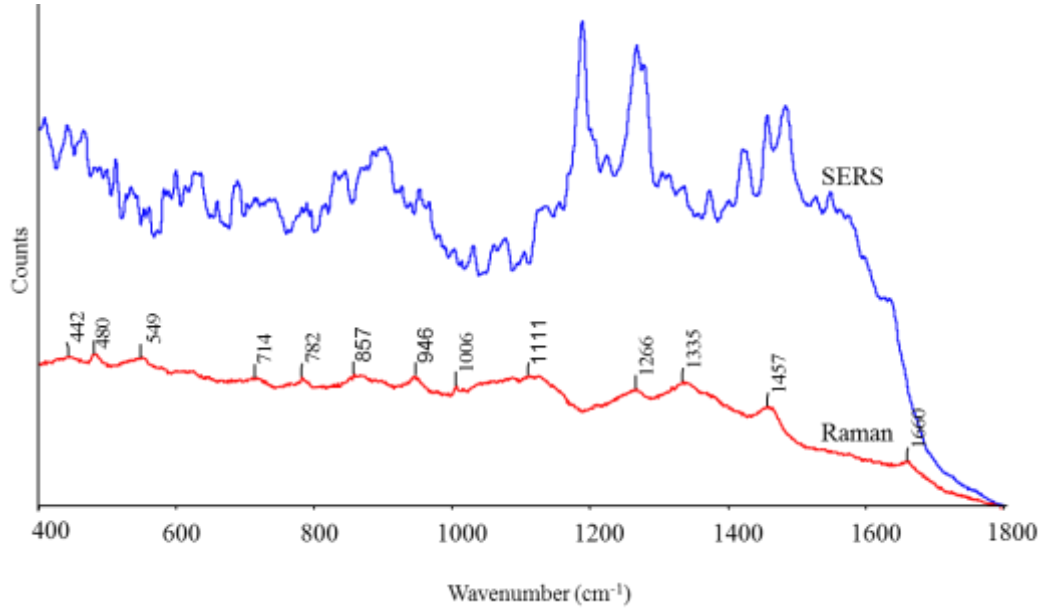

Figure 3.6: Comparison of Raman and SERS spectra of AAE1 hyphae. Spectra are on a common scale and offset for clarity.

The tentative selected Raman band assignments of AAE1 cell are listed in Table 3.3. This indicates that the Raman spectra give us information about the whole cell composition. SERS spectra were a result of the interaction of gold colloids with the outer cell wall components of the AAE1 cells. As shown in Figure 3.6, the SERS spectrum contains many sharper and enhanced signals compared to the Raman spectrum. Because of the time required to generate the spectrum, the spectra is a result of multiple SERS scattering events. Moreover, the laser power utilized to obtain the SERS spectrum was much lower, which decreases the laser-induced degradation of the sample. A high background signal was observed in the SERS spectra from 1200-1650 cm^{-1}, which may indicate that partial oxidation of the sample may have occurred. Some SERS activity was observed with significantly enhanced signals at 1150 and 1250 cm^{-1}. However the

challenge with assigning functional groups to this spectrum is that the time required to obtain the spectrum was long (~1 minute) when compared to the time of a SERS event. The SERS signals also have significant noise and Raman and SERS signals are not overlapped.

Table 3.3. Tentative band assignments from AAE1 spectrum, Figure 3.6.

peak position/cm^{-1}	assignment[a] [32,33]
442	CCC ring def
549	COC glycosidic ring def
857	CO, CC, CH def
946	Ring vibrations
1006	CC ring breathing
1266	CH def, CH_2OH group, amide III
1335	CH, OH def
1457	CH_2, COH def
1660	Amide I

[a]str=stretching; def=deformation; sym=symmetric; asym=antisymmetric.

The Raman spectra in the region 700-1800 cm^{-1} were collected by raster scans of a single AAE1 hypha from the control sample (hypha had not been exposed to gold colloids). Sample was mounted and dried onto ZnSe window. Figure 3.7A shows the optical microscope image of the hypha and the area where the Raman map was obtained. Figure 3.7 C shows the Raman spectra corresponding to the pixels marked in Figure 3.7B. The spectra were recorded with 785 nm laser with ~15 mW laser light, 10 s exposure times (36 pixels; 360 s total exposure time) and 1 scan. All spectra are displayed on a common scale with a broad weak Raman signal with maximum ~1300 cm^{-1}. The Raman spectra collected from the points on the hypha (Figure 3.7B, pixels 1, 2 and 3; Figure 3.7C, Spectra 1, 2 and 3) display the same profile with the spectra obtained from the background (Figure 3.7B, pixels 4 and 5; Figure 3.7C, Spectra 4 and 5). The

only difference is the elevated fluorescence background for the spectra coming from the hyphae. Thus, Raman mapping of the control sample does not provide information about the AAE1 molecular composition even with high laser power (~30 mW).

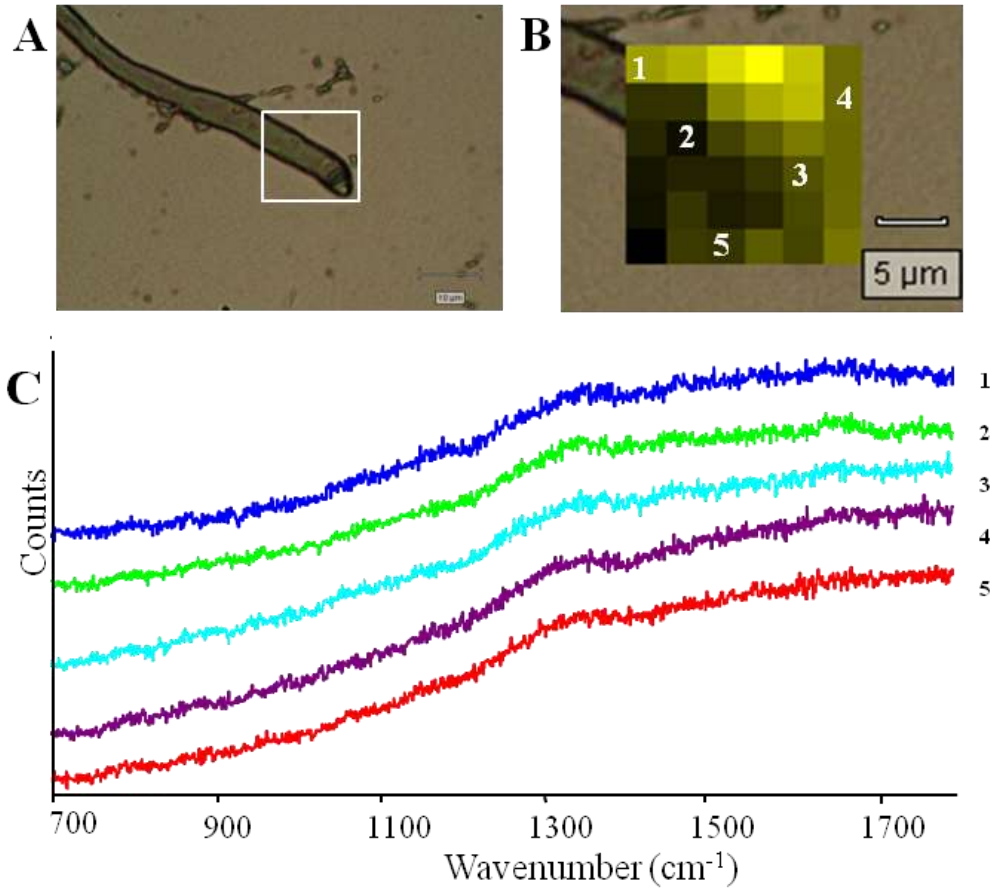

Figure 3.7: Attempted Raman imaging from AAE1 hypha (control). All spectra were recorded with 785 nm laser, ~30 mW, 1 scan and exposure time of 10 s (Raster scan). A) Photoimage of hypha on ZnSe substrate with a box showed the location of the recorded map; Scale bar =10µm. B) Close-up of the box shown in A; Scale bar =5µm. C) Spectra obtained from pixels marked in B. Spectra are on a common scale and offset for clarity.

SERS measurements of *A. nidulans* hyphae were obtained using gold colloidal particles prepared by reduction of $HAuCl_4$ with MSG. Figure 3.8 shows the SERS mapping from raster scans of AAE1 colonies exposed to AuNPs for 2 hours and mounted onto ZnSe window. The spectra were collected with 785 nm excitation wavelength with

~3 mW laser, 10 s exposure times and 1 scan. Figure 3.8A displays the optical microscope image and the location of the recorded map. Figure 3.8B displays the pixels relevant to the SERS spectra shown in Figure 3.8D. Figure 3.8C exhibits the SERS map processed on band intensity at 1516 cm^{-1}. The SERS spectra associated with the AAE1 hypha (Figure 3.8B, pixels 1, 2 and 3; Figure 3.8D, Spectra 1, 2 and 3) are enhanced and showed high signal-to-noise ratio compared to the Raman spectra of the control sample (Figure 3.7C).

It was known that Raman signals can be enhanced when the molecules are in close vicinity or in direct contact with the metal particles. In addition, molecules should have a particular spatial orientation to the metal particles.[34,35] Strong SERS signals at 1000, 1516 and 1586 cm^{-1} were achieved from point 1 on the hypha (Figure 3.8B, pixel 1: Figure 3.8D, Spectrum 1) which could be due to absorption and aggregation of AuNPs on the outer surface of AAE1. These bands were assigned to C-C stretching of aromatic ring (phenylalanine), symmetric and asymmetric stretching of COO^- respectively.[13,36] Several variations in the number, positions and intensities of the signals detected in the SERS spectra of AAE1 (Figure 3.8D, Spectra 1-3). This may associated with the inhomogeneity of the fungal cell surface.[37] Sujith et al. extracted yeast cell wall sugars and reported a weak SERS response from wall sugars.[37] Since mannoproteins are the main components of the fungal outer surface, it suggests the possibility of SERS response from proteins.

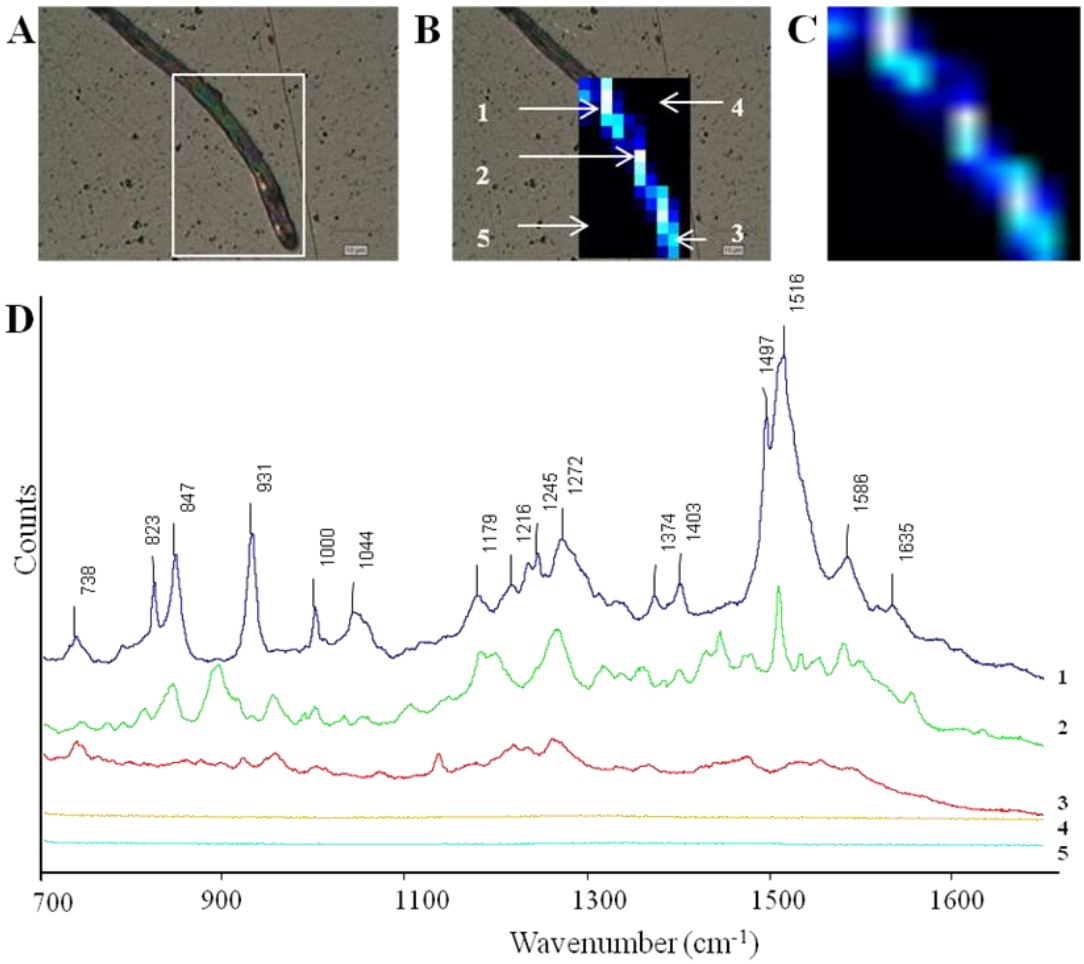

Figure 3.8: SERS imaging from AAE1 colony incubated with AuNPs. All spectra were recorded with 785 nm laser, ~3 mW, 1 scan and exposure time of 10 s (Raster scan). A) Photoimage of hypha on ZnSe substrate with a box showed the location of the recorded map; Scale bar =10µm. B) Same area with marked pixels; Scale bar = 10µm. C) Same area processed to show intensity at 1516 cm^{-1}. D) Spectra obtained from pixels marked in B. Spectra are on a common scale and offset for clarity.

The proposed assignments of the peaks observed in spectrum 1 (Figure 3.8D) are given in table 3.4. The peaks correspond to the responses from both oxygen containing groups and amide group. This suggests the high affinity of Au to bind to oxygen atom of the amino acids or to nitrogen atom of the proteins.[38,39] Metal particles have different affinities for different kinds of proteins and amino acids,[39,40] which could be another reason for the variation observed in SERS spectra.

Table 3.4: Tentative band assignments from AAE1 colony incubated with AuNPs. Figure 3.8D, spectrum 1.

peak position/cm^{-1}	assignment[a 33,41-43]
738	CH_2 def
823	CC str
847	CO, CC, CH def
931	Ring vibrations
1000	CC ring breathing
1044	CC str
1179	C-O, C-C str
1216	CN str
1245	Amide III
1272	CH def, CH_2OH group, amide III
1374	COO^- str (sym)
1403	NH def
1497	CH_2 def
1516	COO^- str (sym), amide II
1586	COO^- str (asym)
1635	Amide I

[a]str=stretching; def=deformation; sym=symmetric; asym=antisymmetric.

SERS mapping of AAE2 colonies incubated with Au colloidal solution for 2 hours and mounted onto ZnSe window is shown in Figure 3.9. The spectra were collected with 785 nm laser with ~3 mW laser, 10 s exposure times and 1 scan. Because a number of pixels used to acquire the map, the SERS spectra are a result of multiple SERS occurring. Figure 3.9A and B display the optical microscope image and the measurement points where the spectra were recorded. The map was processed for the band intensity at 1531 cm^{-1} and the image is shown in Figure 3.9C. The SERS spectra from the marked points (Figure 3.9B) are displayed in Figure 3.9D. Spectra 1-4 were recorded from the marked points (Figure 3.9B) on the hyphae and revealed signal enhancement. The SERS spectra of AAE2 are characterized by the bands at 1318, 1429, 1571 and 1631 cm^{-1}

which are attributed to amide III, symmetric stretching of COO^-, asymmetric stretching of COO^- and amide I respectively.[13,36,37] Spectra 5 and 6 were obtained from the points on the background and showed the typical Raman spectra of the ZnSe window.

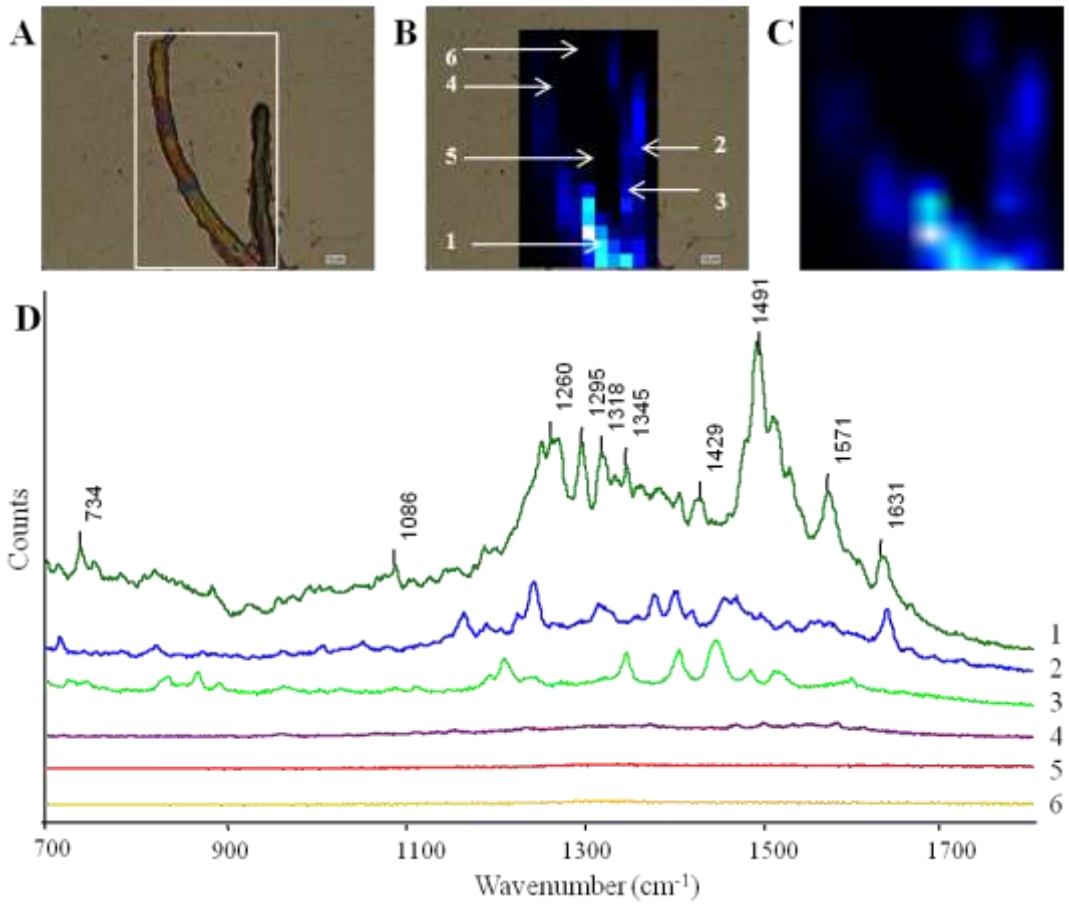

Figure 3.9: SERS imaging from AAE2 colony incubated with AuNPs. All spectra were recorded with 785 nm laser, ~3 mW, 1 scan and exposure time of 10 s (Raster scan). A) Photoimage of hypha on ZnSe substrate with a box showed the location of the recorded map; Scale bar =10µm. B) Same area with marked pixels; Scale bar = 10µm. C) Same area processed to show intensity at 1631 cm^{-1}. D) Spectra obtained from pixels marked in B. Spectra are on a common scale and offset for clarity.

Tentative assignment of the bands observed in spectrum 1 (Figure 3.9D) is given in Table 3.5. Differences in the positions and intensities of the signals can be detected in the SERS spectra of AAE2 (Figure 3.9D, spectra 1-4). For example, the bands at 847 and 931 cm^{-1} were not observed in the SERS spectra of AAE2. The differences observed in

the Raman spectra of AAE1 and AAE2 could be a result of the sample heterogeneity and the apparent random behaviour of the SERS event. Like AAE1, the SERS responses of AAE2 are from amide group and oxygen containing groups. The outer surface of both AAE1 and AAE2 are covered with mannoproteins which is apparent by the similar SERS responses from these 2 strains between 1200 and 1700 cm^{-1}, but not below 1200 cm^{-1}.

Table 3.5. Tentative band assignments from AAE2 colony incubated with AuNPs. Figure 3.9D, spectrum 1.

peak position/cm^{-1}	assignment[a 33,41-43]
734	CH_2 def
1086	COH bending, CH bending
1260	Amide III, CH def, CH_2OH group
1295	CH_2 def
1318	Amide III, CH def
1345	CH_2 def
1429	COO^- str (sym)
1491	CH_2 def
1571	COO^- str (asym)
1631	Amide I

[a]str=stretching; def=deformation; sym=symmetric; asym=antisymmetric.

Figure 3.10 displays the SERS spectra from an AuNPs aggregation on an AAE1 cell wall. AAE1 colony was exposed to Au colloids for 30 minutes and mounted and dried onto commercially used aluminum foil slide. The spectra were recorded with static scan centered at 700 cm^{-1} at 30 s intervals using 785 nm excitation wavelength with ~0.1 mW laser, 1 s exposure and 1 scan. As represented in Figure 3.10, the bands at 682, 731 and 877 cm^{-1} persisted in all spectra. The bands at 655 and 757 cm^{-1} can be identified in 3 spectra (4-6), while the strong band at 585 cm^{-1} was observed only in one spectrum. These variations may be a result of dynamic change in Au nanoaggregates adsorption on the proteins of the outer surface of fungal cell.[44]

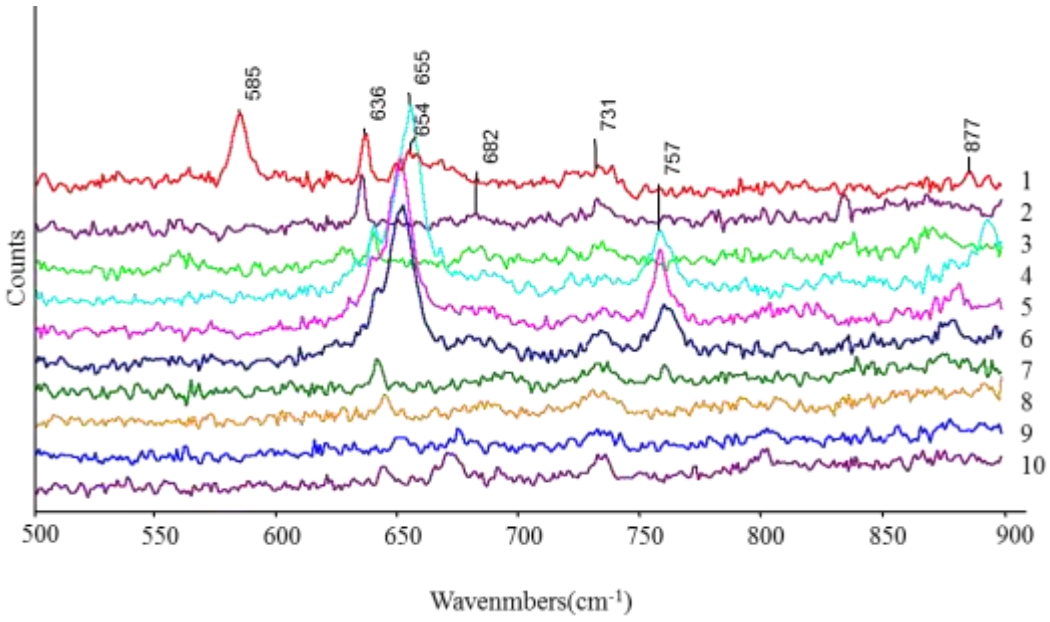

Figure 3.10: SERS spectra from aggregation of AuNPs on AAE1 cell wall recorded at 30 s intervals. AAE1 colonies were mounted and dried on aluminum foil slide. All spectra were recorded with 785 nm laser, ~0.1 mW, 1 scan and exposure time of 1 s (static scan centered at 700 cm^{-1}).

3.4 Conclusions

Raman spectroscopy is a technique yielding chemical composition information on a molecular level. Raman and SERS were used to explore fungal cell wall composition of two strains of *A. nidulans* which differ from each other in the cell wall thickness. Several Raman and SERS maps were recorded from *A. nidulans* hyphae and enhanced signals were observed when the cell wall components were in the vicinity of the NPs. For some spectra strong SERS signals were achieved which suggests that AuNPs aggregated on the outer surface of *A. nidulans* hyphae. Most of the peak assignments from the SERS were from carbohydrates and outer surface proteins, likely mannoproteins. Outer surface of both AAE1 and AAE2 strains were covered with mannoproteins, however they showed inconsistent SERS responses.

Nanoparticles synthesized by MSG were stable over time, but poor reproducibility with fluctuations of spectral features in the SERS spectra of *A. nidulans* was observed. The reasons for this can be explained by the fact that the time scale for SERS events are much shorter than the time required to a generate SERS map. Moreover, both nanoparticles and analyte must be present with the proper geometry. Experimental parameters such as size, aggregation of the nanoparticles and wavelength of the laser light can also affect the SERS spectra of fungi. Differences in sample preparation or positioning (sample heterogeneity) greatly affected the positions and number of peaks which made the interpretation of the SERS spectra of fungi very challenging. Although the work described in chapters 2 and 3 were focused mainly on SERS studies of *A. nidulans* hyphae, several FTIR-ATR, Raman and SERS spectra of *A. nidulans* spores were also collected in order to test the feasibility of using AuNPs for detecting chemical compounds in the conidial wall. A summary of the achieved results from this study is provided in chapter 4.

3.5 References

1. M. Harz, P. Rosch , J. Popp, *Cytom Part A*, 2009, 75A, 104-113.

2. W. E. Huang, M. Li, R. M. Jarvis, R. Goodcare, S. A. Banwart, *Adv Appl Microbiol*, 2010, 70, 153-186.

3. J. M. Chalmers, P. R. Griffiths. Vibrational spectroscopic studies of microorganisms. Chichester: John Wiley, 2002, 3308-3334.

4. P. Rosch, M. Harz, M. Schmitt, K. D. Peschke, O. Ronneberger, H. Burkhardt, H. W. Motzkus, M. Lankers, S. Hofer, H. Thiele, J. Popp, *Appl Enviro Microbiol*, 2005, 71, 1626-1637.

5. G. J. Pupples, W. Colier, J. H. F. Olminkhof, C. Otto, F. F. M. Mul, J. Greva, *J Raman. Spectrosc*, 1991, 22, 217-225.

6. R. M. Jarvis and R. Goodacre, *Anal Chem*, 2004, 76, 40-47.

7. E. C. Le Ru, P. G. Etchegoin. Principles of Surface Enhanced Raman Spectroscopy and Related Plasmonic Effects. Amsterdam: Elsevier, 2009.

8. Z. Xiaoyu, M. A. Young, O. Lyandres, R. P. Van Duyne, *J Am Chem Soc*, 2005, 12, 4484-4489.

9. S. Efrima, L. Zeiri, *J Raman Spectrosc*, 2009, 40, 277–288.

10. R. M. Jarvis, R. Goodacre, *Chem Soc Rev*, 2008, 37, 931–936.

11. A. Sujith, T. Itoh, H. Abe, K. Yoshida, M. S. Kiran, V. Biju, M. Ishikawa, *Anal Bioanal Chem*, 2009, 394, 1803–1809.

12. A. F. Chrimes, K. Khoshmanesh, S. Tang, B. R. Wood, P. R. Stoddart, S. S. E. Collins, A. Mitchell, K. Kalantar-zadeh, *Biosens Bioelectron*, 2013, 49, 536–541.

13. A. Szeghalmi, S. G. W. Kaminskyj, P. Rosch, J. Popp, K. M. Gough, *J Phys Chem B*, 2007, 111, 12916-12924.

14. M. A. Prusinkiewicz, F. Farazkhorasani, J. J. Dynes, J. Wang, K. M. Gough, S. G. W. Kaminskyj, *Analyst*, 2012, 137, 4934-4942.

15. R. M. Jarvis, N. Law, I. T. Shadi, P. O'Brien, J. R. Lloyd, R. Goodcare, *Anal Chem*, 2008, 80, 6741–6746.

16. J. E. Galagan, M. R. Henn, L. Ma, C. A. Cuomo, B. Birren, *Genome Res*, 2005, 15, 1620-1631.

17. S. D. Harris, *Mycologia*, 2008, 100, 823-832.

18. S. Isaac. Fungal-plant interactions. Cambridge: Chapman & Hall, 1992.
19. J. Ruiz-Herrera. Fungal cell wall: Structure, synthesis, and assembly. New York: Taylor & Francis group, 2012.
20. S. M. Bowman, S. J. Free, *BioEssays*, 2006, 28, 799–808.
21. B. Tefsen, A. F. Ram, I. V. Die, F. H. Routier, *Glycobiology*, 2012, 22, 456–469.
22. A. M. El-Ganiny, D. A. R. Sanders, S. G. W. Kaminskyj, *Fungal Genet Biol*, 2008, 45, 1533-1542.
23. S. A. Dalrymple, I. Sheoran, S. G. W. Kaminskyj, D. A. R. Sanders, *Acta Cryst*, 2011, F67, 885–887.
24. A. Sugunan, P. Melin, J. Schnürer, J. Hilborn, *Adv Mater*, 2007, 19, 77-81.
25. A. Sugunan, C. Thanachayanont, J. Dutta, J. G. Hilborn, *Sci Tech Adv Mater*, 2005, 6, 335-340.
26. W. Haiss, N. T. K. Thanh, J. Aveyard, D. Fernig, *Anal Chem*, 2007, 79, 4215-4221.
27. K. Faulds , R. E. Littleford, D. Graham, G. Dent, W. Smith, *Anal Chem*, 2004, 76, 592-598.
28. D. Lin-Vien , N. B. Colthup, W. G. Fateley, J. G. Grasselli. The Handbook of Infrared and Raman Characteristic Frequencies of Organic Molecules. San Diego: Academic Press Inc., 1991.
29. J. T. Edsall, *J Chem Phys*, 1937, 5, 508-517.
30. N. Peica, C. Lehene, N. Leopold, S. Schlucker, W. Kiefer, *Spectrochim Acta A Mol Biomol Spectros*, 2007, 66, 604–615.
31. I. Chourpa, F. H. Lei, P. Dubois, M. Manfait, G. D. Sockalingum, *Chem Soc Rev*, 2008, 37, 993–1000.
32. K. Maquelin, C. Kirschner, L. P. Choo-Smith, N. van den Braakb, H. P. Endtz, D. Naumann, G. J. Puppels, *J Microbiol Methods*, 2002, 51, 255 - 271.
33. K. De Gussem, P. Vandenabeele, A. Verbeken, L. Moens, *Spectrochim Acta A Mol Biomol Spectros*, 2005, 61, 2896–2908.
34. W. R. Premasiri, D. T. Moir, M. S. Klempner, N. Krieger, G. Jones, L. D. Ziegler, *J Phys Chem B*, 2005, 109, 312–320.
35. N. P. Ivleva, M. Wagner, A. Szkola, H. Horn, R. Niessner, C. Haisch, J Phys Chem B, 2010, 114, 10184–10194.

36. K. Maquelin, L. Choo-Smith, T. van Vrees, H. P. Endtz, B. Smith, R. Bennett, H. A. Bruining, G. J. Puppels, *Anal Chem*, 2000, 72, 12-19.

37. A. Sujith, T. Itoh, H. Abe, K. Yoshida, M. S. Kiran, V. Biju, M. Ishikawa, *Anal Bioanal Chem*, 2009, 394, 1803–1809.

38. R. K. DeLong, C. M. Reynolds, Y. Malcolm, A. Schaeffer, T. Severs, A. Wanekaya, *Nanotechnol Sci Appl*, 2010, 3, 53–63.

39. E. Podstawka, Y. Ozaki, L. M. Proniewicz, *Appl Spectrosc*, 2004, 58, 581-90.

40. E. Podstawka, Y. Ozaki, L. M. Proniewicz, *Appl Spectrosc*, 2004, 58, 570-80.

41. K. De Gussem, P. Vandenabeele, A. Verbeken, L. Moens, *Anal Bioanal Chem*, 2007, 387, 2823-2832.

42. H. G. M. Edwards, N. C. Russell, R. Weinstein, D. D. Wynn-Williams, *J Raman Spectrosc*, 1995, 26, 911-916.

43. S. Ghosal, J. M. Macher, K. Ahmed, *Environ Sci Technol*, 2012, 46, 6088−6095.

44. A. Sujith, T. Itoh, H. Abe, A. Anas, K. Yoshida, *Appl Phys Lett*, 2008, 92, 103901-103904.

Chapter 4: FTIR-ATR, Raman and SERS Spectroscopy of *Aspergillus nidulans* Spores

4.1 Introduction

Fungi play many critical roles in ecosystems, influencing carbon and mineral cycling, forming symbiotic relationships with plants, as well as being pathogenic agents for humans, animals and plants.[1] Fungal cell wall is a heterogeneous and dynamic network that protects fungi against lysis and maintains cellular shape and integrity.[2] The fungal cell wall defines an interface between the fungal hypha and its surroundings and allows the fungus to adapt to environmental stresses and express its genetic differences.[2,3] A better understanding of the fungal cell and its wall composition is of great interest for further investigation of their activities and interactions.

Fungal spores are microscopic biogenic particles that have significant effects on medical, industrial and agricultural activities in human life.[4] Asexual sporulation is a common reproductive method for many fungi and provides effective reproduction, dispersion and survival during adverse environmental conditions.[4,5] Electron microscopy and atomic force microscopy (AFM) of the conidia surface have shown that the outermost layer of many fungal conidia is covered with regularly assembled fascicles known as rodlets, 10±1 nm in diameter.[6-9] Electron microscopy of the conidial wall of *Aspergillus nidulans* (*A. nidulans*) has shown globose particles, 3-3.5 μm in diameter.[6] Chemical analysis of the rodlet layer of the wild-type *A. nidulans* strain has shown that proteins, carbohydrates and melanin are the main components of this layer.[10,11] Hydrophobins are a family of small, cysteine-rich, hydrophobic proteins that primarily compose the rodlet layer of *A. nidulans*.[9,12] The hydrophobic nature of the rodlet layer

performs several functions in fungal growth and development including effective spore dispersion by air, a protective barrier against chemical attack, and adhesion to host cells and surface interaction with other hydrophobic surfaces.[9] Neutral sugars such as glucose (the most abundant), galactose and mannose containing polysaccharides are the major carbohydrates of the conidial wall of *A. nidulans* strains.[11] The α-1,3-glucan is the predominant polysaccharide in the conidial wall of wild-type strain of *A. nidulans*.[11]

Rapid and reliable techniques for identification, determination and differentiation between fungal species and strains are essential due to the significant ecological and microbiological roles that fungi play in nature. To date, several phenotypic and genotypic methods have been recognized for identification of fungal species.[13,14] However, the use of these methods is limited due to lack of detailed information on a molecular level and high costs, labor and time consuming nature of these methods. There is a great need to employ alternative fast, economical, and nondestructive techniques to provide information on a molecular level. Vibrational spectroscopic methods including FTIR and Raman spectroscopy are fast and noninvasive methods for molecular structure examination of the biological structures. IR and Raman techniques require minimal sample preparation and provide detailed chemical composition information from both inside and the surface composition of the complex fungal cells.[15]

Raman spectroscopy is hampered by its low scattering efficiency. As an alternative, surface enhanced Raman scattering (SERS) enhances molecules low Raman scattering when they are placed on a roughened metal surface or in contact with colloidal metal particles. SERS is a sensitive and selective method that allows one to obtain specific information about the components in or on a cell.[16] .

In this study, FTIR attenuated total reflectance (ATR) and Raman techniques were utilized to study chemical composition among the conidia of various strains of *A. nidulans*. Glucans (polymers of D-glucose) are the main cell wall polysaccharides present in the cell wall of filamentous fungi. According to the type of glycosidic linkages between glucose units, glucans have been classified into α and β configurations.[17] In this research 5 strains of *A. nidulans* (wild type, AAE2, AXH17, AXH2 and AXH21) with different wall α-1,3-glucan contents,[18-20] were used as test samples to determine the feasibility of using vibrational techniques to assess the differences in wall composition. In addition, conidial structure alterations during germination were examined by Raman spectroscopy and distinct changes in spectral features were detected between the germinated spore and the germ tube. The chemical structure of the conidial wall of *A. nidulans* was investigated by means of SERS microscopy. Several SERS maps were collected from spore and enhanced signals were observed at several points on the conidial wall surface.

4.2 Materials and Methods

4.2.1 Fungi

Strains of *A. nidulans* utilized in this study are shown in Table 4.1. These strains were supplied by Prof. Susan Kaminskyj from the Biology Department, University of Saskatchewan. The colonies on PDA (both wild and non-wild) were green in appearance which is an indication that they have similar levels of pigmentation which indirectly shows that they are likely similar in maturity. Information about wild type gene deletion was described by El-Ganiny et al.[21] UDP-galactofuranose is synthesized from UDP-galactopyranose through UDP galactopyranose mutase (UGM). In strain AAE2, *ugmA*Δ

was deleted. [21] Alpha-1,3-glucans are synthesized by transmembrane enzymes, named α-1,3-glucan synthases.[22] *A. nidulans* has two genes (*agsA* and *agsB)* with different functions responsible for α-glucan synthesis. Alpha-glucan synthesis is mainly affected by *agsB* which creates 95% of the α-1,3-glucan cell wall composition while disruption of agsA has marginal effect on α-1,3-glucan levels.[23,24] Deletion of *agsB* affects the cell wall α-1,3-glucan contents. AXH21 strain presented a reduction in the cell wall α-1,3-glucan formation due to [*agsA*Δ, *agsB*Δ] double deletion. [22,25] The α-amylase gene, *amyD* appears to inhibit or perhaps to degrade α-1,3-glucan synthesis of the cell wall. In the AXH2 strain, the content of α-1,3-glucan was increased compared to wild type as a result of *amyD* gene knockout. AXH17 (*actA*(p)-*agsB),* a *agsB*-over-expression strain, possessed about 3 times more cell wall α-1,3-glucan (~291 %) compared to the wild type.[18]

Table 4.1: *Aspergillus nidulans* strains used for this study.

Strain	Relevant genotype	Colonies on PDA	Relative glucose (%) in alkaline soluble fraction (mean±SD)*
Wild type	wild type	Green	100.0±6.0
AAE2	ugmAΔ	Green	-
AXH2	*amyD*Δ	Green	152.5±13.5
AXH17	*actA*(p)-*agsB*	Green	291.0±25.7
AXH21	*agsA*Δ, *agsB*Δ	Green	1.2±1.0

* Values are those published by Kaminskyj et al.[18]

All strains were grown on potato dextrose agar (PDA) at 37 ºC for 3 days. The growth medium pH was adjusted to 6.5 with 1 M NaOH. The α-1,3-glucan content of these strains was determined by Xiaoxiao He in Kaminskyj group.[18]

4.2.2 Gold Colloid Preparation

A colloidal solution of AuNPs was prepared using the method described elsewhere.[26,27] Briefly, 0.84 mL of 0.5 % (21 mM) $HAuCl_4$ solution was added to 50 mL distilled water and the mixture was heated to boiling. Then, 2.8 mL of 0.42 % (25 mM) of MSG was added to the solution while heating and stirring. The solution was heated and stirred for five minutes until the color changed from light yellow to red. Finally, the reaction was removed from the heat and the solution was rapidly quenched in an ice bath. The maximum absorption of colloidal Au was at ~530 nm, ascribed to AuNPs with average size of 40-50 nm.[28]

4.2.3 Sample Preparation

Spores were collected from the freshly inoculated PDA culture plates using a sterile micropipette tip and transferred to a ZnS window or commercially used aluminum foil slide prior to FTIR and Raman measurements of each strain, respectively.
For Raman analysis of germinated spores, 5 µL of spore suspension in sterilized ultrapure water was placed on a square of gold-coated silicon wafer and a block of PDA was placed on it. Gold-coated silicon wafers were attached to microscope glass slides with double-sided tape. Each slide was incubated in a moist chamber at 30 ºC for 20-24 hours.[29] The sample was frozen at -80 ºC and then dried at room temperature. Hyphae grown across the PDA block were mature and capable of spore production. Germinated spores on the gold-coated silicon wafer substrate were used for Raman measurements. The number of AAE1 and AAE2 germinated spores examined with Raman is shown in Table 4.2.

Table 4.2: Number of germinated spores examined for each strain with the Raman technique.

Technique	Substrate	# of germinated spores (AAE1)	# of germinated spores(AAE2)
Raman	Gold-coated silicon wafer	8	7

Freshly harvested spores of the wild type were transferred to a 1.5 mL microfuge tube containing 200 µL of 25 mM monosodium glutamate (MSG) solution. An aliquot of this mixture was deposited on commercially used aluminum foil slides and dried at room temperature. This sample was used for Raman measurement and since nanoparticles were not added these spectra could be compared with SERS spectra. For SERS measurement, 200 µL of Au colloidal solution was added to wild type spore in MSG and mixed for 0.5-2 hours depending on the experiment. An aliquot of the final mixture was placed on available aluminum foil slide and dried at room temperature prior to SERS measurement.

4.2.4 FTIR Measurements

ATR spectra were obtained from several clusters of spores using a Varian 670 FTIR spectrometer coupled with a Varian 620 FTIR microscope equipped with a liquid nitrogen-cooled mercury-cadmium-telluride (MCT) focal planar array detector and a germanium (Ge) attenuated total reflectance (ATR) accessory. Mid-IR spectra were recorded from 4000 to 900 cm^{-1} at 4 cm^{-1} resolution by co-adding 256 scans. A background (air) was collected with a Ge crystal in place before each sample measurement.

All spectra were baseline corrected using OMNIC (7.2 a) software. This baseline correction was carried out for presenting the spectra on a similar scale which allowed for easier comparison of the individual spectra. Intensities of individual peaks were not

altered as a result of this baseline correction. Table 4.3 shows the number of spore analysed for each strain.

Table 4.3: Number of spore examined for each strain with FTIR-ATR, Raman and SERS techniques.

Technique	Substrate	# of spore (AAE1)	# of spore (AAE2)	# of spore (AXH2)	# of spore (AXH17)	# of spore (AXH21)
FTIR-ATR	ZnS	5	4	4	4	4
	Glass	5	5	2	2	2
Raman	Aluminum foil	25	24	17	17	17
SERS	Aluminum foil	7	6			

4.2.5 Raman and SERS Measurements

Raman and SERS spectra were collected from single spores using a Renishaw inVia Raman microscope in conjunction with a motorized x-y stage for map creation. A 785 nm excitation wavelength of a diode laser was focused onto a sample through a 50x objective with a laser power in the range of ~0.1-30 mW. The spectrometer was equipped with an electronically cooled charge-coupled device (CCD) and a 1200 l mm^{-1} holographic grating. Raman spectra were obtained between 400 and 1800 cm^{-1} using 1-10 s exposure times and 1-10 scans. Total exposure times for these spectra varied from 1-100s. The Raman spectrometer was wavelength-calibrated using a silicon wafer, and collected spectra were centered at 520 cm^{-1}. All spectra were baseline corrected using OMNIC (7.2 a) software. The number of spore examined for each strain is displayed in Table 4.3.

4.3. Results and Discussion

Alpha-1,3-glucans are one of the major polysaccharides found in *A. nidulans* cell wall. *Aspergillus nidulans* strains with different cell wall α-glucan content were used (Table 4.1). In AXH21, AXH2 and AXH17, due to deletion of particular α-glucan synthesis genes, the wall α-glucan content was changed to dramatically lower or higher α-glucan content, respectively.[18] The α- glucan content in AAE2 strain is increased as reported by Damveld et al. and Alam et al.[19,20]

4.3.1 ATR-FTIR of *A. nidulans* Spore

Figure 4.1A shows the ATR spectra of three different substrates including a microscope glass slide, ZnS window and a ZnSe window. Since the microscope glass slide showed a strong absorption in the 1200 - 900 cm^{-1} region, ATR measurements of spores were obtained using the ZnS window.

Spores of the 5 strains of *A. nidulans* were placed on a ZnS window, then mid-IR absorption spectra were collected (Figure 4.1 B-D). In order to obtain reproducible spore spectra, ATR spectra of each spore strain were collected from 3 spore clusters. The most dominant absorption bands in the low wavenumber region were at 1200-900, 1500-1200 and 1800-1500 cm^{-1}. These bands were mainly attributed to carbohydrates, amide III and amide I (C=O stretching vibration), amide II (NH bending coupled to CN stretching) and carbonyl vibration respectively.[30]

The main spectral feature in the high wavenumber ascribed to CH_2 absorption bands (carbohydrates and proteins) at 3050-2800 cm^{-1} region.[31] The IR band position for each strain, together with tentative band assignments is presented in Table 4.4. As can be seen in Figure 4.1B and C, the IR spectra of *A. nidulans* wild type and mutant strains

exhibited similar features in most absorption regions. However, variations in shape and intensity of some of the bands were observed. The small peaks that were observed (994 and 936cm^{-1}) for one strain (AXH17) is consistent with the highest level of α-1,3-glucan (~291%). It is interesting to note that the very weak peak at 936 cm $^{-1}$ was not observed in others strains.

The IR spectra of all strains presented intense bands in the 1200-900 cm^{-1} (mainly CC and CO stretching) and 1700-1200 cm^{-1} (amide I, II and III) regions.[32] The presence of these bands indicates that polysaccharides and proteins are the main components of *A. nidulans* strains. The variations in strains IR spectra were mainly associated with carbohydrates and proteins and to a lesser extent to lipids absorption bands. The band at ~1074 cm^{-1} were assigned to CC stretching vibration of β-glucan linkage (Figure 4.1D).[33-35] The presence of this band in strains of *A. nidulans* suggests that β-glucans are the main polysaccharides in *A. nidulans* spore wall composition.

As mentioned earlier, α-glucans are one of the main components of the rodlet layer. The conidial wall α-1,3-glucans performs an essential role in the interaction between the germinating conidia.[36] It was reported that in the agsB mutants with a lower level of cell wall α-1,3-glucan, less aggregation was observed between swollen conidia.[18,22] It indicates that the lower content of the cell wall α-1,3-glucan may disorganize the rodlet layer and affect its functions.

The IR spectrum of D-glucose was reported and showed vibrational bands at 1035, 1078, 1149 and 1456 cm^{-1}.[33] Similar bands were detected in the IR spectra of *A. nidulans* strains (Figure 4.1C). These results indicated that glucose was the main monosaccharaide in the composition of *A. nidulans* wall carbohydrates.

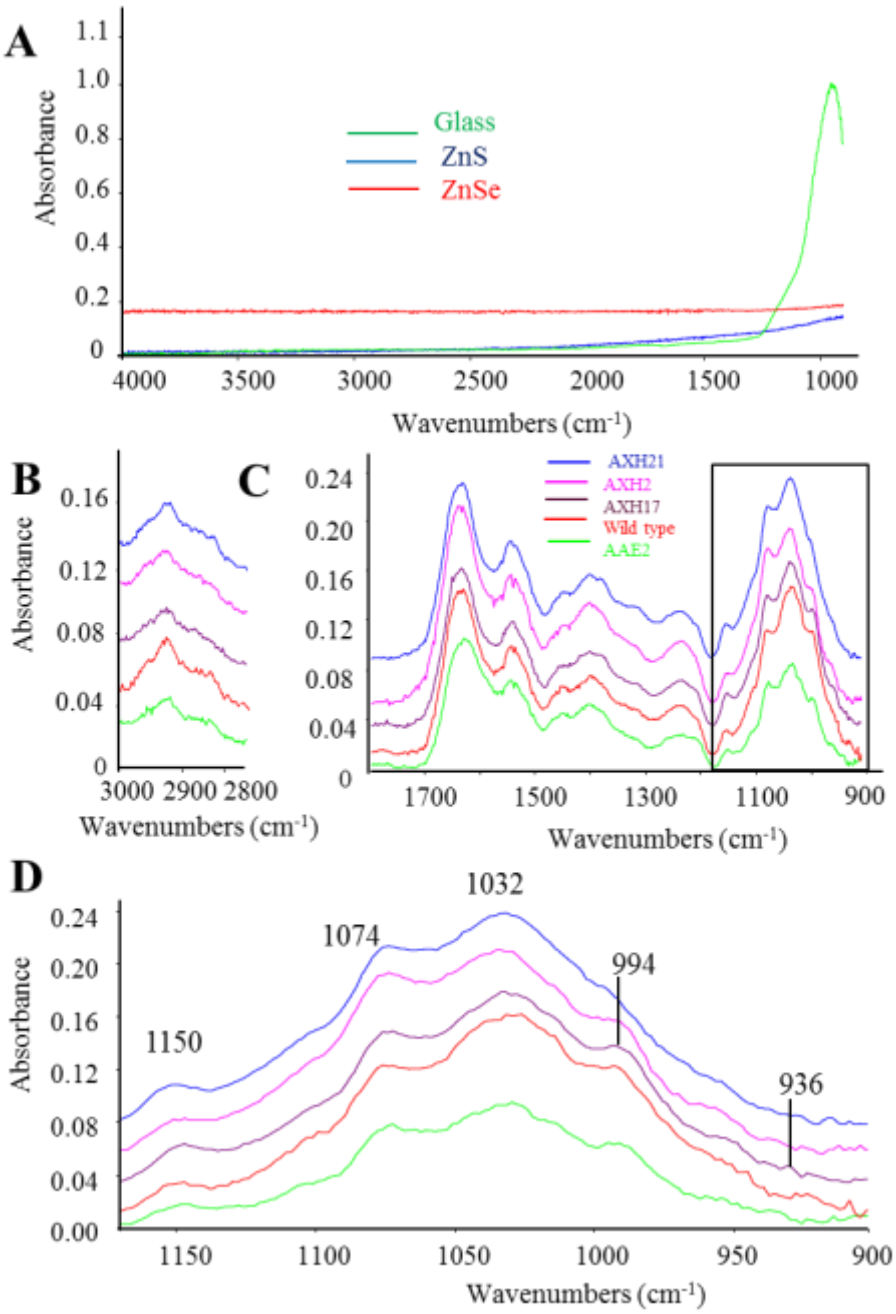

Figure 4.1: FTIR-ATR spectra of *Aspergillus nidulans* asexual spores. A) Different substrate. B) Cluster of spores from 5 strains of *A. nidulans* on ZnS slide in the 2800-3000 cm^{-1} region. C) Cluster of spores from five strains of *A. nidulans* on ZnS slide in the 900-1800 cm^{-1} region. Box shows the carbohydrate absorption region (1170-900 cm^{-1}). D) Close-up of the box shown in C. Spectra are on a common scale and offset for clarity.

Table 4.4: Positions of the observed FTIR bands (in cm^{-1}) of the various *A. nidulans* strain spores

Wild type	AAE2	AXH17	AXH2	AXH21	Band assignment [a]
3282	3268	3282	3282	3276	OH str (sym)[31]
2926	2921	2927	2927	2921	CH str (asym) of CH_2 [37]
2856				2851	CH str (sym) of CH_2 [37]
1632	1630	1635	1638	1632	Amide I [15]
1543	1544	1541	1544	1545	Amide II[15]
1453	1449	1448	1444	1448	CH_2 def [37,38]
1399	1401	1399	1399	1400	COH bending,[38] C=O str (sym) of COO^- [37]
1234	1236	1230	1231	1236	Amide III,[39] P=O str (asym) of PO_2^- [37]
1148	1147	1147	1147	1150	CO str [37]
1075	1072	1072	1073	1074	CC & CO str (glycosidic link, β-Glucans)[32,33] P=O str (sym) of PO_2^- [37]
1031	1029	1032	1034	1032	CC str (glucans, β- anomer)[35,38]
993	995	993	994		CO, CC str (glucans, β- anomer) [35]
		936			CH deformation (glucans, α- anomer)[35,38,40]

[a]str=stretching; def=deformation; sym=symmetric; asym=antisymmetric.

4.3.2 Raman of *Aspergillus nidulans* Spore

Figure 4.2A presents the Raman spectra of *A.nidulans* strains single spores along with the microscopic image of wild type single spores as an example. Each spectrum shown in this figure is the average of 10 single spore spectra. All spectra were recorded with 785 nm laser with ~0.4 mW laser at the sample, 10 s exposure time and 4 scans in the 400-1800 cm^{-1} spectral region. Depending on the experiment, total exposure time varied from 1-4 minutes. The Raman spectra of the *A. nidulans* spore were mainly dominated by proteins, carbohydrates and lipids. As represented in Figure 4.2A, the Raman spectral features of different strains showed a few differences mostly in intensity of the peaks at 515, 1215, 1426, 1553 and 1643 cm^{-1}. The proposed peak assignments as well as the observed peak positions are listed in Table 4.5. All spectra were shown in common scale.

Raman and IR methods present complementary information about the chemical structure of the fungi. The intensity of the Raman and IR bands are different as a result of different selection rules. As can be seen in Figure 4.2A, strong signals at 1643, 1553 and 1215 cm^{-1} were associated with amide I, amide II and amide III respectively. In IR spectra, these three bands can be found at 1632, 1543 and 1234 cm^{-1}. Further contribution of proteins in *A. nidulans* fungal spore composition was observed at 1002 cm^{-1} due to CC stretching of the aromatic ring (phenylalanine). The bending and stretching vibrations of COC of glycosidic link can be detected at 515 and 865 cm^{-1} respectively. More carbohydrate contributions can be observed at 1051 cm^{-1} due to CO stretching vibration.[41]

The Raman spectra of the spore of *A. nidulans* analyzed in this study reflected similar spectral signatures to the Raman spectrum of the spore of *A. versicolor* as described by Ghosal et al.[42] It was reported that fungal spores of different species in the similar genus displayed similar spectral features.[38] The spectral resemblances between the various species within the same genus may be linked to taxonomical relationship.[43]

Figure 4.2B compares the Raman spectra of a single spore and a cluster of spores. Microscopic images of the single spore and cluster of spores were also shown in Figure 4.2B. The laser light, exposure time and number of scans for collecting of both spectra were similar. The Raman spectra of single spore and cluster of spores showed uniform vibrational bands with slight differences in intensity of some of the bands. Most of the bands in the Raman spectrum of spore cluster were similar compared to the same bands in the Raman spectrum of single spore with respect to peak resolution and signal-to-noise ratio.

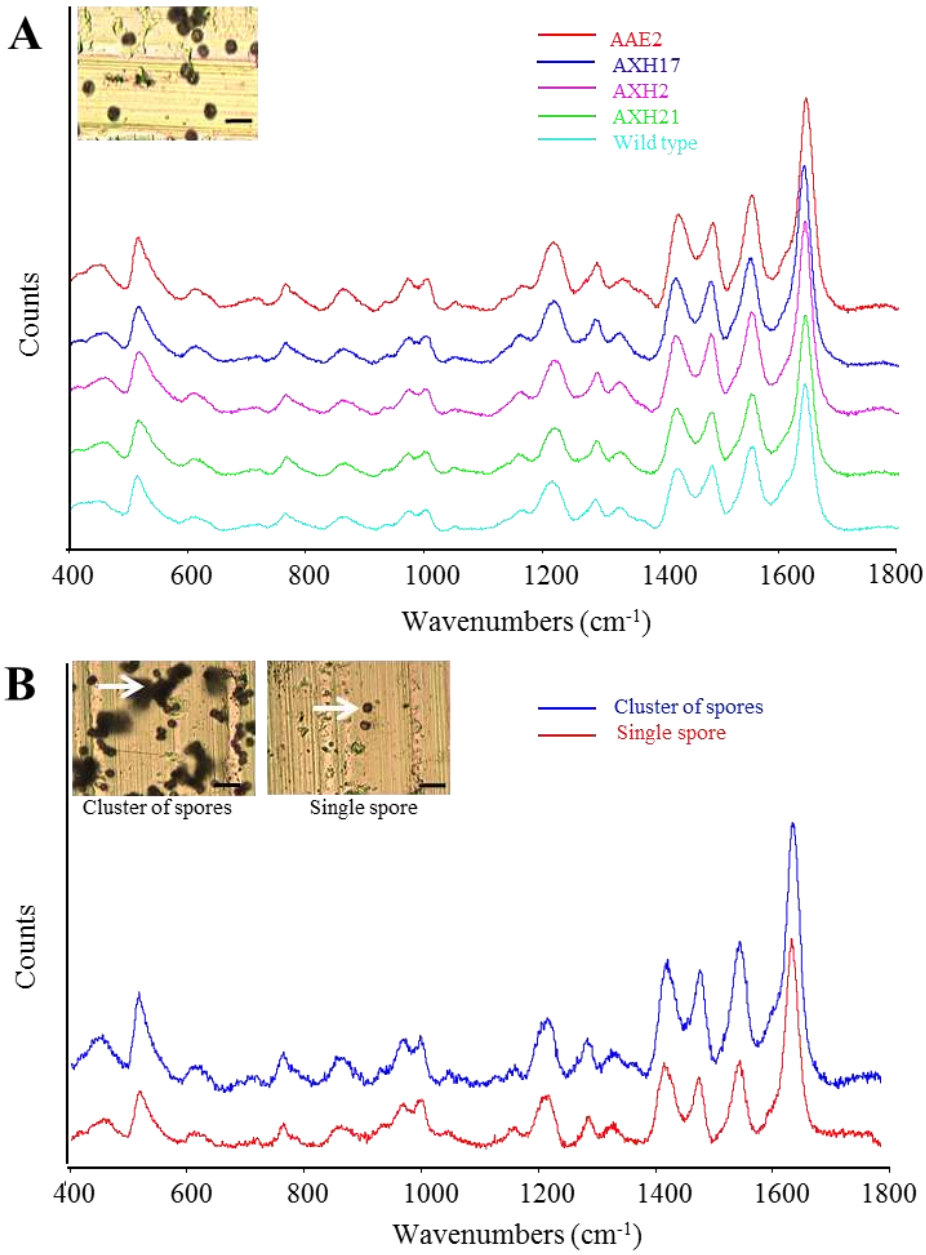

Figure 4.2: Raman spectroscopy of *Aspergillus nidulans* asexual spores.

A) Photoimage of wild type spore on aluminum foil slide; Scale bar = 10 µm. Average Raman spectra from 10 single spores from five strains of *A. nidulans.* All spectra were recorded with a 785 nm laser, power, ~0.4 mW and exposure times of 10 s.

B) Photoimage of wild type single spore and cluster of spores on aluminum foil slide; Arrow indicated the location where the spectrum was recorded; Scale bar = 10 µm. Comparison of Raman spectra of a single spore and a cluster of spores. Spectra were recorded with 785 nm laser power, ~0.1 mW and exposure time of 10 s. Spectra are on a common scale and offset for clarity.

Table 4.5: Positions of the observed Raman bands (in cm^{-1}) of the various *A. nidulans* strain spores

Wild type	AAE2	AXH17	AXH2	AXH21	Band assignment [a]
449	451	460	459	454	CCC ring def [44]
512	515	516	516	515	CCC ring def,[45]COC def (glycosidic ring)[46]
863	860	861	859	865	CC str, [37,43] COC str (1,4 glycosidic link)[37,43]
972	970	972	973	971	CH_2 def [45]
999	1001	1002	1002	998	CC str aromatic ring [37,45]
1052	1051	1053	1050	1051	CO str [45]
1166	1164	1161	1162	1158	C-C, C-N str[37]
1215	1216	1217	1218	1219	Amide III[44 45]
1289	1290	1289	1292	1290	Amide III[37,48], CH_2 def [45]
1330	1335	1329	1328	1331	C-H def [45]
1425	1427	1424	1424	1426	CH_2 def [41,45,49]
1484	1485	1483	1483	1485	Ring breathing[47, 48]
1553	1553	1552	1551	1551	Amide II[50]
1643	1644	1641	1642	1643	Amide I,[41] C=C st[43,45]

[a]str=stretching; def=deformation; sym=symmetric; asym=antisymmetric.

4.3.3 Raman of *Aspergillus nidulans* Germinated Spore

The conidium cell wall showed major ultrastructural changes during germination. These changes include: increased conidium size, decreased wall thickness, disruption of the rodlet layer and appearance of an amorphous layer that was mainly composed of polysaccharides (hydrophilic) from the inner spore wall and finally variations in the capacity for adhesion to occur. In particular, poor adhesion for spores that were not germinating to strong adhesion for germinating spores.[9,51,52]

Figures 4.3A and B display a microscopic image of a wild type germinated spore and the Raman spectra that were collected from the germinated spore and along the germ tube. The positions of the collected spectra were marked in the image. All spectra were collected in the 400-1800 cm^{-1} region using ~30 mW laser with 10 s exposure time and 10 scans except for the germinated spore (Figure 4.3A, arrow 1; ~0.4 mW laser light, 10 s exposure time and 10 scans). The germinated spore showed similar spectral signatures

as ungerminated spore (Figure 4.3A, arrow 1; Figure 4.3B, spectrum 1) which are rich in proteins and carbohydrates. Distinct differences were observed in the Raman spectrum of the spore compared to those of the germ tube**.** By increasing the distance of the germ tube from the spore, the intensity of vibrational bands were reduced and a few bands disappeared (Figure 4.3A, arrows 2 and 3; Figure 4.3B, spectra 2 and 3). When the germ tube measurements were made at distances from the spore by more than 60 µm, most of the vibrational bands that were linked to proteins, carbohydrates and lipids disappeared (Figure 4.3A, arrows 4-6; Figure 4.3B spectra 4-6) and the spectra were similar to mature hyphal spectra. Previously the same results from the FTIR spectra of a germinated *Neurospora* spore were observed. [53]

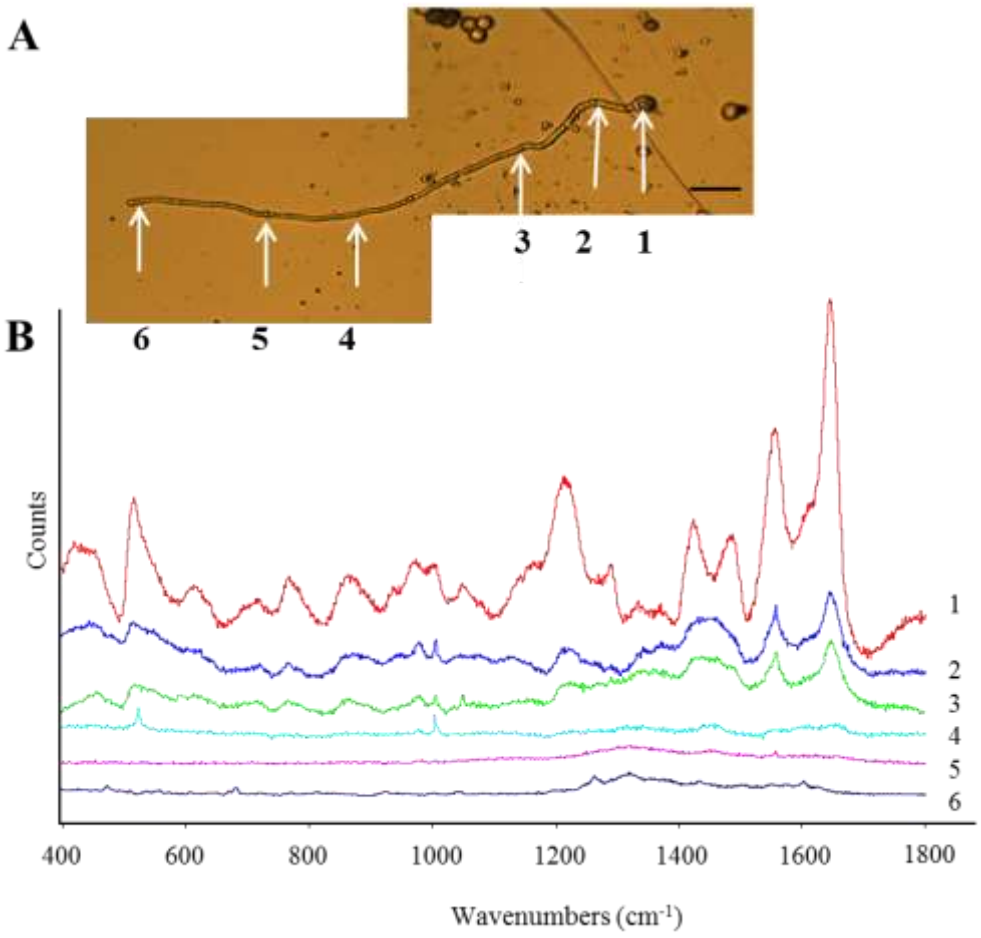

Figure 4.3: Wild type spore germination. A) Photoimage of a germinated spore grown on a gold-coated silicon wafer; Scale bar = 10 µm. B) Raman spectra of germinated spore and different positions of germ tube correspond to the arrows marked on the image. Spectra are on a common scale and offset for clarity.

One of the important factors that must be considered during analysis of biological samples is laser-induced degradation of the sample. It is essential to collect Raman spectra with sufficient signal-to-noise ratio while avoiding laser degradation of the sample. Since fungal spores are rich in biological components, low laser power was used to collect the Raman spectra. Figure 4.4 A and B represent the images of the spore before and after laser-induced degradation. Raman spectra of a single spore with different laser power on the sample were collected and shown in Figure 4.4C. As can be seen, when low

laser power (~0.4 mW) was used, the *A. nidulans* spore spectrum was detected without any visible sign of sample degradation (Figure 4.4A; Figure 4.4C, spectrum 1). By increasing the laser power on the sample, the fluorescence background was elevated in the 1200-1700 cm^{-1} region compared to spectrum 1 (Figure 4.4C, spectra 2, 3). Excessive power (~30 mW) on the sample resulted in spore damage and sample degradation was apparent in the Raman spectrum (Figure 4.4B; Figure 4.4C, spectrum 4).

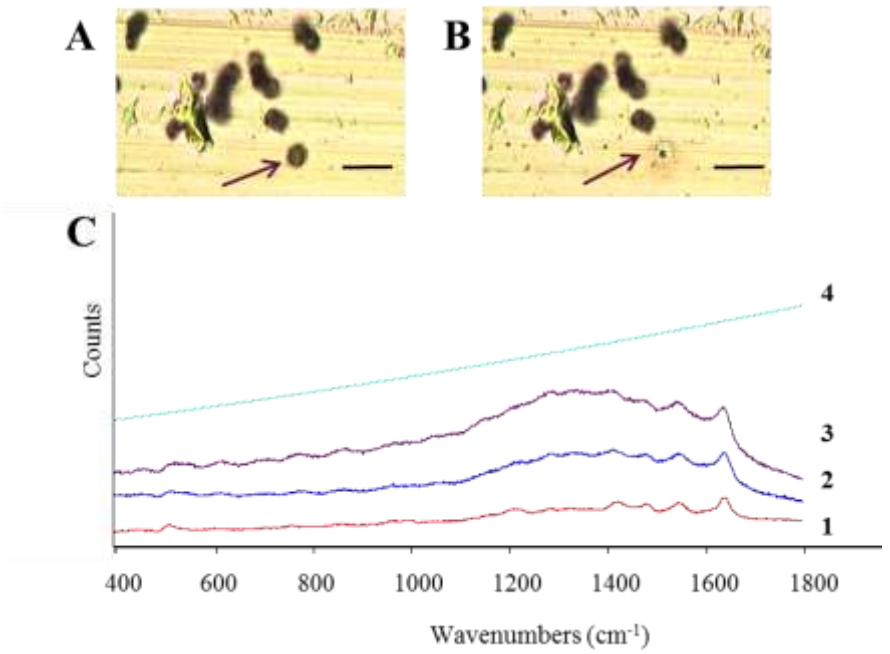

Figure 4.4: Laser induced degradation of wild type spore. A) Photoimage of a wild type spore on Aluminum foil slide before spore damage; Scale bar = 10 µm. B) Photoimage of wild type spore on Aluminum foil slide after analysis with the strong laser illumination (30 mW); Scale bar = 10 µm. C) Raman spectra of spore collected with different laser power; Spectra 1-4 were recorded with laser power of 0.4 mW, 8 mW, 16 mW and 30 mW, respectively. Spectra are on a common scale and offset for clarity.

4.3.4 Surface Enhanced Raman Scattering Activity of *Aspergillus nidulans* Spore

The Raman and SERS spectra of wild type spores are shown in Figure 4.5. The SERS spectrum was acquired from the wild type spores that were exposed to AuNPs. A Raman spectrum was collected from the control sample that had not been treated with

gold colloidal particles. Both Raman and SERS spectra were collected with 785 nm laser with ~0.4 mW laser light on the sample. Most of the bands in SERS spectrum of spore are enhanced and showed high signal-to-noise ratio compared to the bands in the control spectrum. For example the SERS bands at 844 and 1083 cm^{-1} which are assigned to COC skeletal mode and COC stretching from glycosidic link respectively[37,47] are significantly larger than the corresponding Raman peaks.

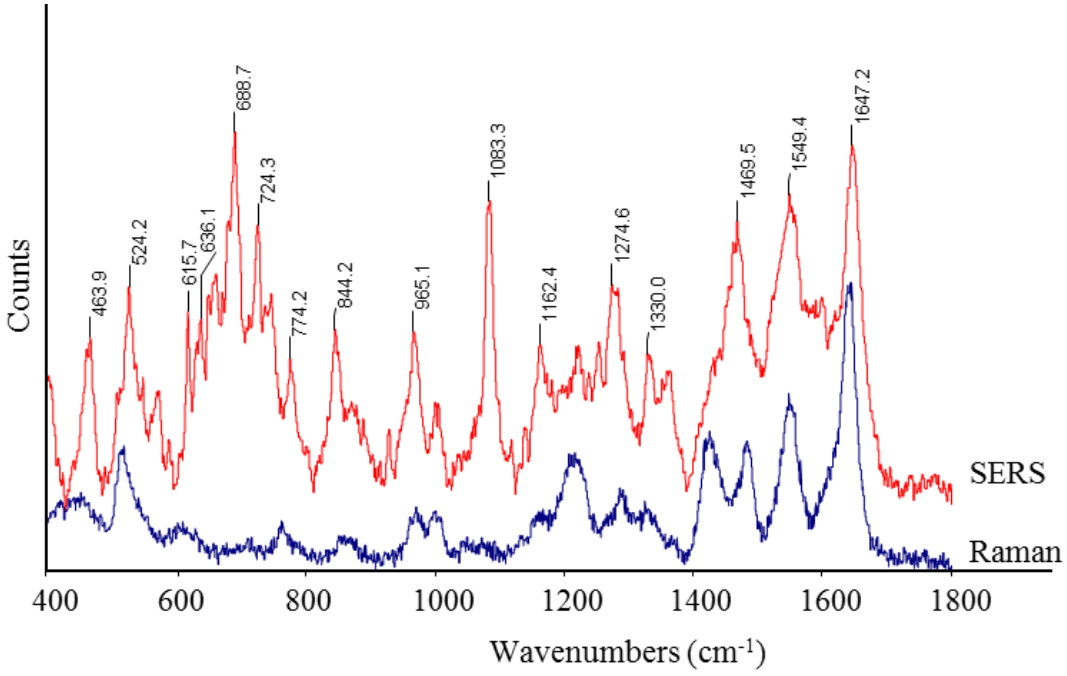

Figure 4.5: Comparison of Raman and SERS single spectra of wild type spore. Spectra were collected with 785 nm laser with ~0.4 mW laser and 10 seconds exposure time. Total time for acquiring spectra was ~1 minute. Spectra are on a common scale and offset for clarity.

SERS mapping was also obtained in the region 400-1800 cm^{-1} from a raster scan of a wild type spore and presented in Figure 4.6. The wild type spores were mixed with AuNPs and a droplet of the mixture was placed on an aluminum foil substrate. The data were recorded with ~1 mW laser light, 10 s exposure time and 1 scan. All spectra are displayed on a common scale. Images of the wild type single spore and the location

where the map was recorded are shown in Figure 4.6A and 6B respectively. Figure 4.6C displays the positions where the spectra were collected. Figure 4.6D shows the SERS spectra corresponding to the pixels (marked in Figure 4.6C) within a single wild type spore. Three of these spectra were collected from points on the spore (Figure 4.6C, pixels 3, 6 and 12; Figure 4.6D, Spectra 3, 6 and 12) and two were shown from the background, where no spore were present (Figure 4.6C, pixels 14, 20; Figure 4.6D, Spectra 14, 20).

Raman signals can be increased by many orders of magnitudes when the molecules are in close vicinity to colloidal metal particles. Strong SERS signals at 998, 1220 and 1600 cm^{-1} was observed from point 3 on the spore (Figure 4.6C, pixel 3; Figure 4.6D, Spectrum 3). These bands were possibly attributed to C-C stretching of aromatic ring (phenylalanine), amide III, and C=C stretching of aromatic ring (phenylalanine), respectively.[44,46] The SERS spectrum of a wild type spore indicates the contributions of proteins and to a lesser extent carbohydrates in wall compositions.

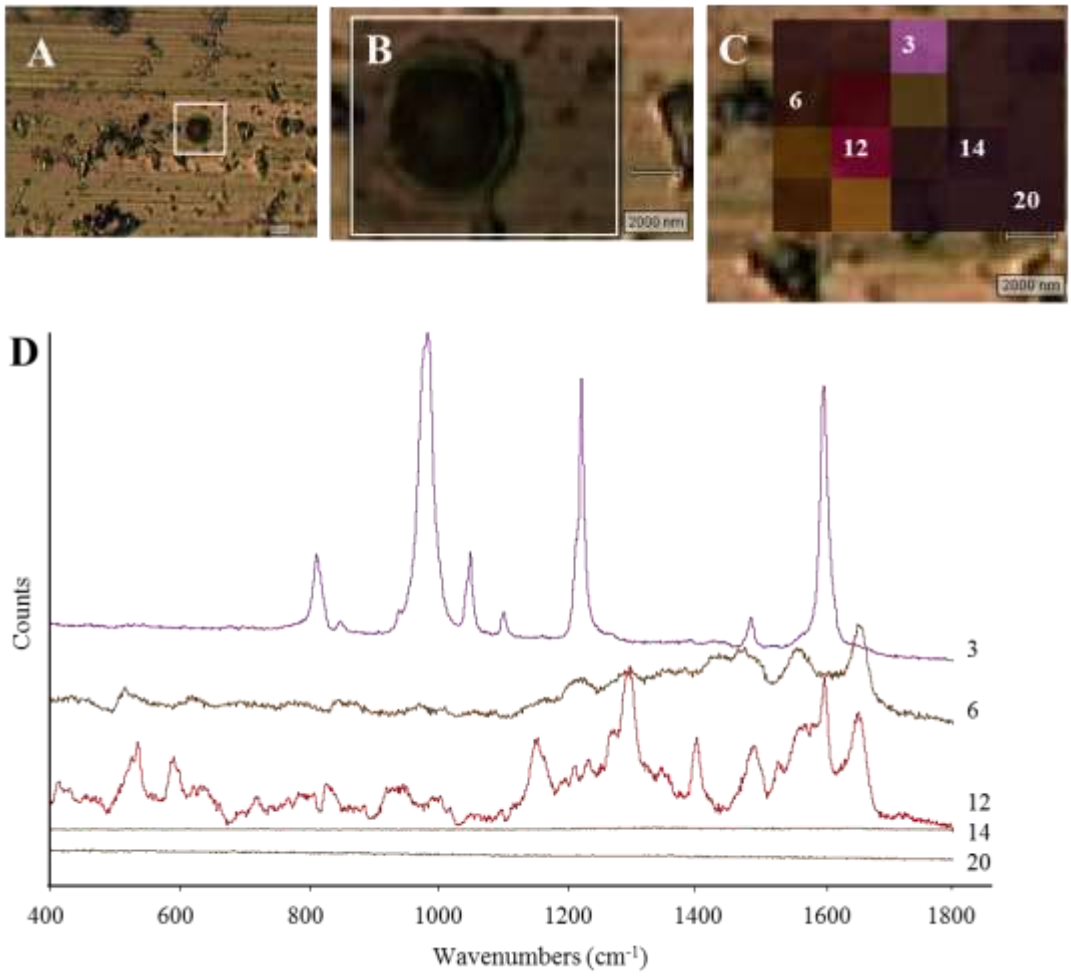

Figure 4.6: SERS imaging from wild type spore incubated with AuNPs. All spectra were recorded with 785 nm laser, ~1 mW, 1 scan and exposure time of 10 s (Raster scan).Photoimage of spore on aluminum foil substrate with a box showed the location of the recorded map; Scale bar =10µm. B) Close-up of the box shown in A; Scale bar =2µm. C) Close-up of the map location, processed to show intensity at 1050 cm^{-1}; Scale bar =2µm. D) Spectra obtained from pixels marked in C. Spectrum number corresponds to the pixel number. Spectra are on a common scale and offset for clarity.

The outer layer of *A. nidulans* conidia is covered by proteins and carbohydrates. Phenylalanine is one of the amino acids constituent the conidial outer and inner wall.[51] It was shown that the SERS response from the cell wall carbohydrates is weak while a strong reaction between the cell wall proteins and AuNPs has been detected.[54] The enhanced Raman signals in the spectra of wild type conidial wall suggests that there is a

high affinity between AuNPs and proteins. It was indicated that there is a strong binding between amine, phosphate, nitro, or thiol moieties and the gold surface. In addition, phenyl groups have a strong affinity with the gold surface as well as a high Raman cross-section that can enhance their Raman signals.[55] As a rule, a mode is enhanced when the polarizability factor is perpendicular to the surface of the metal particle. Then, the orientation of the phenyl ring to the metal particle surface affects the intensities of the ring vibrational modes.[56] In phenylalanine, the modes at 1000 cm^{-1} and 1600 cm^{-1} were enhanced regardless of the orientation of the ring to the metal surface due to presence of polarizability components in all directions.[56,57] Spectral inhomogeneity that was observed in the SERS spectra of wild type conidia may mainly arise from the changes in molecular orientation.[58]

4.4. Conclusions

In this chapter, the potential of vibrational techniques (FTIR and Raman spectroscopy) to examine fungal spores as well as to study the chemical composition of different strains of *A. nidulans* were presented. Proteins and carbohydrates were the dominant components of the *A. nidulans* spores. Several strains of *A. nidulans* with different cell wall α-glucan content were analyzed and very slight differences in their IR and Raman spectra were observed (994 cm^{-1}). The application of SERS to investigate the chemical composition of the wall of the fungal spores was explored and strong binding between the spore wall proteins and AuNPs was observed. SERS enhance the intensity of inherently weak Raman signals to several orders of magnitude and may be used as an efficient tool to study the surface structure of the biological systems. Reproducibility was

the main problem in SERS investigations of fungi which made spectral analysis challenging.

4.5 References

1. K. A. Borkovich, D. J. Ebbole. Introduction to the Filamentous Fungi. Texas A& M University: American Society for Microbiology (ASM), 2010.

2. S. M. Bowman, S. J. Free, *BioEssays,* 2006, *28*,799–808.

3. A. Firon, G. Lesage, H. Bussey, *Curr Opin Microbiol*, 2004, *7*, 617–623.

4. T. H. Adams, J. K.Wieser, J. Yu, *Microbiol Mol Biol Rev*, 1998, *62*, 35-54.

5. N. Osherov, G. May, *Genetics*, 2000, 155, 647-656.

6. W. M. Hess, D. L. Stocks, *Mycologia,* 1969, 61, 560-571.

7. B. C. van der Aa, M. Asther, Y. F. Dufrene, Colloids Surf B, 2002, 24, 277–284.

8. L. Zhao, D. Schaefer, M. R. Marten, *Appl Eniron Microbiol*, 2005, 71, 955–960.

9. E. Dague, D. Alsteens, J. Latge, Y. F. Dufrene, *Biophys J*, 2008, 94, 656–660.

10. F. Claverie-Martin, M. R. Diaz-Torres, M. J. Geoghegan, *Curr Microbiol,* 1986,14, 221-225.

11. F. Claverie-Martin, M. R. Diaz-Torres, M. J. Geoghegan, *Curr Microbiol*, 1988, 16, 281-287.

12. J. Bayry, V. Aimanianda, J. I. Guijarro, M.Sunde, J.Latge, *PLoS Pathog*, 2012, 8, e1002700.

13. L. Hall, S.Wohlfiel, G. D. Roberts, *J Clin Microbiol*, 2004, 42, 622-626.

14. G.Liguori, A.Lucariello, G.Colella, A. De Luca, P. Marinelli, *J Clin Pathol,* 2007, 60, 1035-1039.

15. K. Maquelin, L. P.Choo-Smith, C. Kirschner, N. A. Ngo-Thi, D. Naumann, G. J. Puppels. Vibrational spectroscopic studies of microorganisms. In Handbook of Vibrational Spectroscopy, Chichester : Wiley, 2002, 3308–3334.

16. K. Kneipp, H. Kneipp, I. Itzkan, R. R. Dasari, M. S. Feld, *J Phys Condens Matter*, 2002, 14, R597-R624.

17. J. Ruiz-Herrera. Fungal cell wall: structure, synthesis, and assembly. Florida : CRC Press, 2012.

18. X. S. He, S. J. Li, S. G. Kaminskyj, *Mol Microbiol*, 2014, 91, 579-595.

19. R. A. Damveld, A. Franken, M. Arentshorst, P. J. Punt, F. M. Klis, C.A.M. J. J. van den Hondel, A .F. J. Ram, *Genetics*, 2008, 178, 873–881.

20. K. Alam, A.M. El-Ganiny, S. Afroz, D. Sanders, J. Liu, S. G. W. Kaminskyj, *Fungal Genet Biol*, 2012, 49, 1033-1043.

21. A. M. El-Ganiny, D. A. R. Sanders, S. G. W. Kaminskyj, *Fungal Genet Biol*, 2008, 45, 1533-1542.

22. C. Henry, J. Latge, A. Beauvais, *Eukaryot Cell*, 2012, 11, 26-29.

23. A.Yoshimi, M. Sano, A. Inaba,Y. Kokubun, T. Fujioka, O. Mizutani, D. Hagiwara, T. Fujikawa, M. Nishimura, S. Yano, S. Kasahara, K. Shimizu, M.Yamaguchi, K. Kawakami, K. Abe, *PLoS One*, 2013, 8, e54893.

24. A. Beauvais, D. Maubon, S. Park, W. Morelle, M. Tanguy, M. Huerre, D. S. Perlin, J. P. Latge, *Appl Environ Microbiol*, 2005, 71, 1531–1538.

25. M. Bernard, J. P. Latge, *Med Mycol*, 2001, 39, 9-17.

26. A. Sugunan, P. Melin, J. Schnürer, J. G, Hilborn, J. Dutta, *Adv Mater*, 2007, 19, 77-81.

27. A. Sugunan, C. Thanachayanont, J. Dutta, J. G. Hilborn, *Sci Tech Adv Mater*, 2005, 6, 335-340.

28. W. Haiss, N. T. K.Thanh, J. Aveyard, D. G. Fernig, *Anal Chem*, 2007, 79, 4215-4221.

29. A. Szeghalmi, S. G. Kaminskyj, P. Rosch , J. Popp, K. M. Gough, *J Phys Chem B*, 2007, 111,12916-12924.

30. D. Naumann, Encyclopedia of Analytical Chemistry. Chichester : Wiley, 2000, 102–131.

31. R. K. Dukor. Handbook of Vibrational Spectroscopy. Chichester : Wiley, 2001.

32. A. Synytsya, K. Mickova, A. Synytsya, I. Jablonsky, J. Spevácek, V. Erban, E. Kováríková, J. Copikova, *Carbohydr Polym*, 2009, 76, 548–556.

33. M. Kaurfikovfi, M. Mathlouthi, *Carbohydr Res*, 1996, 284,145-157.

34. M. Kacurakova, P. Capeka,V. Sasinkova, N. Wellnerb, A. Ebringerova, *Carbohydr Polym*, 2000, 43,195-203.

35. J. Sandula, G. Kogan, M. Kacurakova, E. Machova, *Carbohydr Polym*, 1999, 38, 247-253.

36. T. Fontaine, A. Beauvais, C. Loussert, B. Thevenard, C. C. Fulgsang, N. Ohno, C. Clavaud, M. Prevost, J. Latge, *Fungal Genet Biol*, 2010, 47, 707–712.

37. K. Maquelin, C. Kirschner, L. P. Choo-Smith, N. Van den Braakb, H. P. Endtz, D. Naumann, G. J. Puppels, *J Microbiol Methods,* 2002, 51, 255 - 271.

38. M. Mohacek-Grosev, R. Bozac, G. J. Puppels, *Spectrochim Acta Mol Biomol Spectros,* 2001,57, 2815-2829.

39. Z. Movasaghi, S. Rehman, I. U. Rehman, *Appl Spectrosc Rev*, 2008, 43, 134–179.

40. A. J. Michell, G. Sourfield, *Aust J biol Sci*, 1970, 23, 345-60.

41. W. E. Huang, M. Li, R. M. Jarvis, R. Goodcare, S. A. Banwart, *Adv Appl Microbiol,* 2010,70,153-186.

42. S. Ghosal, J. M.Macher, K. Ahmed, *Environ Sci Technol,* 2012, 46, 6088–6095.

43. K. De Gussem, P. Vandenabeele, A. Verbeken, L. Moens, *Anal Bioanal Chem,* 2007, 387, 2823-2832.

44. U. Neugebauer, U. Schmid, K. Baumann, W. Ziebuhr, S. Kozitskaya, V. Deckert, M. Schmitt, G. J. Pupples, *ChemPhysChem,* 2007, 8, 124-137.

45. K. De Gussem, P. Vandenabeele, A. Verbeken, L. Moens, *Spectrochim Acta Mol Biomol Spectros*, 2005, 61, 2896–2908.

46. K. Maquelin, L. Choo-Smith, T. van Vrees, H. P. Endtz, B. Smith, R. Bennett, H. A. Bruining, G. J. Puppels, *Anal Chem*, 2000, 72, 12-19.

47. Z. Movasaghi, S. Rehman, I. U. Rehman, *Appl Spectrosc Rev,* 2007, 42, 493–541.

48. K. C. Schuster, E. Urlaub, J. R. Gapes, *J Microbiol Methods*, 2000, 42, 29–38.

49. N. Uzunbajakava, A. Lenferink, Y. Kraan, B. Willekens, G. Vrensen, J. Greve, C. Otto, *Biopolymers,* 2003, 72, 1-9.

50. H. G. M. Edwards, N. C. Russell, R. Weinstein, D. D. Wynn-Williams, *J Raman Spectrosc,* 1995, 26, 911-916.

51. G. T. Cole, T. Sekiya, R. Kasai, T. Yokoyama, Y. Nozawa, *Exp Mycol,* 1979, 3, 132-156.

52. G. Tronchin, J. P. Bouchara, M. Ferron, G. Larcher, D. Chabasse, *Can J Microbiol,* 1995, 41, 714-721.

53. K. Jilkine, K. M. Gough, R. Julian. S. G. W. Kaminskyj, *J Inorg Biochem*, 2008, 102, 540–546.

54. A. Sujith, T. Itoh, H. Abe, K. Yoshida, M. S. Kiran, V. Biju, M. Ishikawa, *Anal Bioanal Chem*, 2009, 394, 1803–1809.

55. M. P. Cecchini, V. A. Turek, J. Paget, A. A. Kornyshev, J. B. Edel, *Nat Mater*, 2013, 12, 165-171.

56. S. Siddhanta, C. Narayana, *Nanomater Nanotechnol*, 2012, 2, 1-13.

57. J. R. Ferraro, K. Nakamoto. Introductory Raman spectroscopy. Boston: Academc press, 1994.

58. A. Kudelski, B. Pettinger, *Chem Phys Lett*, 2004, 383, 76-79.

Chapter 5: Conclusions and Future Studies

5.1 Conclusions

In this thesis, Raman and SERS methods were used to investigate the chemical structure of two strains of *A. nidulans*. To the best of my knowledge, this is the first SERS study of *A. nidulans* using *in vivo* and *in-situ* synthesized AuNPs. A number of conclusions can be drawn from this research.

Aspergillus nidulans has the potential to biosynthesize AuNPs intra-cellularly and extra-cellularly. These AuNPs were showed surface plasmon resonance and used as SERS substrates for SERS measurements of *A. nidulans.*

Parameters such as temperature, pH and gold concentration were important to prepare NPs with appropriate sizes and shapes for SERS study. It was very difficult to control the size, shape and location of the NPs which were prepared by colonies of *A. nidulans.*

Characterization of AuNPs synthesised by *A. nidulans* colonies revealed that most of the particles were associated with the hyphal walls and cytoplasm. However, the exact mechanism for the synthesis of NPs using *A. nidulans* is not yet known since there are various biomolecules that could be involved in the synthesis of NPs.

Aspergillus nidulans colonies that contained AuNPs showed SERS activity. Bands from the SERS spectra were attributed primarily to proteins and carbohydrates.

Stable AuNP was synthesized by MSG. These particles displayed surface plasmon resonance. Incubation of the pre-formed NP with *A. nidulans* cells resulted in

aggregation of NPs on the outer surface of fungal walls. Most of the SERS responses were from the outer surface proteins (mannoproteins of *A. nidulans*).

Raman spectra of the control samples (colonies which had not been incubated with AuNPs) of AAE1and AAE2 strains showed similar spectral features. Significant differences were not detected between the SERS spectra of AAE1 and AAE2 colonies which were incubated with AuNPs. Unfortunately, poor reproducibility of SERS spectra was observed (not shown) which generally made data interpretation very challenging.

FTIR-ATR studies of various strains of *A. nidulans* conidia indicated that glucose-containing polysaccharides are the main compounds in the composition of *A. nidulans* wall. Significant differences were detected in the Raman spectrum of the spore compared to those of the germ tube. The Raman spectra of the germ tube were similar to the spectra of mature hyphae. SERS studies of AAE1 spores revealed that there was a strong binding between the spore wall proteins and AuNPs.

5.2 Future Studies

Characterization of pre-formed AuNPs with Transmission electron microscopy (TEM) could provide useful information about the exact size and shape of the NPs. Characterization of *A. nidulans* cell surface with TEM and Scanning electron microscopy (SEM) would indicate the location of NPs within or on the surface of the cell. Structural information that can be acquired with these microscopic techniques may also provide clues about how NPs affect growth and structure of the cell walls of fungi in general. Furthermore, imaging of live hyphae before and after incubation with NPs would provide information about the effect of NPs on the chemical composition of the cells.

The SERS spectra of the fungal cell wall were complex. Differences in the spectra of different *A. nidulans* colonies (AAE1 and AAE2) were subtle which suggests that a statistical approach would be required. Although not investigated in these studies, chemometrics data analyses such as principle component analysis (PCA) and cluster analysis of the SERS data could aid in the comparison of complex spectral data.